Chemical characterization and biological assessment of *Euterpe oleracea* Mart. (açaí) for *in vitro* botanical-drug interactions with anticancer drugs

by

Kabre Lynne Heck

A dissertation submitted to the Graduate Faculty of
Auburn University
in partial fulfillment of the
requirements for the Degree of
Doctor of Philosophy

Auburn, Alabama
May 3, 2024

Keywords: *Euterpe oleracea* Mart.; Açaí; botanical-drug interaction; chemical fingerprinting, metabolomics, PAMPA

Approved by

Dr. Angela I. Calderón, Chair, Gilliland Professor of Drug Discovery and Development
Dr. Randall Clark, Gilliland Professor of Drug Discovery and Development
Dr. Jack DeRuiter, Hill Crest Professor of Drug Discovery and Development
Dr. Douglas Goodwin, Professor of Chemistry and Biochemistry
Dr. Satyanarayana R. Pondugula, Professor of Anatomy, Physiology and Pharmacology

Abstract

Cancer is the leading cause of death worldwide, with an estimated 19.3 million new cases in 2020 and almost 10 million cancer deaths. Botanical dietary supplements (BDS) are consumed more by cancer patients than otherwise healthier patients without cancer to alleviate side effects of chemotherapy drugs and/or increase quality of life; up to 80% of cancer patients have reported using BDS following their initial cancer diagnoses. However, many patients do not know the risks of concomitant use of BDS with anticancer drugs and the possibility for increased AEs, which may be life-threatening.

Euterpe oleracea Mart. (Arecaceae), commonly known as açaí, is a fruit that grows on the açaí palm tree native to the Amazon region. Açaí presents many health benefits, the most prominent being antioxidant and anti-inflammatory activities. In recent years, it has been introduced into the BDS market, and its popularity is steadily rising. Açaí is now among the top 40 botanicals used in the U.S., and cancer patients increasingly use açaí BDS to complement their conventional chemotherapeutic agents. This rise in popularity has also led to challenges regarding the quality, safety, and efficacy of açaí fruit products. Our group previously found that both passively and non-passively diffused compounds in MeOH açaí fruit extract displayed significant inhibition of hepatic CYP3A4 – suggesting potential for interactions between açaí BDS and CYP3A4-interactive drugs. Before testing this hypothesis, analytical methods to chemically characterize and standardize açaí products prior to *in vitro* testing are needed.

The first objective of this work was to develop a chemical fingerprinting method for untargeted characterization of açaí samples from a variety of sources, including food products and botanical dietary supplement capsules, made with multiple extraction solvents. An optimized LC-

MS method was generated for in-depth untargeted fingerprinting of chemical constituents in açaí extracts. Statistical analysis models were used to describe relationships between the açaí extracts based on molecular features found in both positive and negative mode electrospray ionization modes. To elucidate the differences in metabolites among açaí extracts from different cultivars, we identified or tentatively identified 173 metabolites from the various extracts. Of these compounds, there are 138 reported in açaí for the first time. Statistical models showed similar yet distinct differences between the extracts tested based on the polarity of compounds present and the origin of the source material. A high-resolution mass spectrometry method was generated that allowed us to greatly characterize 16 complex extracts made from different sources of açaí with different extraction solvent polarities.

Quantitation of bioactive constituents is a crucial preliminary step before utilizing extracts for biological assays so they may be normalized and administered according to a specific constituent concentration. Açaí has four main anthocyanin analytes: cyanidin 3-*O*-glucoside, cyanidin 3-*O*-sambubioside, cyanidin 3-*O*-rutinoside, and peonidin 3-*O*-rutinoside. This is the first comparison of açaí anthocyanin profiles between fresh fruits, processed powders, and botanical dietary supplement capsules. The materials examined shared a similar anthocyanin profile, with cyanidin 3-*O*-rutinoside being the most abundant, followed by cyanidin 3-*O*-glucoside. Among the botanical dietary supplement capsules, the two formulations varied greatly in anthocyanin concentration despite both being aqueous extracts. Previous LC-MS methods range from 35-120 min per injection, while we report a 10 min quantitative method for analysis of anthocyanins in various açaí materials that is fast, reproducible, and accurate. The method produced is useful to assure the quality, efficacy and safety of food and dietary supplement materials containing açaí.

We then tested our chemically standardized açaí BDS extracts for inhibition of hepatic CYP3A4. A parallel artificial membrane permeability assay (PAMPA) was utilized to filter intestinal passive diffusion of the four extract constituents so that compounds could be tested for inhibition of hepatic CYP3A4. Passively and non-passively diffused constituents of extracts from PAMPA assays were injected into the LC-MS and characterized for visualization and comparison of chemical entities. To elucidate the non-passively diffused compounds responsible for significant CYP3A4 inhibition, the Bioactivity – GNPS tool was used to hypothesize which compounds within the formulation extract were potentially active to accelerate their identification. We found no significant inhibition of CYP3A4 by passively diffused constituents for any extract. There was, however, significant inhibition by non-passively diffused constituents of both F1ME and F1AC extracts with 50% CYP3A4 inhibition at the donor compartment concentrations 5.764 and 15.58 ng/mL cyanidin 3-*O*-glucoside, respectively. Six compounds were predicted to be inhibitors of CYP3A4 from F1ME, including betaine and 5 unknown compounds. This indicates that BDS containing açaí may not inhibit CYP3A4 through passively diffused compounds. Compounds from açaí BDS that inhibit CYP3A4 may be absorbed through other mechanisms, such as transporters.

Acknowledgements

I would first like to thank my primary advisor, Dr. Angela Calderón, for all her guidance over the last five years, both personally and professionally. Thank you for pushing me to be the best scientist and person that I could be, and for your words of encouragement when I did not see that person in me. It has been your exceptional mentorship that I have to thank for my accomplishments during my time in Auburn. Thank you for taking a chance on the young woman who came to visit here in Auburn in May of 2019. She grew into the investigator that can write these words and it now prepared to take on the world – but she could not have done it without you.

Next, I would like to thank my committee members, Dr. Randall Clark, Dr. Jack DeRuiter, Dr. Douglas Goodwin, and Dr. Satyanarayana Pondugula for their support and advice they have given me during my graduate career. Thank you for all the letters of support and recommendation, as these were instrumental for me in my searches for extramural funding and now a research career.

I would like to state my appreciation for the Harrison College of Pharmacy and the Department of Drug Discovery and Development for the resources that have been provided to me as a graduate student. I would like to thank Jenny Johnston, Kaleia Williams, John Folmar, and Chris Smith for having the answers to any of my administrative needs or questions.

Thank you to the department for also granting my Graduate Teaching Assistantship, where I gained an additional mentor, Dr. April Staton, as my supervisor. Thank you for the care you have always shown me and the lessons I will take away with me about teaching and about life. Because of you, I remained confident that there was always at least one person looking out for me.

Thank you to my lab mates Kelli, Zarna, and Destini for teaching me how to be a team player and a better teacher. Thank you for your support, perspectives, and most of all your friendship. I will miss our weekly lunches before lab meeting.

Thank you to the National Center for Complementary and Integrative Health (NCCIH) and the Office of Dietary Supplements (ODS) from the National Institutes of Health (NIH) for providing R15AT011047 and F31AT012266 grants that allowed me to conduct research that I am passionate about while increasing the diversity of our research team through undergraduates and new graduate students. I am thankful for all the training I have received because of this funding.

A special thank you to members from Agilent Technologies for insight, training, and inspiration over the years. Jennifer Hitchcock, Timothy Bolduc, Kevin Quinn, Alexis Owens, and Karen Yannell have each been instrumental to different sections of this dissertation or to the development of my professional career.

Lastly, I would like to thank my family and friends – from home and those I have made while here in Auburn – for all the love and support during this time. Special recognition is reserved for Lauren Lucas and Charlotte Muse who I leaned on most during this time here at Auburn.

Table of Contents

Abstract ii

Acknowledgements v

List of Figures x

List of Tables xiv

List of Abbreviations xvi

Chapter 1: Introduction 1

1.1 BDS usage by cancer patients 1

1.2 Botanical-drug interactions 1

1.3 *Euterpe Oleracea* Mart (Açaí) 2

1.3.1 Risk for CYP3A4 interference 2

1.3.2. Risk for UGT inhibition 5

1.4 Importance of chemical characterization and standardization 7

1.4.1 Untargeted metabolomics and chemical fingerprinting of botanicals 7

1.4.1.1 Methods of chemometric analyses using liquid chromatography-mass spectrometry 8

1.4.1.2 Chemical characterization of açaí extracts 9

1.4.2 Quantitation of anthocyanins by LC-MS 12

1.4.3 Standardization of açaí extracts for *in vitro* assays 10

1.4.4 Tools for identification of bioactive compounds from complex mixtures 12

Chapter 2. Materials and Methods 15

2.1 Chemicals and reagents 15

2.2 Selection and authentication of açaí fruits, raw materials, and capsules 16

2.3 Preparation of açaí extracts 17

2.3.1 Extraction of açaí whole fruit 17

2.3.2 Extraction from plant powder 18
2.3.3 Extraction from capsules 18
2.4 Chemical fingerprinting 19
2.4.1 Method development 19
2.4.2 Data Analysis 20
2.4.2.1 Statistical Analysis 20
2.4.2.2 Qualitative analysis and metabolite identification 23
2.5 Anthocyanin quantitation 24
2.5.1 LC-ESI-MS method development 24
2.5.2 Preparation of calibration curves 24
2.5.3 Validation of method 25
2.6 Assessment of açaí BDS extracts for CYP3A4 inhibition 25
2.6.1 PAMPA assay 25
2.6.2 CYP3A4 inhibition assay 26
2.6.3 LC-MS permeability profiling of BDS extracts 28
2.6.4 Prediction of CYP3A4 inhibitors from F1ME 28
2.6.5 Structural elucidation of F1ME inhibitors 29
2.7 Assessment of açaí extracts for UGT inhibition 31
2.7.1 Generation of LC-MS method for UGT metabolite quantitation 31
Chapter 3. Results and Discussion 32
3.1 Chemical fingerprinting 32
3.1.1 Untargeted fingerprinting analysis of açaí extracts 32
3.1.2 Statistical analyses of açaí extracts 76
3.1.2.1 Principal component analysis 76
3.1.2.2 Correlation matrices 79

3.1.2.3 Hierarchical clustering analysis 83
3.2 Anthocyanin quantitation 87
3.2.1 Quantitation method development 87
3.2.1.1 Optimization of separation parameters 87
3.2.1.2 Calibration curve 91
3.2.1.3 Validation 93
3.2.2 Anthocyanins in various açaí materials 95
3.2.3 Anthocyanin stability testing 100
3.3 CYP3A4 103
3.3.1 Inhibition potential of BDS extracts on CYP3A4 103
3.3.2 LC-MS-based chemical characterization of BDS extracts 106
3.3.3 Structural elucidation of constituents with CYP3A4 inhibition activity 110
3.4 UGT inhibition studies 114
3.4.1 Method development for quantitation of glucuronide metabolites 114
4. Conclusions and Future Directions 120

List of Figures

Figure 1. Structures of anthocyanins, cyanidin 3-glucoside (**1**), cyanidin 3-sambubioside (**2**), cyanidin 3-rutinoside (**3**), and peonidin 3-rutinoside (**4**). 11

Figure 2. Workflow for bioactive compound identification using the automated GNPS-Bioactivity dashboard. 30

Figure 3. Mass versus retention time plot showing 2,510 features in positive electrospray (ESI^+) (A) and 1,492 features found in negative electrospray (ESI^-) (B) found amongst all açaí sample types. The y-axis provides the uncharged mass of the feature; the x-axis represents the elution times for each feature. The size and color of the point represent the frequency at which a feature was found amongst the 64 samples. 33

Figure 4. MS/MS spectra of compounds in açaí extracts that were assigned tentatively (L2 annotations) by extensive querying and comparison with spectral libraries. Red lines indicate fragment matches between experimental spectra and library spectra. MS/MS scores are indicated in [ ] and were obtained using either Agilent Qualitative Analysis, GNPS, or SIRIUS for their respective libraries. Numbers shown in the spectra match those corresponding in Table 4. 46

Figure 5. MS/MS spectra for compounds present in açaí extracts that were identified using authentic standards (L1 annotations). MS/MS score is indicated in [ ]. 72

Figure 6. PCA showing similarities between extract types based on features found in ESI^+. Each set of dots (technical quadruplicates) represents an açaí extract from 16 different accessions. 77

Figure 7. PCA showing similarities between extract types based on features found in ESI^-. Each set of dots (technical quadruplicates) represents an açaí extract from 16 different accessions. 78

Figure 8. Correlation matrix between the different açaí extracts based on positive mode PCA features. Each extract is an average of the four replicates. 81

Figure 9. Correlation matrix between the different açaí extracts based on negative mode PCA features. Each extract is an average of the four replicates. 82

Figure 10. Heatmap visualizing the average area under the curve for 100 compounds used in PCA for positive mode. (A) Heatmap with clustering with metabolite clustering on the x-axis (top) and sample clustering on the y-axis. (B) Close-up examination of sample dendrogram for positive features showing extract similarities. 85

Figure 11. Heatmap visualizing the average area under the curve for 100 compounds used in PCA for negative mode. (A) Heatmap with clustering with metabolite clustering on the x-axis (top) and sample clustering on the y-axis. (B) Close-up examination of sample dendrogram for positive features showing extract similarities. 86

Figure 12. Extracted ion chromatogram of anthocyanins **1** (**A**), **2** (**B**), **3** (**C**), and **4** (**D**) present in acMeOH extracts of açaí raw materials (MRAC), anthocyanin standards (**E**-**H**), and internal standard (IS) reserpine (**I**). 89

Figure 13. Illustration of anthocyanin contents in various açaí extracts. AC, acidic methanol extract; AQ, aqueous extract; EO, *Euterpe oleracea* Mart. fruits; ET, ethanol extract; F1,

BDS formulation 1; F2, BDS formulation 2; ME, methanol extract; MR, Mountain Rose powder (raw material)..... 97

Figure 14. Depiction of average anthocyanin stability in acMeOH for 30 days at -80°C. Data shows is percent analyte recovery calculated by dividing the anthocyanin concentration on day 30 by the anthocyanin concentration on day 0 and multiplying by 100. 101

Figure 15. Illustration of differences in average anthocyanin stability for various extract types stored in acMeOH for 30 days in -80°C. Data shows is percent analyte recovery calculated by dividing the anthocyanin concentration on day 30 by the anthocyanin concentration on day 0 and multiplying by 100. 102

Figure 16. Inhibition curves for the inhibition of CYP3A4 by non-passively diffused (from PAMPA donor compartment) and passively diffused (from PAMPA acceptor compartment) compounds in açaí BDS formulations. Activity expressed as the percentage of the remaining activity compared with DMSO control (F1AC and F2AC extracts required no DMSO). Data expressed as mean ± SD of three independent experiments. IC_{50} values were calculated based on concentrations of PAMPA donor compartment at time 0..... 105

Figure 17. Venn diagram of BDS extract compounds present in each of the four BDS extracts. Compounds unique to F1ME (23) which were further examined are highlighted in green. 108

Figure 18. Venn diagrams of BDS extract compound passive permeability. Entities from DMSO buffer control were excluded as part of Profinder analysis. 109

Figure 19. Structures of UGT metabolites used in development of LC-MS assay. Compounds are labeled according to Table 10. 117

Figure 20. Comparison of (**A**) traditional C18 and (**B**) phenyl-hexyl stationary phases for the separation of UGT metabolites (**1-6**) and IS (**7**). Metabolites are labeled according to Table 10..... 118

List of Tables

Table 1. Symptoms and serious outcomes associated with açaí single ingredient supplements AEs, CAERS 2004-2019 [20]. 4

Table 2. List of anticancer agents metabolized by glucuronidation which are also associated with cardiovascular AEs. 6

Table 3. Batch Recursive Feature Extraction method parameters used in Agilent MassHunter Profinder software. Reported parameters are those that have been changed from the default values for Batch Recursive Feature Extraction for small molecules/peptides. 22

Table 4. Parameters for identified or tentatively identified compounds detected in various açaí extracts using positive and negative electrospray ionization modes. Compounds confirmed using authentic chemical standards are shown in **bold**. Compounds which were tentatively identified but have not previously been reported for açaí to our knowledge are denoted with an (*). 34

Table 5. LC-ESI-MS data of anthocyanins present in MRAC extract and IS reserpine. 90

Table 6. Regression equation, correlation coefficient, lower limit of detection (LLOD), lower limit of quantitation (LLOQ), and linearity range for anthocyanins by high resolution LC-ESI-MS. 92

Table 7. Intraday (0 day) and interday (2 and 4 day) accuracy for anthocyanins **1**, **2**, **3**, and **4** in MRAC, EOAC, and F2AC extracts. 94

Table 8. Anthocyanin content in various extracts of açaí purée, raw material, and dietary supplement capsules..... 98

Table 9. Predicted bioactive compounds for CYP3A4 inhibition from F1ME extract..... 112

Table 10. LC-MS detection of glucuronide metabolites from in-vitro assay conditions..... 116

List of Abbreviations

acMeOH	acidic methanol (70% MeOH, 0.1% formic acid)
ACN	acetonitrile
AEs	adverse events
BDI	botanical-drug interaction
BDS	botanical dietary supplements
BMN	bioactive molecular network
CYP3A4	cytochrome P450 3A4
DMSO	dimethyl sulfoxide
EIC	extracted ion chromatogram
ESI^+	positive electrospray ionization
ESI^-	negative electrospray ionization
FA	formic acid
FAERS	Food and Drug Administration Adverse Event Reporting System
FBMN	feature based molecular networking
FDA	U.S. Food and Drug Administration

GNPS	Global Natural Product Social Molecular Networking
HCA	hierarchical clustering analysis
HLM	human liver microsomes
IS	internal standard
LC-MS	liquid chromatography-mass spectroscopy
LLOD	lower limit of detection
LLOQ	lower limit of quantification
MeOH	methanol
MFE	molecular feature extraction
MPP	Mass Profiler Professional
MS/MS	tandem mass spectrometry
NADPH	nicotinamide adenine dinucleotide phosphate
NCCIH	National Center for Complementary and Integrative Health
NIH	National Institutes of Health
PAMPA	parallel artificial membrane permeability assay
PCA	principal component analysis
QC	quality control

RSD	relative standard deviation
RT	retention time
SA	similarity analysis
UGT	UDP-glucuronosyltransferase

Chapter 1: Introduction

1.1 BDS usage by cancer patients

Cancer is the leading cause of death worldwide, with an estimated 19.3 million new cases in 2020 and almost 10 million cancer deaths [1]. Polypharmacy is more likely amongst cancer patients and can be as prevalent as 84% [2]. Cancer patients receiving a combination of drugs are more likely to experience drug-drug interactions as well as related adverse events (AEs) [3-6]. Botanical dietary supplements (BDS) are consumed more by cancer patients than otherwise healthier patients without cancer to alleviate side effects of chemotherapy drugs and/or increase quality of life [7-10]. Studies have shown that up to 80% of cancer patients have reported using BDS following their initial cancer diagnoses [11]. BDS have also been shown to be used by cancer patients in hopes of strengthening the immune system, helping them cope with stress, and increasing their chance of a cure [12]. Evidence supports that some BDS benefit cancer treatment when administered alone [13]. However, concomitant use of BDS with anticancer drugs can be precarious when it leads to life-threatening AEs.

1.2 Botanical-drug interactions

Most anticancer drugs contain one active pharmaceutical ingredient with a specific mechanism of action. BDS have numerous chemical constituents that can interact with various cell targets of both healthy and cancerous cells. The enzyme responsible for the metabolism of most anticancer drugs is cytochrome P450 isoform 3A4 (CYP3A4), an enzyme predominantly located in the liver. In previous studies, it has been found that many interactions between anticancer agents and BDS are due to the pharmacokinetic factors generated by the change in functionality or expression of CYP3A4 enzymes [14]. The botanical-drug interactions (BDIs) involving anticancer

agents that have been previously shown to decrease the effectiveness include those between cisplatin and black cohosh (Ranunculaceae *Actaea racemose* L.), fluorouracil and beta carotene, and paclitaxel and quercetin. An additional study has shown an interaction that causes increased anticancer agent toxicity when using methotrexate with kava-kava (Piperaceae *Piper methylsticum* G. Forst.) [15].

1.3 *Euterpe Oleracea* Mart (Açaí)

Euterpe oleracea Mart. (Arecaceae), commonly known as açaí, is a fruit that grows on the açaí palm tree native to the Amazon region. Açaí is harvested for various parts of the palm tree that provide a wide range of functions. Specifically, the açaí fruits are harvested for multiple industries including that of food and cosmetics. Açaí presents many health benefits, the most prominent being antioxidant and anti-inflammatory activities. Several compound classes are present in açaí that research has shown to be the source of these effects: compounds such as anthocyanins, polyphenolic compounds, and flavonoids are of most interest in studying the benefits of using açaí as a BDS [16].

1.3.1 Risk for CYP3A4 interference

In recent years, açaí has been introduced into the BDS market, and its popularity is steadily rising. Açaí is now among the top 40 botanicals used in the U.S., and cancer patients increasingly use açaí BDS to complement their conventional chemotherapeutic agents [17, 18]. This rise in popularity has also led to challenges regarding the quality, safety, and efficacy of açaí fruit products [19].

Upon examination of the U.S. Food and Drug Administration (FDA) Adverse Event Reporting System (FAERS) database, our research team found an increased probability for vascular AEs when patients used anticancer drugs and BDS containing açaí synchronously, but the mechanism of this interaction remains unknown [18]. Then, the FDA Center for Food Safety and Applied Nutrition Adverse Event Reporting System (CAERS) was used to find AEs specifying the use of açaí dietary supplements together with other products and drugs. Out of the AEs reported from January 2004 – December 2019, at least 127 involved BDS containing açaí of which 113 (89%) were suspect use and 14 (11%) were concomitant use (**Table 1**). In addition, 20% of all symptoms from suspected use AEs and 57% of symptoms of concomitant use AEs were symptoms of cardiovascular disorders. Of the 14 AEs in which açaí was used synchronously, these AEs required hospitalization for 50% of these occurrences. The symptoms chosen, including chest pain, high blood pressure and pulmonary thrombosis, have been previously connected with concomitant use of BDS and anticancer drugs [18].

Our group then examined the potential risk between CYP3A4-interactive cancer drugs and açaí and found that both passively and non-passively diffused compounds in methanol açaí fruit extract displayed significant inhibition of hepatic CYP3A4 – suggesting potential for interactions between açaí BDS and CYP3A4-interactive drugs.

Table 1. Symptoms and serious outcomes associated with açaí single ingredient supplements AEs, CAERS 2004-2019 [20].

Symptom(s)/Serious outcomes	Suspect AEs[b]	Concomitant AEs[c]
Any Symptoms	**113**	**14**
CV Symptom(s)	**23**	**8**
Heart rate abnormal	2	
Cardiac disorder		2
Chest pain	7	1
Heart rate irregular	1	1
Heart rate increased	4	
Blood pressure increased	1	1
Blood pressure fluctuation	1	1
Pulmonary thrombosis		1
CV Serious Outcomes	**23**	**8**
Death	1	1
Life-threatening condition	5	
Hospitalization	6	4
Disability	1	
Intervention to prevent permanent impairment	6	3
Less serious outcome	4	

[a] Symptom(s) related to cardiovascular disorders as specified by the reporter and coded by FDA according to the MedDRA.

[b] Suspect açaí products. Products indicated by the reporter to have "caused a reaction".

[c] Concomitant açaí products taken at the same time as the Suspect product.

1.3.2. Risk for UGT inhibition

UDP-glucuronosyltransferases (UGTs) are a phase II hepatic enzyme responsible for the glucuronidation of xenobiotics by electrophilic addition of glucuronic acid. About 55% of the majority of prescribed drugs are inactivated by UGTs, including over 70 anticancer drugs [21, 22]. UGT inhibition is a clinically significant form of drug-drug interactions that can lead to toxicity. An example of a clinically relevant drug interaction is known to occur with UGT1A1, where known inhibitors of UGT1A1 could put a patient taking irinotecan at significant risk for bone marrow suppression since irinotecan is largely dependent on this UGT for its metabolism (of metabolite SN-38) [23]. Many anticancer drugs metabolized by UGTs are also associated with cardiovascular AEs. A literature review was performed to examine the extent to which BDIs could be caused by the inhibition of UGTs by açaí constituents. First, a search was performed for FDA-approved anticancer drugs which have been shown to be metabolized by glucuronidation. Then, anticancer drugs which were shown to be metabolized by UGTs were investigated for reports of AEs related to cardiovascular disease when taken singularly (not in combination with other pharmaceuticals). **Table 2** shows the results of these searches and supports that many anticancer drugs metabolized by UGTs may have serious AEs related to cardiovascular symptoms if taken concomitantly with a UGT inhibitor. For example, inhibition of these UGTs by açaí constituents could produce cardiotoxicities due to decreased metabolism and increased blood plasma half-life of a drug which can cause cardiovascular AEs when taken alone.

Table 2. List of anticancer agents metabolized by glucuronidation which are also associated with cardiovascular AEs.

UGT	Anticancer drug
1A1	Axitinib [24, 25], Belinostat [26, 27], Binimetinib [28, 29], Encorafenib [28, 29], Etoposide [30, 31], Flavopiridol [32, 33], SN-38 (Irinotecan) [34, 35], Nintedanib [36, 37], Panobinostat [38, 39], Raloxifene [40, 41], Tamoxifen [42, 43], Trabectedin [38, 44]
1A3	Axitinib [24, 25], Lorlatinib [29, 38], Panobinostat [38, 39]
1A4	Abiraterone [45, 46], Acalabrutinib [47, 48], Anastrozole [49, 50], Axitinib [24, 25], Bendamustine [48, 51], Ibrutinib [22, 52], Imatinib [53, 54], Trabectedin [38, 44]
1A6	Methotrexate [55, 56]
1A9	Axitinib [24, 25], Flavopiridol [32, 33], Fostamatinib [57, 58], Glasdegib [29, 38], SN-38 (Irinotecan) [34, 35], Letrozole [49, 59], Panobinostat [38, 39], Raloxifene [40, 41], Regorafenib [25, 60], Sorafenib [53, 61], Vandetanib [38, 62]
2B7	Belinostat [26, 27], Cobimetinib [28, 63], Epirubicin [64, 65], Sorafenib [53, 61], Tamoxifen [42, 43], Tretinoin [38, 66]
UNK	Bleomycin [67, 68], Dasatinib [69], Daunorubicin [64], Doxorubicin [64], 5-Fluorouracil [70], Mitoxantrone [71], Niraparib [38], Pomalidomide [38, 72], Ruxolitinib [73, 74], Selinexor [75, 76], Sunitinib [53]
UNK, unknown which isoform responsible for glucuronidation of anticancer drug.	

1.4 Importance of chemical characterization and standardization

Unlike single active pharmaceutical ingredients, natural products are complex mixtures which may be known or unknown in their chemical composition and concentration. Extracts from botanical natural products should be chemically standardized to certain concentrations of bioactive or marker compounds which are unique to a species [77]. The quantitative description of these active compounds is essential for reporting the safety and efficacy of the botanicals [78]. When performed, standardization allows for the selection and adjustment of dosages of botanical natural products which is advantageous for researchers, healthcare professionals, and consumers alike [79]. Standardization is a process that allows for reproducibility and rigor, which is required by the National Institutes of Health's (NIH) National Center for Complementary and Integrative Health (NCCIH) as part of their Policy on Natural Product Integrity [80]. Many botanical natural products are sensitive to changes due to various environmental factors such as temperature, light, and other growing conditions which can drastically change the chemical makeup [81]. This variability makes quantitation even more crucial because bioactive compounds can change in concentration from batch to batch. Chemical characterization and quantitation of compounds in açaí fruit purée, raw material, and supplement capsules is a crucial preliminary step to complete before utilizing extracts for *in vitro* and *in vivo* assays to provide consistency across products.

1.4.1 Untargeted metabolomics and chemical fingerprinting of botanicals

For hundreds of years, the prevention and treatment of human ailments have largely relied on herbal remedies. Since the year 2020, herbal dietary supplement sales have been the highest they have ever been reported, reaching over $10 billion [17]. Plant extracts are often complex blends of hundreds of different chemicals with synergistic actions. The quality of botanical

products is influenced by several factors and depends on the number of chemical constituents occurring and their concentration. Metabolites with even low concentrations may be important for the quality, safety and efficacy of the herbal formulation [82]. The chemistry of plants is influenced by a wide range of elements, such as genetic diversity, plant ecotype, nutrition, geographic location, seasonal fluctuations, stress, as well as post-harvest drying and storage [83].

To address the variety and quality of plant metabolites, metabolomic fingerprinting of a botanical extract is crucial. Examination of product authenticity and the ability to spot adulteration may both be aided by obtaining the plant's unique chemical fingerprint [84]. A thorough examination of the chemical components of BDS is challenging and time-consuming due to the complexity of these materials [85]. A strong tool for separating the various components and creating a distinctive profile of the sample is provided by chromatography when used in conjunction with an appropriate detection technology to assess the overall pattern [82]. For the identification, quality assurance, and authenticity of botanical extracts, chromatographic fingerprints are being created.

1.4.1.1 Methods of chemometric analyses using liquid chromatography-mass spectrometry

The chromatographic results are subjected to chemometric analysis in order to get pertinent data from the plant profile about seasonal, regional, and taxonomic characteristics [84]. It may also be used for process improvement, quality assurance, and authentication [84]. Due to the vast amount of data that is produced using chromatographic fingerprinting, exploratory data analysis is important for identifying general patterns in the data by recognizing potential connections between samples and/or variables [82, 84]. The analyses used for this work include principal component analysis (PCA), hierarchical clustering analysis (HCA), and similarity analysis (SA) (will also be

referred to as correlation matrix). The most popular exploratory method for visualizing and reducing the original data's dimensionality while maintaining the greatest amount of data variability is PCA [84]. PCA is used to identify outliers and identify sample similarities and differences [86]. The goal of the clustering analysis is to identify patterns or clusters in the data based on commonalities, such as proximity, correlation, or a mix of both [87]. The method that is most frequently employed to examine similarities among chemical fingerprints for botanicals is HCA [84]. It organizes the data into a hierarchical structure that reveals underlying patterns and relationships within the data. HCA groups similar data points based on their features into clusters, displaying as a dendrogram, a tree-like structure. SA is a suitable approach for assessing the similarity or difference between individual fingerprints [88]. It quantifies the proximity or closeness between objects within a dataset, offering a numerical value that quantifies the degree of similarity or dissimilarity between two objects. These statistical analyses will help us to describe well our botanical extracts for this study.

1.4.1.2 Chemical characterization of açaí extracts

In the past, many compound classes have been reported in açaí. Açaí fruits have previously been unattainable outside of Brazil, therefore this is the first report of having fresh, whole fruits in the U.S. for chemical and biological studies [89]. Açaí pulp's lipid composition accounts for half of its chemical makeup, which is partly why it is categorized as an energy-dense food. Even though this is the case, few fatty acids have been identified in açaí fruit pulp extracts. Açaí fruits, seeds, and leaves have been somewhat chemically characterized in the past and have been found to contain predominantly flavonoids, non-flavonoid phenolic compounds, lignoids, and fatty acids [85, 90-103]. Other compound classes that have been found in açaí include terpenes, tannins,

lignans, stilbenes, quinones, and norisoprenoids [16]. Amino acids and carbohydrates as well as vitamins and minerals have also been found in açaí fruits as part of their nutrient profile [90, 104].

1.4.2 Standardization of açaí extracts for *in vitro* assays

Anthocyanins are flavonoid glycosides with a 4-hydroxyflavilium ion. These have been identified as the components that determine the vibrant purple, red, and orange hues of many fruits and vegetables, as well as the antioxidant properties of açaí [90]. Açaí has four characteristic anthocyanin analytes: cyanidin 3-glucoside (**1**), cyanidin 3-sambubioside (**2**), cyanidin 3-rutinoside (**3**), and peonidin 3-rutinoside (**4**) (**Figure 1**) [19, 85, 96, 98]. While some botanical natural products containing açaí are standardized to total polyphenol or total anthocyanin content, we are standardizing to a specific amount of cyanidin 3-glucoside because it has been previously quantified in human plasma after açaí pulp or purée consumption (1.138 – 2.321 ng/mL) [105]. Thus, the complete identification and quantification of the anthocyanin compounds present in commercially available plant raw materials, conventional preparations, and BDS is a requirement for *in vitro* studies to meet these concentrations.

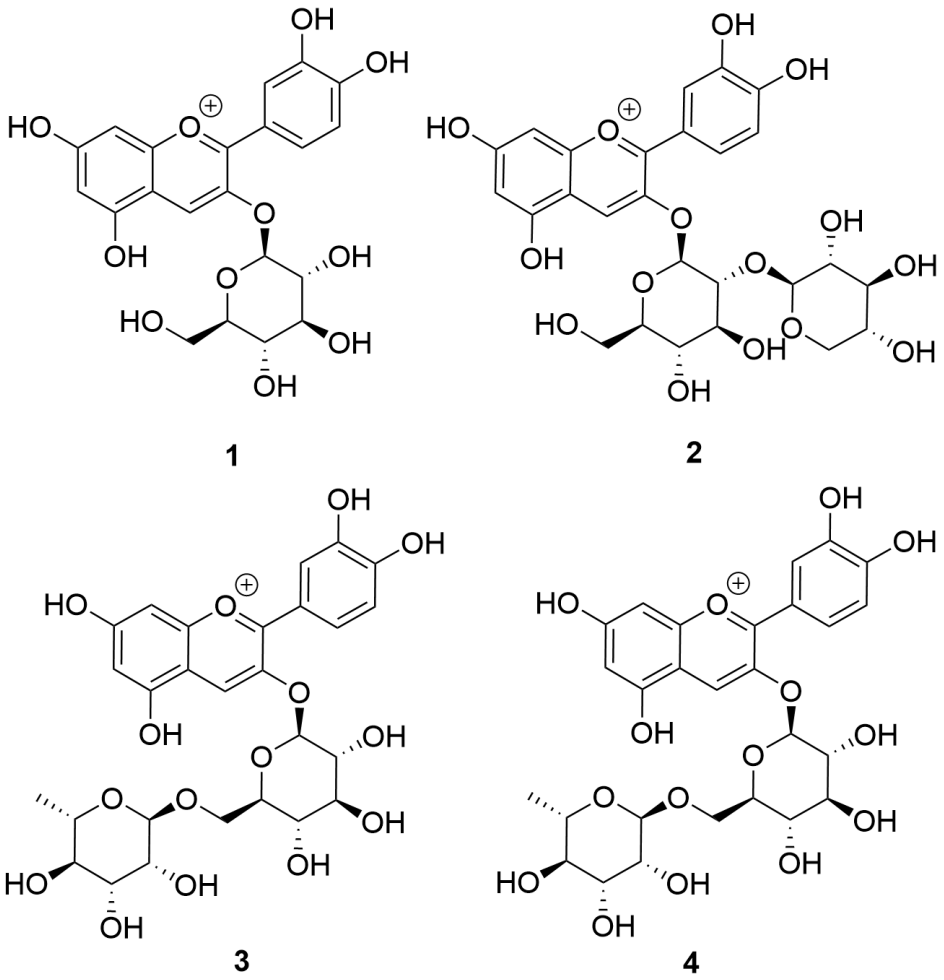

Figure 1. Structures of anthocyanins, cyanidin 3-glucoside (**1**), cyanidin 3-sambubioside (**2**), cyanidin 3-rutinoside (**3**), and peonidin 3-rutinoside (**4**).

1.4.3 Quantitation of anthocyanins by LC-MS

In past literature, there has been a variety of columns and methods used to identify these anthocyanins with liquid chromatography-mass spectrometry (LC-MS) using electrospray ionization (ESI) [85, 95, 96, 98, 106, 107]. However, previous methods using ESI-MS as the detector range from 35-120 minutes per injection. These methods with long run times make the quantitation of a large number of samples very difficult and time consuming. In this study, we report a 10-minute quantitative method for anthocyanins in various açaí materials that is fast while remaining reproducible, sensitive, and accurate. As part of a project to study the potential for BDIs, our goal was to enhance our previously published method for quantifying major anthocyanins in açaí. This method was then employed to describe the anthocyanin variability between açaí fruits, powders, and BDS capsules, ultimately, to identify if fresh fruits from Hawaii would exhibit similar anthocyanin profiles to commercial products containing fruits originating from Brazil.

1.4.4 Tools for identification of bioactive compounds from complex mixtures

It is not enough to know that a plant extract inhibits a drug-metabolizing enzyme, but further research should be done to elucidate which compounds from a complex mixture are responsible for the inhibition. The current method for the discovery of bioactive natural products is bioassay-guided fractionation. This process requires numerous and laborious tasks such as extraction of metabolites using solvents, chromatographic fractionation of the extract, screening of each fraction for bioactivity, isolation and identification of bioactive compounds, and verification of the isolated compound bioactivity [108]. Bioassay-guided fractionation often results in fractions that have lost their bioactivity due to compound degradation during purification or failure in isolation of the bioactive compound due to the low concentration of the analytes [109].

Computational approaches have played an increasingly prominent role in natural product-based drug discovery. One tool that natural product researchers use to generate molecular networks is the Global Natural Product Social Molecular Networking (GNPS) coupled with bioactivity to predict bioactive compounds [109]. Bioactive molecular networks (BMN) visualize and predict potential known and unknown chemical compounds with high bioactivity within chemical families based on having similar tandem mass spectrometry (MS/MS) fragmentation patterns [110]. Using feature-based molecular networking (FBMN) is more accurate and concise than traditional Classical Molecular Networking due to its ability to differentiate isomers with similar MS/MS spectra and integrate relative quantitative information [111, 112]. FBMN can also be combined with a bioactivity score that allows for the generation of a hypothesis for which compounds are bioactive. A bioactivity score can be any measure of therapeutic effect such as an IC_{50}, minimum inhibitory concentration, or measure of targeted metabolite/genetic material concentration field [109]. Our group has recently accomplished the automation of combining GNPS with bioactivity by designing an integrated dashboard that includes the necessary tools for creating a bioactive molecular network including MZmine2, GNPS, and Cytoscape [113]. MZmine2 is used for pre-processing the data for FBMN and includes filters for noise, duplicate peaks, and isomers. This pre-processing software is preferred over others because it is the most universally used across multiple fields of research [114]. Cytoscape is an open-source platform used for network visualization that can clearly show which compounds are known and/or bioactive [109, 115]. Even if an extract is not bioactive, all extracts will be used for this objective so that the tool can filter out compounds from the non-bioactive extracts to help determine unique compounds from extracts that are bioactive. These networks enable efficient compound discovery by guiding targeted isolation and accurate hypothesis generation of novel bioactive constituents.

In order to elucidate which compounds in açaí BDS may cause interactions with CYP3A4, our group will be using our previously published automated workflow for the bioactive compound identification [113]. The bioactive networking workflow is a multi-step process requiring many different bioinformatics tools. The automation tool streamlines each step of this workflow to make it much faster and more user-friendly with a straightforward user interface. Some successful uses of this workflow include bioactive compound identification from guava (Myrtaceae *Psidium guajava* L.), isolation of neuroprotective natural products in Chinese sweet plum (Rhamnaceae *Sageretia theezans* (L.) Brongn) extracts, identification of bacterial metabolites from the actinomycete genus *Planomonospora* (Streptosporangiaceae), discovery of monoterpene indole alkaloids found in Asegai tree (Apocynacaea *Alstonia balansae* Guillaumin), and in the comparison of the diterpene ester profiles of grey hedgehog (Euphorbiaceae *Euphorbia pithyusa* L.), and *Euphorbia cupanii* Guss. (Euphorbiaceae) [116-120]. This workflow is useful in a wide range of different areas for identifying and discovering compounds and metabolites, and this will be the first time it will be used to predict chemical constituents responsible for BDIs. This study aims to assess potential for BDIs involving CYP3A4 inhibition by açaí *in vitro* and subsequently identify the compounds responsible for inhibition using the newly automated Bioactivity – GNPS tool.

Chapter 2. Materials and Methods

2.1 Chemicals and reagents

All solvents used were LC-MS grade and purchased from Fisher Scientific (Fair Lawn, NJ, USA). Coumarin, cyanidin 3-*O*-glucoside chloride, dimethyl sulfoxide (DMSO), EDTA, isovanillic acid, isovitexin, KH_2PO_4, kaempferol, $MgCl_2$, Na_2HPO_4, NADPH, naringenin, oleamide, oleic acid, palmitic acid, quercetin 3-glucoside, Trizma® hydrochloride (Tris HCl), UDPGA and LC-MS grade formic acid (FA) were purchased from Sigma-Aldrich (St. Louis, MO, USA). Cyanidin 3-*O*-rutinoside chloride (98%) was purchased from INDOFINE Chemical Company, Inc. (Hillsborough, NJ, USA). Cyanidin 3-*O*-sambubioside chloride, peonidin 3-*O*-glucoside chloride, and peonidin 3-*O*-rutinoside chloride were purchased from EXTRASYNTHESE (Genay, France). Chrysoeriol, gallic acid, orientin, taxifolin, and vitexin were purchased from Chromadex (Los Angeles, CA, USA). Additional analytical standards purchased include catechin from Ambeed (Arlington Heights, IL, USA), dihydrokaempfrol from Carbosynth (San Diego, CA, USA) and quercetin and acacetin from TargetMol (Boston, MA, USA). Internal standard (IS) reserpine (>99%) was purchased from Agilent Technologies (Little Falls, DE, USA). Alamethicin, chenodeoxycholic acid 24-acyl-β-D-glucuronide, beta-Estradiol 3-(β-D-glucuronide) sodium salt, propofol β-D-glucuronide, serotonin β-D-glucuronide, and trifluoperazine N-glucuronide were purchased from Cayman Chemical Company (Ann Arbor, MI, USA). Naloxone 3-β-D-glucuronide was purchased from Toronto Research Chemicals (North York, ON, CA). IS chlorpropamide was purchased from 1PlusChem (San Diego, CA, USA). IS $^{13}C_3$-1′-hydroxymidazolam was bought from Corning (Woburn, MA, USA). Genotyped HLM (Product no. 456202) and Corning BioCoat Pre-coated PAMPA Plates (Cat. No. 353015) were

sourced from Corning® Life Sciences (Tewksbury, MA, USA). Gentest® Insect Cell Control Supersomes™ (Product no. 456200) were sourced from Discovery Life Sciences (Huntsville, AL, USA). All the chemical standards listed above were purchased at LC-MS grade purity or at least 97% by LC-MS.

2.2 Selection and authentication of açaí fruits, raw materials, and capsules

Certified organic açaí berry powder (MR) (Catalog no. AÇAÍ4, Lot #26579) was supplied by Mountain Rose Herbs (Eugene, OR, USA) in the quantity of 10 kilograms. This powder was chosen due to its representative nature of what most individuals are consuming when eating açaí food products such as smoothies. The fruit pulp was freeze dried with 0.4% lime juice added for acidification and stability. Verification of sample was performed by Alkemist Labs (Costa Mesa, CA, USA) by high performance thin-layer chromatography through comparison to reference samples. The MR powder was stored at 4ºC in light resistant bags until time of extract preparation.

Euterpe oleracea Mart. fruits were collected by Jeff Marcus on April 15, 2021, at Floribunda Palms and Exotics (Mt. View, HI). The fruits were taxonomically authenticated by Andrew Henderson from the New York Botanical Garden and the voucher specimen #04272225 has been deposited at the New York Botanical Garden. Upon arrival to the lab, açaí fruits were rinsed with deionized water to remove debris and potential contaminant growth before being stored at -80ºC. In alignment with the preparation of açaí for traditional use in Brazil, *Euterpe oleracea* Mart. fruit purée (EO) was made in the lab by warming the fruits in deionized water at 40ºC for one hour. After warming, pre-soaked berries were de-seeded, and the outer shell layer was puréed with the warm soaking water using a blender. This aqueous extract was lyophilized until powder dry to make açaí fruit powder. From 750 g of dry fruits, 71.11 g of fruit powder was obtained.

Two U.S. manufacturers of dietary supplement capsules containing aqueous extracts of açaí two separate lots from each in 2019 and 2022 have been supplied or purchased from Nature's Way (NW) (Green Bay, WI, USA, 2019 batch #20099227 and 2022 batch #20137327) and Natrol (Chatsworth, CA, USA, 2019 lot #2070593 and 2022 lot#2086344). The BDS capsules will be referred to as F1 (NW 2019), F2 (Natrol 2019), F3 (NW 2022), and F4 (Natrol 2022). These two supplement brands were chosen based on Amazon market reports (2019) in addition to the commercial availability for consumers both online and in retail pharmacies. F1 capsules contain 1,040 mg of açaí extract per serving, which has been standardized to 10% polyphenols or 104 mg. F3 capsules also contain 1,040 mg of açaí extract per serving; however, this batch has been standardized to 2% polyphenols or 20.8 mg. Both the F2 and F4 capsules contain 1000 mg of açaí extract per serving, which was extracted with water in a 4:1 ratio of açaí berry to water. Both supplements include other ingredients, silica, and magnesium stearate, and F1 additionally includes maltodextrin. Product integrity dossiers are kept at the Calderón Laboratory for all herbal extracts, plant materials, and botanical dietary supplement capsules.

2.3 Preparation of açaí extracts

2.3.1 Extraction of açaí whole fruit

Açaí purée (EO) was weighed out and extracted by acidic methanol (acMeOH, MeOH:H_2O 70:30, 0.1% HCl v/v), 95% ethanol, methanol (MeOH), and water individually. These extracts will be referred to as EOAC, EOET, EOME, and EOAQ, respectively. Powders were added to Erlenmeyer flasks and solvent was added until the powder/solvent ratio was 40 g/L. Materials were extracted for 24 hours with gentle shaking at 75 rpm at 25°C. Organic extractions were performed twice, while aqueous extraction was performed only once to avoid the risk of microbial

contamination. The extracts were filtered with Whatman filter paper no. 1 and all extracts were rotary evaporated and nitrogen dried before lyophilization except for aqueous extracts which were lyophilized only. Açaí purée yielded 12.03%, 17.20%, 17.46%, and 18.76% for EOAQ, EOAC, EOME, and EOET extracts, respectively. All dried extracts were stored at -20°C until use.

2.3.2 Extraction from plant powder

Açaí raw materials (MR) were weighed out and extracted in same manner as described in *2.3.1 Extraction of açaí whole fruit.* MR was weighed out and extracted by acMeOH, 95% ethanol, MeOH, and water individually. These extracts will be referred to as MRAC, MRET, MRME, and MRAQ, respectively. Açaí raw material had yields of 12.03%, 17.02%, 17.46%, and 18.76% for MRAQ, MRAC, MRME, and MRET extracts, respectively. All dried extracts were stored at -20°C until use.

2.3.3 Extraction from capsules

For MeOH extracts of F1 and F2 (commonly F1ME and F2ME), the powder obtained from 5 capsules of each formulation were extracted with 50 mL of MeOH three times. The MeOH extracts were combined and centrifuged at 4000 rpm and 4°C for 20 minutes. The produced supernatant was filtered through 0.45 µm PTFE syringe filters, dried under 218 mbar at 40 °C, and further dried by nitrogen evaporation and lyophilization. The yields were 22.2% (w/w) for F1ME and 11.0% (w/w) for F2ME. For acMeOH extracts, the powder from 5 capsules from each formulation was extracted twice with 25 mL of acMeOH to generate our F1AC and F2AC extracts. The procedures that followed match that of the MeOH extracts. The yields of acMeOH extracts were 19.3% (w/w) for F1AC and 18.6% (w/w) for F2AC. All dried extracts were stored at -20°C until use.

For extracts of F3 and F4, powder obtained from 120 capsules each were weighed out and extracted in same manner as described in *2.3.1 Extraction of açaí whole fruit.* Açaí BDS extracts were extracted with either acMeOH (F3AC and F4AC) or MeOH (F3ME or F4ME). The extractions had yields of 18.51%, 37.05%, 43.21%, and 11.21% for F3AC, F3ME, F4AC, and F4ME extracts, respectively. All dried extracts were stored at -20°C until use.

2.4 Chemical fingerprinting

2.4.1 Method development

For each extract, four biological replicates were made for each açaí extract for a total of 64 samples. Dried extracts were reconstituted at 1 mg/mL in acMeOH and sonicated for 10 minutes prior to centrifugation for 10 minutes at 8000 rpm and 4°C. Supernatants were then syringe filtered with 0.22 µm PTFE filters to remove and insoluble particulates. A pooled sample was generated to use for quality control (QC) that was made by mixing equal parts of all 64 samples. The chemical fingerprinting method was generated by running this QC sample with a variety of mobile phases, gradient elutions, and columns. When the optimal conditions were found, the method was tested for interday and intraday reproducibility by running the same sample for multiple injections both in the same day and on multiple different days.

For the chemometrics analysis, samples were injected randomly across the worklist. The QC sample was injected every 5 injections to allow for retention time (RT) alignment and for internal mass calibration using a reference mass solution. Extract samples were analyzed using a 2.1 x 100 mm, 2.7 µm Poroshell 120 EC-C18 (Agilent Technologies, New Castle, DE). The flow rate was set at 0.35 mL/min, the sample injection volume was 10 µL, the acquisition rate was set at 1.41 scans, and complete mass scanning ranged from *m/z* 100–1000. MS conditions were

optimized with capillary voltage 3200 V and 3400 V for positive mode ESI (ESI^+) and negative mode ESI (ESI^-), respectively; drying gas temperature 350°C, fragmentor voltage 175 V, and skimmer 65 V. Nitrogen was supplied as a nebulizing gas at 25 psi and as a drying gas at 10 L/min. LC separation for açaí extract samples was conducted with a gradient mobile phase consisting of (A) water, 0.1% FA and (B) MeOH, 0.1% FA. The linear gradient was: 0 min, 15% B; 6 min, 65% B; 15 min, 80% B; 25-40 min, 95% B, 45 min, 15% B with a 5-minute post-time for re-equilibration. The column temperature was set to 25°C. Both ESI^+ and ESI^- were utilized. The same method was utilized for MS/MS acquisition, with the addition of collision energies of 10, 20, and 40 eV to gain fragmentation information.

2.4.2 Data Analysis

2.4.2.1 Statistical Analysis

MassHunter Profinder (Agilent Technologies, Little Falls, DE) software was used for data pre-processing prior to statistical analyses. Batch recursive feature extraction for small molecules/peptides was used to align compound features in the 64 extract samples plus a matrix blank. The peak height threshold was set to a signal-to-noise ratio (S/N) of 10.0 for both positive and negative features. For each polarity dataset, manually established parameters including ion species, mass filters, RT, mass tolerances, scoring, and grouping are listed in **Table 3**. Compounds found in the matrix blank were excluded. The compound groups and abundances in height were exported in CSV format prior to statistical analysis in RStudio.

In the abundance data, we observed numerous zero abundances under specific RT and mass spectra conditions. To remove redundant features, we implemented a preprocessing step focusing on RT and mass spectra with significant non-zero abundances. Specifically, we conducted feature

selection by detecting peaks in abundance. Initially, we identified 100 peaks for each sample, counted the occurrence of each feature recognized as a peak, and sorted them. Subsequently, we retained the first 100 features that were most frequently identified as peaks across 64 samples. For each selected feature, we recorded the corresponding abundance value. The processed dataset, which includes abundances associated with the identified mass spectra and RT, was then subjected to further statistical analysis.

PCA is a commonly employed technique for significantly reducing the dimensionality of the dataset while retaining maximal information, particularly in the case of complex datasets [84]. Consequently, we applied PCA to the reconstructed dataset. After applying PCA, the reconstructed data matrices were reorganized and compressed into a set of principal components (PCs). Each PC was derived via a linear combination of variables from the original dataset, with the loading coefficients of PCs indicating the importance of each original variable. To visualize the relationships among the 16 classes, we utilized biplots for the PCs, creating two-dimensional scatter plots. Additionally, considering the proportion of variance explained by each PC, we selected the first eight PCs as new variables for the subsequent analysis.

HCA is used to explore similarity relationships between objects [84]. The result can be visualized using heat maps and dendrograms. In this study, we utilize the Euclidean distance metric to measure the similarity among 64 samples and 100 selected features from the reconstructed dataset respectively. A complete agglomeration method is employed for clustering. Specifically, at the beginning of the process, each sample/feature is treated as a cluster of its own. Then, these clusters are sequentially combined into larger clusters based on distance until all elements ultimately belong to a single cluster.

Table 3. Batch Recursive Feature Extraction method parameters used in Agilent MassHunter Profinder software. Reported parameters are those that have been changed from the default values for Batch Recursive Feature Extraction for small molecules/peptides.

Parameter Name	**ESI^+ Ions**	**ESI^- Ions**
MFE[a] – Extraction Parameters		
Peak Filters: Signal-to-Noise	10.0	10.0
Allowed Ion Species	+H, +Na, +K	-H, +Cl, +HCOO
Allowed Neutral Losses	-[H_2O], -[CH_3]	-[H_2O], -[CH_3]
Isotope Model	Common organic (no halogens)	Common organic (no halogens)
Charge State	1-2	1-2
Compound Binning and Alignment		
RT tolerance	± (0.00% + 0.15 min)	± (0.00% + 0.15 min)
Mass tolerance	± (20.00 ppm + 2.00 mDa)	± (20.00 ppm + 2.00 mDa)
MFE – Post-Processing Filters		
Absolute height	5000 counts	2500
Score (MFE)	70.00	70.00
Minimum Filter Matches	2 file(s) in at least one sample group	2 file(s) in at least one sample group
Limit to largest	N/A	4000 compound groups
Find by Ion – Match Tolerances and Scoring		
Masses	± 20.00 ppm	± 20.00 ppm
Retention times	± 0.150 minutes	± 0.150 minutes
Low Score Matches: Warn if score	< 75.00	< 75.00
Low Score Matches: Do not match if score is	N/A	< 70.00
Find by Ion – EIC[b] Peak Integration and Filtering		
Filter on	Peak height	Peak height
Absolute Height	≥ 3000 counts	≥ 1,500 counts
Find by Ion – Post-Processing Filters		
Absolute height	N/A	2500 counts
Score (Target)	≥ 50.00	≥ 50.00
Minimum Filter Matches	2 file(s) in at least one sample group	2 file(s) in at least one sample group

[a]Molecular Feature Extraction

[b]Extracted Ion Chromatogram

2.4.2.2 Qualitative analysis and metabolite identification

Annotation confidence was obtained according to criteria for chemical analysis previously reported by Alcazar Magana et al. [121]. For Level 1 (L1) annotations, accurate mass, fragment ion pattern similarity, and RT were employed based on authentic commercially available standards. For tentative identifications (Level 2 or L2), exact mass, isotopic pattern and spacing, and MS/MS fragmentation data were used with the following thresholds to be met: (1) accurate mass was to be detected with deviation less than 5 ppm, (2) isotopic pattern and spacing is above 90%, and (3) MS/MS fragmentation similarity is above 70% when compared to library spectra. It is vital to note that these compounds are only putative annotations and will need to be further validated in subsequent studies if they are believed to have biological activity.

Data analysis including molecular feature extraction, molecular formula and fragment formula generation, and database searching was performed using MassHunter Qualitative Analysis software ver. B.10.00 and ChemVista library manager including METLIN™ and Agilent LCQTOF Applied Markets Personal Compound Database and Library (PCDL). Compound fragmentation data was also uploaded to SIRIUS+CSI:FingerID version 5.8.2 for MS/MS library searching using obtained spectra in the following libraries: Biocyc, CheBI, COCONUT, HMDB, HSDB, KEGG, KNApSAck, MaConDa, MeSH, NORMAN, Natural Products, Plantcyc, PubChem, YMDB, and Zinc Bio [122, 123]. Additional compounds were found as matches through Classical Molecular Networking in GNPS.

2.5 Anthocyanin quantitation

2.5.1 LC-ESI-MS method development

Agilent 6520 Q-TOF mass spectrometer with a 1220 rapid resolution liquid chromatography system was used for quantitation of anthocyanins on an Agilent 2.1 x 100 mm, 2.7 µm Poroshell 120 SB-C18 column (Little Falls, DE, USA). The flow rate was set at 0.35 mL/min, and the sample injection volume at 10 µL while the acquisition rate was 1.41 scan/s with the complete mass scanning range from m/z 100–1000. The MS conditions were optimized with ESI^+-MS analysis performed at a capillary voltage 3400 V; drying gas temperature 350 °C; fragmentor voltage 175 V and skimmer 65 V. Nitrogen was supplied as a nebulizing gas at 25 psig and as a drying gas at 10 L/min. MS/MS experiments were conducted with a collision energy of 15 and 30 eV. LC conditions consisted of a gradient mobile phase with (A) water containing 0.1% FA and (B) MeOH:acetonitrile (ACN) (50:50) containing 0.1% FA. The gradient was optimized to 0-1 min, 5% B; 1-5 min, 5-99% B; 5-6 min, 99-5% B; 6-10 min, 5% B. The column temperature was 25°C. All standards and standard solutions were injected in triplicate. Reserpine was used as an IS at 50 ng/mL. Qualitative and quantitative LC-MS data were analyzed using MassHunter Qualitative Analysis software ver. B.10.00 and MassHunter Quantitative Analysis software ver. B.08.00 (Wilmington, DE, USA).

2.5.2 Preparation of calibration curves

Individual stock solutions of cyanidin 3-glucoside (**1**), cyanidin 3-sambubioside (**2**), cyanidin 3-rutinoside (**3**), and peonidin 3-rutinoside (**4**) were prepared in MeOH at 10 mM concentration. Serial dilutions of standard stock solutions were prepared in MeOH and water (70:30, 0.1% FA) to afford concentrations ranging from 0.0011-2.24, 0.0014-2.90, 0.0014-2.97,

and 0.0014-3.04 ug/mL, for **1**, **2**, **3** and **4** respectively. All samples were spiked with a fixed amount of reserpine (50 ng/mL) as the IS. The powdered samples were stored at -20°C until use. The liquid samples used for interday and stability studies were stored at -80°C between analyses.

2.5.3 Validation of method

The modified LC-ESI-MS method was validated for linearity, accuracy, and precision. The linearity of the method was evaluated by triplicate analysis of standard solutions from 0.002 µM to 5 µM (concentrations of each analyte described in *Preparation of calibration curves*). A calibration curve, lower limit of detection (LLOD) and lower limit of quantitation (LLOQ) for each standard were generated through injecting series of serial dilutions of known concentrations and use of MassHunter Quantitative Analysis software. Accuracy of the method was assessed through recovery experiments in which samples were spiked with 0.1 µM of anthocyanin standards and analyzed five days apart to assess intraday (0 day) and interday (2 and 4 day) accuracy and reproducibility. The percent accuracy of the method was calculated by dividing the mean measured concentration by the nominal concentration and multiplying by 100%. Dilutions of samples were performed for extracts whose analytes exceeded the linearity range.

2.6 Assessment of açaí BDS extracts for CYP3A4 inhibition

2.6.1 PAMPA assay

The physiologically relevant concentration range to test açaí extracts for CYP3A4 inhibition has been determined based on a human pharmacokinetic study where a single oral dose of açaí pulp produced a maximum plasma concentration (C_{max}) of cyanidin 3-*O*-glucoside (CG) of 2.321 ng/mL [105]. Therefore, our extracts were made in concentrations of 1.59 – 1000 ng/mL of

CG in the donor side of the parallel artificial membrane permeability assay (PAMPA). These concentrations contain the 2.321 ng/mL plasma concentrations for pulp while accounting for typical intestinal concentrations prior to absorption mechanisms, overexposures, and variability among commercialized extracts.

The PAMPA plate was warmed to room temperature for at least 30 minutes prior to use. The donor compartment of the 96-well microplate system simulated intestinal content pre-absorption, while the acceptor compartment simulated passively absorbed compounds. A serial dilution of açaí extract solution (25 µg/µL to 0.195 µg/µL) was prepared in PAMPA buffer (0.014 M KH_2PO_4 and 0.054 M Na_2HPO_4, pH 7.4) with an optimized DMSO concentration of 0.417%. Açaí extract solution (300 µL/well) was added in the receiver plate (donor), and PAMPA buffer (200 µL/wells) was added to wells in the pre-coated filter plate (acceptor). The filter plate was then coupled with the receiver plate and the plate assembly was incubated at room temperature and/or 37°C for 5 hours without shaking or with shaking at 75 rpm. For shaking, two different shakers were used (Shaker 1: Thermo Scientific MaxQ™ 5000 Floor-Model; Shaker 2: Beckman Coulter Biomek 4000 Automated Liquid Handler using Inheco Single Temperature Control). At the end of the incubation, the plates were separated and the contents in the donor compartment plate were stored directly, whereas contents from the acceptor compartment were transferred to a new 96-well clear microplate for storage and subsequent studies.

2.6.2 CYP3A4 inhibition assay

CYP3A4 enzymatic reaction matrices contained permeable (acceptor side) and non-permeable diffused (donor side) compounds of açaí extracts from PAMPA plates and 0.2 mg/mL single donor human liver microsome (HLM) CYP3A5*3*3 (nonexpresser used to assess only

CYP3A4 activity) from various manufacturers in inhibition buffer (5 mM $MgCl_2$ and 1 mM EDTA in 100 mM potassium phosphate buffer, pH 7.4). Ketoconazole (10 µM) was used as a positive control in place of açaí extract, while DMSO control from PAMPA plates was used as a negative control to delineate the CYP3A4 inhibition effect of açaí extracts from DMSO. Midazolam (gold standard probe for CYP3A4/5 activity) stock solution prepared in MeOH:buffer (30:70 v/v) was added at its K_m concentration (3 µM) [124]. The reaction mixtures were preincubated at 37°C for 10 min. with shaking (75 rpm), after which the reactions were initiated by the addition of 1 mM NADPH and incubated at 37°C with shaking (75 rpm for 15 min.). Reactions were stopped by the addition of 20 µL water/ACN/FA (92:5:3, *v/v/v*) with stable isotope labeled IS ($13C^3$ 1'-Hydroxymidazolam, 1.0 µM) to minimize the error generated from dilution bias. Subsequently, reaction mixtures were vortexed for 1 min. and centrifuged at 8,000 x g at 4°C for 15 min. The filtrates were 10-fold diluted with water containing 0.1% FA and subjected to LC-MS analysis to quantitate the production of metabolite 1'-hydroxymidazolam.

Briefly, Agilent 6520 Q-TOF mass spectrometer with a 1220 rapid-resolution liquid chromatography system was used for the quantitation of 1'-hydroxymidazolam. Nitrogen was used as a nebulizing gas at 25 psi and as a drying gas at 10L/min. LC conditions consisted of a gradient mobile phase with (A) water containing 0.1% FA and (B) MeOH containing 0.1% FA. Detection was performed in ESI^+. The ratio of the peak areas of IS and metabolites produced by LC-MS and other calculations were performed using Microsoft® Excel. Log dose-response curves and half maximal inhibitory concentration (IC_{50}) values were calculated using GraphPad Prism 5.02 software (GraphPad Software).

2.6.3 LC-MS permeability profiling of BDS extracts

The permeability of açaí compounds was analyzed as previously reported with the following exemptions [125]. At the end of the 5-hour incubation period, wells of the same concentration from either the acceptor or donor plates had their contents removed and pooled. Pooled samples each had MeOH and FA added until the concentration reached the concentration of the previously described acMeOH solution. A portion of the supernatant was removed and injected into the LC-MS with the same method as below in 2.6.4 except for an additional time segment where the flow from 0-2 min was diverted to waste to avoid buffer salts entering the MS source. LC-MS analysis was performed with triplicate injection in both ESI^+ and ESI^-.

2.6.4 Prediction of CYP3A4 inhibitors from F1ME

Each BDS extract was dissolved at a standardized concentration of 1000 ng/mL of CG in an acMeOH solution and analyzed in triplicate on a 2.1 x 100 mm, 2.7 µm Poroshell 120 EC-C18 (Agilent Technologies, New Castle, DE). The flow rate was set at 0.35 mL/min, the sample injection volume was 10 µL, the acquisition rate was set at 1.41 scans, and complete mass scanning ranged from *m/z* 100–1000. Both ESI^+ and ESI^- were utilized. MS conditions were optimized with capillary voltage 3200 V and 3400 V for ESI^+ and ESI^-, respectively; drying gas temperature 350 °C, fragmentor voltage 175 V, and skimmer 65 V. Nitrogen was supplied as a nebulizing gas at 25 psi and as a drying gas at 10 L/min. LC separation for açaí BDS extract samples was conducted with a gradient mobile phase consisting of (A) water, 0.1% FA and (B) MeOH, 0.1% FA. The linear gradient was: 0 min, 15% B; 6 min, 65% B; 15 min, 80% B; 25-40 min, 95% B, 45 min, 15% B with a 5-minute post-time for re-equilibration. The column temperature was set to 25°C.

The same method was utilized for MS/MS acquisition, adding collision energies of 10, 20, 40 and 60 eV to gain fragmentation information.

2.6.5 Structural elucidation of F1ME inhibitors

All information regarding the use of or obtaining the GNPS-Bioactivity automated interface can be found in our previous publication with the following exception: instead of using MS/MS data for our tool, full scan MS data was used in MZmine2 to allow for the examination of compounds which may not be observed during MS/MS data acquisition [113]. This exemption does not allow for a bioactive molecular network to be created, but the statistical analysis is still performed to hypothesize which compounds in a mixture are most bioactive.

Using MSConvert software, MS/MS data files will be converted to .mzXML files with the noise levels set to MSlevel1 and MSlevel2. The automation tool will run the batch of files in MZmine2, where data is processed and then automatically exported to GNPS where a FBMN job is performed. Once the FBMN job is finished, the Cytoscape data folder can be saved and uploaded to the automated dashboard. Then, the outputs of GNPS, MZmine2, and the .csv file including the R script are uploaded into Cytoscape where the BMN is created. The compounds predicted to be the most bioactive will be used in Subaim 1B.3. These compounds will be indicated by a statistical p-value under 0.05 (95% Cl) and will show as the largest nodes in the BMN. The workflow of this outline can be found in **Figure 2**.

Data analysis including molecular feature extraction, molecular formula and fragment formula generation, and database searching was performed using MassHunter Qualitative Analysis software ver. B.10.00 and MassHunter PCDL Manager with METLIN™. Compound fragmentation data was processed with SIRIUS+CSI:FingerID version 5.8.2 for MS/MS library

searching in the following libraries: Biocyc, CheBI, COCONUT, GNPS, HMDB, HSDB, KEGG, KNApSAck, MaConDa, MeSH, NORMAN, Natural Products, Plantcyc, PubChem, YMDB, and Zinc Bio [122, 123]. Manual searches were performed in LIPID MAPS.

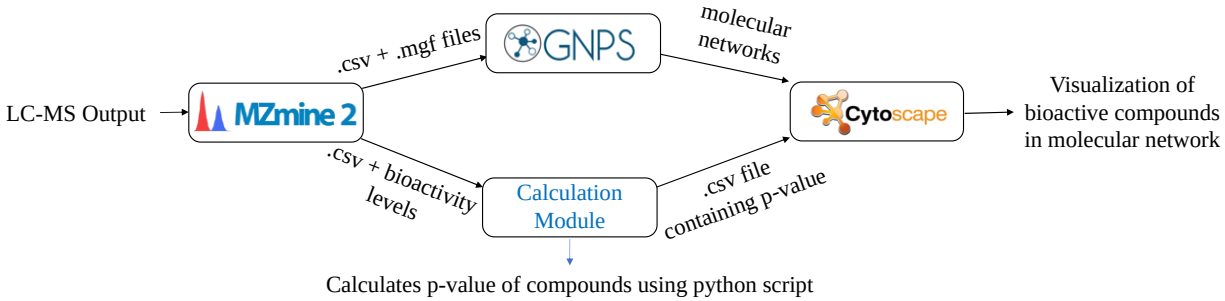

Figure 2. Workflow for bioactive compound identification using the automated GNPS-Bioactivity dashboard.

2.7 Assessment of açaí extracts for UGT inhibition

2.7.1 Generation of LC-MS method for UGT metabolite quantitation

This method was developed to assess potential UGT inhibition by açaí constituents *in vitro*. Samples mimicking *in vitro* assay conditions were made including 0.25 mg/mL UGT Supersome Control, 25 µg/µL alamethicin, 5 mM $MgCl_2$, and 5 mM UGPGA in 50 mM Tris-HCl buffer (pH 7.4). Each of the 6 UGT metabolite analytical standards was added at 1 µM. The total volume of the mimicked reaction mixture was 100 µL. The sample was then spiked with 100 µL of ACN containing IS chlorpropamide before centrifugation at 10,000 rpm for 15 min (4ºC). This was the sample that was used to generate the LC-MS quantitation method.

Optimal separation of the UGT metabolite mixture was achieved using a 4.6 x 100 mm, 3.5 µm ZORBAX Eclipse Plus Phenyl-Hexyl column (Agilent Technologies, New Castle, DE). The flow rate was set at 0.5 mL/min, the sample injection volume was 10 µL, the acquisition rate was set at 1.41 scans, and complete mass scanning ranged from *m/z* 200–700. LC separation for UGT inhibition assay samples was conducted with a gradient mobile phase consisting of (A) water, 0.1% FA and (B) ACN, 0.1% FA. The linear gradient was: 0 min, 30% B; 0.5 min, 30 % B; 1.5 min, 60% B; 3 min, 90% B; 4 min, 90% B; 4.5 min, 60% B; 5 min, 15% B; 8 min, 15% B. The column temperature was set to 25°C. Both ESI^+ and ESI^- were utilized. MS conditions were optimized with capillary voltage 3200 V and 3400 V for ESI^+ and ESI^-, respectively; drying gas temperature 350 °C, fragmentor voltage 100 V, and skimmer 65 V. Nitrogen was supplied as a nebulizing gas at 25 psi and as a drying gas at 10 L/min.

Chapter 3. Results and Discussion

3.1 Chemical fingerprinting

3.1.1 Untargeted fingerprinting analysis of açaí extracts

We developed a chromatographic method for chemical fingerprinting of açaí samples using a C18 stationary phase. This column was chosen because of previous success with using this column to separate and quantitate anthocyanins from these same complex açaí extracts [126]. This method requires 50 minutes per chromatographic run including re-equilibration time. **Figure 3** shows a mass versus retention plot for all 64 açaí extract samples and the most frequently found molecular features found in full scan spectra using both ESI^+ and ESI^-.

From the 4,002 total mass features detected in ESI^+ (2,510 features) and ESI^- (1,492 features), 173 compounds were annotated after feature alignment and MS/MS library searches (**Table 4**). To our knowledge, this analysis includes 138 compounds that had previously been identified in plants but have now been found for the first time in açaí extracts. The MS/MS spectra and spectral matches of tentatively identified compounds in açaí are provided in **Figure 4**. The MS/MS spectra and spectral matches of positively identified compounds in açaí using authentic chemical standards of LC-MS grade purity are provided in **Figure 5**. When a compound was detected in both ion modes, the one with the best MS/MS fragmentation match was included. Annotated compounds include 82 fatty acids, 32 flavonoids, 18 phenols, 13 organic acids, and 12 amino acid derivatives among other constituents. Because fatty acids, organic acids, and amino acids are primary metabolites and ubiquitous to all plants, we see no reason that any of these compounds could not be made biosynthetically by açaí [127]. Flavonoids and phenols have been

previously reported in açaí many times; therefore, they should be easily biosynthesized via the shikimate, pentose phosphate, and phenylpropanoid pathways [16, 19, 94, 98, 106, 125-129].

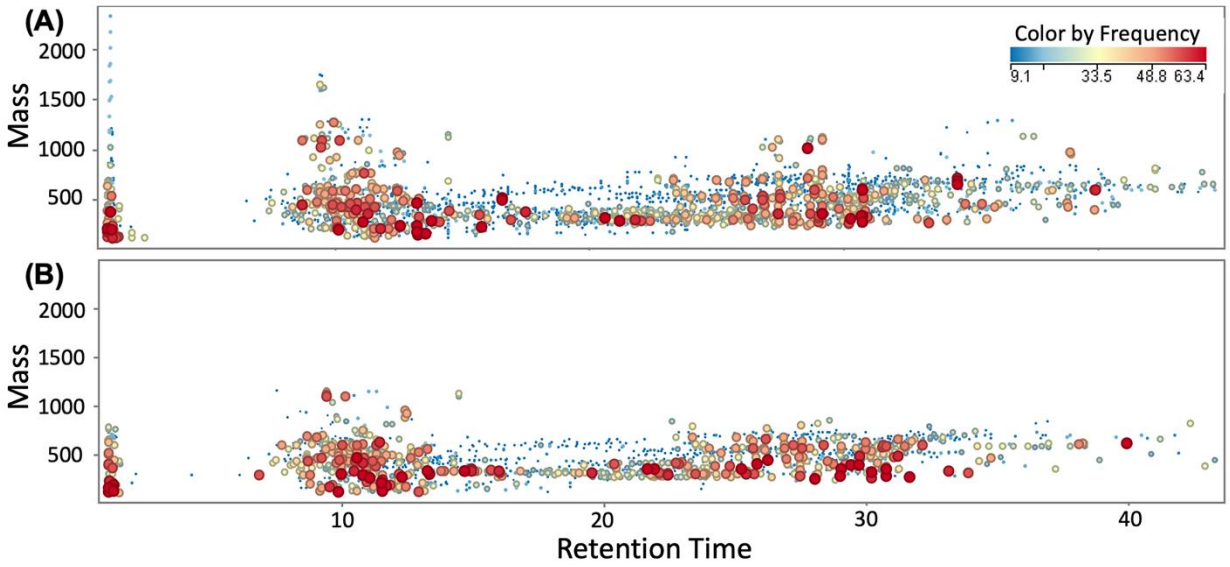

Figure 3. Mass versus retention time plot showing 2,510 features in ESI^+ (A) and 1,492 features found in ESI^- (B) found amongst all açaí sample types. The y-axis provides the uncharged mass of the feature; the x-axis represents the elution times for each feature. The size and color of the point represent the frequency at which a feature was found amongst the 64 samples.

Table 4. Parameters for identified or tentatively identified compounds detected in various açaí extracts using ESI^+ and ESI^-. Compounds confirmed using authentic chemical standards are shown in **bold**. Compounds which were tentatively identified but have not previously been reported for açaí to our knowledge are denoted with an (*).

	Compound	***m/z***	**RT (min)**	**Detected Adducts**	**Δ ppm**	**Neutral Formula**
1	(*R*)-2-hydroxycaprylic acid*	159.1023	12.8	$[M-H]^-$	-2.31	$C_8H_{16}O_4$
2	1-(2,4-dihydroxyphenyl)-3-(3,4-dihydroxyphenyl)-1-propanone*	273.0777	11	$[M-H]^-$	3.12	$C_{15}H_{14}O_5$
3	1-monopalmitin*	331.2860	28.6	$[M+H]^+$	-1.17	$C_{19}H_{38}O_4$
4	1-oleoyl lysophosphatidic acid*	435.2517	28.2	$[M-H]^-$	-0.03	$C_{21}H_{41}O_7P$
5	1-palmitoyl lysophosphatidic acid*	409.2365	29.9	$[M-H]^-$	2.04	$C_{19}H_{39}O_7P$
6	1,1-dimethylpyrrolidinium-2-carboxylate*	144.1004	1.26	$[M]^+$	5.6	$C_7H_{14}NO_2$
7	2-ethyl-7-propyloctanedioic acid*	243.1612	20.1	$[M-H]^-$	4.18	$C_{13}H_{24}O_4$
8	2-hydroxy-4-(methoxycarbonyl)benzoic acid*	195.0310	10.9	$[M-H]^-$	-0.22	$C_9H_8O_5$
9	2-hydroxyheptanoic acid*	145.0866	11.5	$[M-H]^-$	-2.88	$C_7H_{14}O_3$
10	2-hydroxypalmitic acid*	271.2270	27.4	$[M-H]^-$	-3.2	$C_{16}H_{32}O_3$

	Compound	*m/z*	RT (min)	Detected Adducts	Δ ppm	Neutral Formula
11	2-hydroxystearic acid*	299.2596	30.1	$[M-H]^-$	1.44	$C_{18}H_{36}O_3$
12	2-methoxy-2-oxoethyltrimethylaminium*	132.1020	1.18	$[M]^+$	0.72	$C_6H_{14}NO_2$
13	2,3-dihydroxy-3-(3,4,5,6-tetrahydroxyoxan-2-yl)propanoic acid*	253.0562	1.21	$[M-H]^-$	-1.21	$C_8H_{14}O_9$
14	2,9-dihydroxynonanoic acid*	189.1133	12.5	$[M-H]^-$	0.36	$C_9H_{18}O_4$
15	2,11-dihydroxyundecanoic acid*	217.1453	14.8	$[M-H]^-$	3.53	$C_{11}H_{22}O_4$
16	3-furoic acid*	111.0085	1.25	$[M-H]^-$	-2.34	$C_5H_4O_3$
17	3-hydroxy-3-methyl-glutaric acid*	161.0453	1.27	$[M-H]^-$	-1.53	$C_6H_{10}O_5$
18	3-hydroxypalmitic acid*	271.2276	26.4	$[M-H]^-$	-0.99	$C_{16}H_{32}O_3$
19	3-methyl-dienelactone*	153.0188	9.26	$[M-H]^-$	-3.48	$C_7H_6O_4$
20	3-*O*-methylgallic acid*	183.0297	6.94	$[M-H]^-$	-1.08	$C_8H_8O_5$
21	3-phenylpropyl beta-*D*-glucopyranoside*	297.1343	11.0	$[M-H]^-$	-0.21	$C_{15}H_{22}O_6$
22	3,10-dihydroxydecanoic acid*	203.1291	13.9	$[M-H]^-$	-3.82	$C_{10}H_{20}O_4$
23	4-hydroxy-6-methylpyran-2-one*	127.0392	3.69	$[M+H]^+$	1.56	$C_6H_6O_4$
24	4-hydroxynonenoic acid*	171.1030	12.2	$[M-H]^-$	2.011	$C_9H_{16}O_3$
25	4-methyl itaconate*	143.0342	2.01	$[M-H]^-$	-5.47	$C_6H_8O_4$
26	4-oxododecanedioic acid*	243.1255	11.5	$[M-H]^-$	1.12	$C_{12}H_{20}O_5$

	Compound	*m/z*	RT (min)	Detected Adducts	Δ ppm	Neutral Formula
27	5-keto-*D*-gluconic acid*	193.0353	1.30	$[M-H]^-$	-0.39	$C_6H_{10}O_7$
28	6-gingerol*	298.1758	15.7	$[M-H]^-$	-0.11	$C_{17}H_{26}O_4$
29	7-(2,3-dihydroxypropoxy)-7-oxoheptanoic acid*	233.1052	8.38	$[M-H]^-$	-0.69	$C_{10}H_{18}O_6$
30	7-keto palmitic acid*	269.2120	24.8	$[M-H]^-$	-0.81	$C_{16}H_{30}O_3$
31	7E-hexadecenoic acid methyl ester*	269.2470	26.3	$[M+H]^+$	-1.88	$C_{17}H_{32}O_2$
32	8-methylnonenoic acid*	167.1247	13.1	$[M-H]^-$	3.57	$C_{10}H_{18}O_2$
33	8-oxoxanthosine*	299.0627	11.6	$[M-H]^-$	-3.44	$C_{10}H_{12}N_4O_7$
34	8,11-dihydroxy-9,12-octadecadienoic acid*	311.2229	19.3	$[M-H]^-$	0.38	$C_{18}H_{32}O_4$
35	8,9-dihydroxystearic acid*	297.2447	23.9	$[M-H_2O-H]^-$	2.94	$C_{18}H_{36}O_4$
36	8E-heptadecenoic acid*	269.2482	30.6	$[M+H]^+$	3.59	$C_{17}H_{32}O_2$
37	9-(2,3-dihydroxypropoxy)-9-oxononanoic acid *	261.1337	11.0	$[M-H]^-$	-2.54	$C_{12}H_{22}O_6$
38	9-HOTrE*	293.2116	20.8	$[M-H]^-$	-2.11	$C_{18}H_{30}O_3$
39	9-Hpode*	311.2243	21.9	$[M-H]^-$	4.87	$C_{18}H_{32}O_4$
40	9-HpOTrE*	309.2076	17.5	$[M-H]^-$	1.51	$C_{18}H_{30}O_4$

	Compound	*m/z*	RT (min)	Detected Adducts	Δ ppm	Neutral Formula
41	9-hydroxynonanoic acid*	173.1182	11.7	$[M-H]^-$	-0.68	$C_9H_{18}O_3$
42	9-oxo-capric acid*	185.1180	12.9	$[M-H]^-$	-1.72	$C_{10}H_{18}O_3$
43	9-OxoODE*	293.2120	22.4	$[M-H]^-$	-0.74	$C_{18}H_{30}O_3$
44	9-OxoOTrE*	291.1978	20.5	$[M-H]^-$	4.23	$C_{18}H_{28}O_3$
45	9,10-dihydroxystearic acid*	315.2551	21.5	$[M-H]^-$	3.23	$C_{18}H_{36}O_4$
46	9,10,13-trihydroxyoctadec-11-enoic acid*	311.2239	18.3	$[M-H_2O-H]^-$	3.59	$C_{18}H_{34}O_5$
47	9,12-octadecadiynoic acid*	277.2164	25.3	$[M+H]^+$	0.7	$C_{18}H_{28}O_2$
48	9(10)-EpOME*	279.2329	22.4	$[M+H-H_2O]^+$	3.74	$C_{18}H_{32}O_3$
49	9S,10S,11R-trihydroxy-12Z,15Z-octadecadienoic acid*	327.2173	15.5	$[M-H]^-$	-1.22	$C_{18}H_{32}O_5$
50	10-hydroxycapric acid*	187.1342	16.2	$[M-H]^-$	1.24	$C_{10}H_{20}O_3$
51	10E-12Z-octadecadienoic acid*	281.2471	24.9	$[M+H]^+$	-1.45	$C_{18}H_{32}O_2$
52	11-hydroxyhexadec-9-enoic acid*	269.2132	20.6	$[M-H]^-$	3.65	$C_{16}H_{30}O_3$
53	11-oxooctadec-12-enoic acid*	295.2279	23.4	$[M-H]^-$	0.11	$C_{18}H_{32}O_3$
54	12,13-DiHOME*	313.2377	19.5	$[M-H]^-$	-2.34	$C_{18}H_{34}O_4$
55	12,13-dihydroxystearic acid*	315.2537	20.5	$[M-H]^-$	-1.22	$C_{18}H_{36}O_4$

	Compound	*m/z*	RT (min)	Detected Adducts	Δ ppm	Neutral Formula
56	12(13)-EpOME*	295.2278	22.4	$[M-H]^-$	-0.23	$C_{18}H_{32}O_3$
57	13-amino-13-oxotridecanoic acid*	242.1768	13.9	$[M-H]^-$	2.61	$C_{13}H_{25}NO_3$
58	13-docosenamide*	338.3434	33.8	$[M+H]^+$	4.85	$C_{22}H_{43}NO$
59	13-HpOTrE*	309.2062	19.9	$[M-H]^-$	-3.02	$C_{18}H_{30}O_4$
60	13-OxoODE*	293.2118	21.8	$[M-H]^-$	-1.43	$C_{18}H_{30}O_3$
61	**acacetin***	285.0760	12.0	$[M-H]^+$	0.27	$C_{16}H_{12}O_5$
62	adenine*	136.0618	1.26	$[M+H]^+$	0.21	$C_5H_5N_5$
63	alpha-12,13-DiHODE*	311.2244	18.5	$[M-H]^-$	4.17	$C_{18}H_{32}O_4$
64	apigenin	269.0455	13.2	$[M-H]^-$	1.31	$C_{15}H_{10}O_5$
65	arginine methyl ester*	189.1340	1.08	$[M+H]^+$	-3.18	$C_7H_{16}N_4O_2$
66	azelaic acid*	187.0976	11.5	$[M-H]^-$	0.09	$C_9H_{16}O_4$
67	betaine*	118.0862	1.42	$[M]^+$	-0.47	$C_5H_{12}NO_2$
68	caprylic acid	125.0977	13.2	$[M-H_2O-H]^-$	3.98	$C_8H_{16}O_2$
69	**catechin**	291.0865	7.21	$[M+H]^+$	0.64	$C_{15}H_{14}O_6$
70	catechol	109.0285	3.84	$[M-H]^-$	-2.49	$C_6H_6O_2$
71	**chrysoeriol**	301.0709	13.3	$[M+H]^+$	0.7	$C_{16}H_{12}O_6$

	Compound	*m/z*	RT (min)	Detected Adducts	Δ ppm	Neutral Formula
72	citric acid	191.0197	1.26	$[M-H]^-$	-0.14	$C_6H_8O_7$
73	corchorifatty acid D*	307.1917	15.1	$[M-H]^-$	0.71	$C_{18}H_{28}O_4$
74	coumaric acid 4-*O*-glucoside*	325.0928	7.30	$[M-H]^-$	-0.28	$C_{15}H_{18}O_8$
75	*o*-coumaric acid*	163.0391	9.95	$[M-H]^-$	-5.32	$C_9H_8O_3$
76	*p*-coumaric acid	163.0398	7.70	$[M-H]^-$	-1.64	$C_9H_8O_3$
77	**coumarin***	147.0436	9.83	$[M+H]^+$	-2.73	$C_9H_6O_2$
78	**cyanidin 3-*O*-glucoside**	449.1083	8.38	$[M]^+$	0.93	$C_{21}H_{21}O_{11}$
79	**cyanidin 3-*O*-rutinoside**	595.1667	8.49	$[M]^+$	1.09	$C_{27}H_{31}O_{15}$
80	**cyanidin 3-*O*-sambubioside**	581.1502	8.40	$[M]^+$	0.3	$C_{26}H_{29}O_{25}$
81	**dihydrokaempferol**	289.0726	10.1	$[M+H]^+$	0.84	$C_{15}H_{12}O_6$
82	*N*,*N*-dimethylpyridin-4-amine*	123.0923	1.37	$[M+H]^+$	5.08	$C_7H_{10}N_2$
83	epigallocatechin*	305.0663	2.21	$[M-H]^-$	-1.23	$C_{15}H_{14}O_7$
84	ethyl palmitate*	285.2796	34.9	$[M+H]^+$	2.78	$C_{18}H_{36}O_2$
85	fisetin*	285.0399	11.4	$[M-H]^-$	-1.97	$C_{15}H_{10}O_6$
86	fructosyl leucine*	294.1563	1.58	$[M+H]^+$	5.34	$C_{12}H_{23}NO_7$
87	galactaric acid*	209.0303	1.35	$[M-H]^-$	0.04	$C_6H_{10}O_8$

	Compound	*m/z*	RT (min)	Detected Adducts	Δ ppm	Neutral Formula
88	**gallic acid**	169.0143	1.51	$[M-H]^-$	0.31	$C_7H_6O_5$
89	glycerophosphocholine*	258.1105	1.36	$[M]^+$	1.55	$C_8H_{21}NO_6$
90	gulonic acid*	195.0503	1.17	$[M-H]^-$	-3.72	$C_6H_{12}O_7$
91	heptanoic acid*	111.0812	10.4	$[M-H_2O-H]^-$	-4.96	$C_7H_{14}O_2$
92	hexadecanedioic acid*	285.2084	14.8	$[M-H]^-$	4.44	$C_{16}H_{30}O_4$
93	homogentisic acid*	167.0344	11.0	$[M-H]^-$	-3.49	$C_8H_8O_4$
94	homoveratric acid*	195.0661	9.70	$[M-H]^-$	-0.94	$C_{10}H_{12}O_4$
95	hydroquinone*	109.0300	3.16	$[M-H]^-$	4.56	$C_6H_6O_2$
96	*DL*-b-hydroxycaprylic acid*	159.1021	12.15	$[M-H]^-$	-3.57	$C_8H_{16}O_3$
97	hyperoside*	463.0882	10.8	$[M-H]^-$	-0.65	$C_{21}H_{20}O_{12}$
98	indoline*	120.0811	12.3	$[M+H]^+$	2.7	C_8H_9N
99	isokaempferide*	301.0716	9.13	$[M+H]^+$	3.11	$C_{16}H_{12}O_6$
100	*L*-isoleucine	132.1025	1.42	$[M+H]^+$	4.76	$C_6H_{12}NO_2$
101	isopalmitic acid*	257.2473	30.1	$[M+H]^+$	-0.8	$C_{16}H_{32}O_2$
102	**isovanillic acid***	167.0355	9.50	$[M-H]^-$	3.1	$C_8H_8O_4$
103	**isovitexin**	431.0992	10.4	$[M-H]^-$	1.92	$C_{21}H_{20}O_{10}$

	Compound	*m/z*	RT (min)	Detected Adducts	Δ ppm	Neutral Formula
104	itaconic acid*	129.0189	1.24	$[M-H]^-$	-3.66	$C_5H_{56}O_4$
105	**kaempferol**	285.0403	13.1	$[M-H]^-$	-0.57	$C_{15}H_{10}O_6$
106	kaempferol 7-*O*-glucoside*	447.0930	8.94	$[M-H]^-$	-0.64	$C_{21}H_{20}O_{11}$
107	*L*-leucine*	132.1025	1.55	$[M+H]^+$	4.48	$C_6H_{12}NO_2$
108	larixinic acid*	127.0392	3.15	$[M+H]^+$	1.56	$C_6H_6O_3$
109	leucyl proline*	229.1544	1.41	$[M+H]^+$	-1.17	$C_{11}H_{20}N_2O_3$
110	leucyl leucine*	245.1873	7.92	$[M+H]^+$	5.64	$C_{12}H_{24}N_2O_3$
111	linolenic acid	279.2316	30.2	$[M+H]^+$	-0.92	$C_{18}H_{30}O_2$
112	linoleoyl ethanolamide*	324.2903	26.3	$[M+H]^+$	1.83	$C_{20}H_{37}NO_2$
113	loliolide	197.1200	10.2	$[M+H]^+$	3.45	$C_{11}H_{16}O_3$
114	luteolin	285.0408	12.5	$[M-H]^-$	1.19	$C_{15}H_{10}O_6$
115	lycaonic acid*	297.2431	23.3	$[M-H]^-$	-1.41	$C_{18}H_{34}O_3$
116	LysoPC(16:0)*	496.3399	26.8	$[M]^+$	0.27	$C_{24}H_{50}NO_7P$
117	LysoPC(18:1)*	522.3556	26.9	$[M]^+$	0.35	$C_{26}H_{53}NO_7P$
118	LysoPC(18:2)*	520.3415	25.6	$[M]^+$	3.33	$C_{26}H_{51}NO_7P$
119	LysoPC(18:3)*	518.3254	26.8	$[M]^+$	2.48	$C_{26}H_{49}NO_7P$

	Compound	*m/z*	RT (min)	Detected Adducts	Δ ppm	Neutral Formula
120	LysoPE(16:0)*	452.2781	26.9	$[M-H]^-$	-0.36	$C_{21}H_{44}NO_7P$
121	maltose	377.0857	1.26	$[M+Cl]^-$	0.23	$C_{12}H_{22}O_{11}$
122	methyl citrate*	205.0400	2.20	$[M-H]^-$	-2.81	$C_7H_{10}O_7$
123	methyl leucine*	146.1178	2.77	$[M+H]^+$	2.33	$C_7H_{15}NO_2$
124	methyl palmitate*	271.2630	33.4	$[M+H]^+$	-0.58	$C_{17}H_{34}O_2$
125	methylgallic acid*	183.0304	9.62	$[M-H]^-$	0.39	$C_8H_8O_5$
126	monoolien*	347.2998	29.1	$[M+H]^+$, $[M+Na]^+$	-0.38	$C_{21}H_{40}O_4$
127	monopalmitin*	353.2671	23.3	$[M+H]^+$, $[M+Na]^+$	2.46	$C_{19}H_{38}O_4$
128	myricetin*	317.0307	11.3	$[M-H]^-$	1.29	$C_{15}H_{10}O_8$
129	myricetin 3-*O*-galactoside*	479.0841	10.1	$[M-H]^-$	2.06	$C_{21}H_{20}O_{13}$
130	**naringenin***	271.0602	12.2	$[M-H]^-$	-3.68	$C_{15}H_{12}O_5$
131	nevadensin*	343.0823	15.6	$[M-H]^-$	-0.08	$C_{18}H_{16}O_7$
132	nicotinic acid*	124.0398	1.51	$[M+H]^+$	4.36	$C_6H_5NO_2$
133	nonanoic acid*	157.1227	14.9	$[M-H]^-$	-4.48	$C_9H_{18}O_2$
134	**oleamide***	282.2793	28.3	$[M-H]^+$	0.35	$C_{18}H_{35}NO$

	Compound	*m/z*	RT (min)	Detected Adducts	Δ ppm	Neutral Formula
135	**oleic acid**	283.2633	30.7	$[M+H]^+$	0.42	$C_{18}H_{34}O_2$
136	oleoyl ethanolamide*	326.3051	28.1	$[M+H]^+$	-0.78	$C_{20}H_{39}NO_3$
137	**orientin**	449.1086	9.83	$[M+H]^+$	1.68	$C_{21}H_{20}O_{11}$
138	palmitamide*	256.2631	27.6	$[M+H]^+$	-1.53	$C_{16}H_{33}NO$
139	**palmitic acid**	255.2339	30.1	$[M-H]^-$	3.71	$C_{16}H_{32}O_2$
140	PE(18:1(9z)/0:0)*	478.2940	27.6	$[M-H]^-$	0.18	$C_{23}H_{46}NO_7P$
141	**peonidin 3-*O*-glucoside**	463.1238	8.9	$[M]^+$	0.59	$C_{22}H_{23}O_{11}$
142	**peonidin 3-*O*-rutinoside**	609.1816	9.34	$[M]^+$	0.4	$C_{28}H_{33}O_{15}$
143	*DL*-phenylalanine	166.0870	2.16	$[M+H]^+$	4.79	$C_9H_{11}NO_2$
144	phloridzin*	435.1293	7.43	$[M-H]^-$	-0.85	$C_{21}H_{24}O_{10}$
145	phytosphingosine*	318.3017	20.8	$[M+H]^+$	4.50	$C_{18}H_{39}NO_3$
146	pimelic acid*	159.0656	8.57	$[M-H]^-$	-4.29	$C_7H_{12}O_4$
147	*DL*-pipecolic acid*	130.0866	1.43	$[M+H]^+$	2.86	$C_6H_{11}NO_2$
148	protocatechuic acid	153.0186	3.15	$[M-H]^-$	-4.79	$C_7H_6O_4$
149	purine*	119.0352	4.29	$[M-H]^-$	-0.29	$C_5H_4N_4$
150	pyrogallol*	125.0243	1.49	$[M-H]^-$	-0.94	$C_6H_6O_3$

	Compound	*m/z*	RT (min)	Detected Adducts	Δ ppm	Neutral Formula
151	**quercetin**	303.0500	12.2	$[M+H]^+$	0.28	$C_{15}H_{10}O_7$
152	**quercetin 3-*O*-glucoside**	465.1030	10.8	$[M+H]^+$	0.19	$C_{21}H_{20}O_{12}$
153	rosilic acid*	299.2604	25.4	$[M-H]^-$	4.11	$C_{18}H_{36}O_3$
154	sambucinol*	267.1587	11.9	$[M+H]^+$	-1.54	$C_{15}H_{22}O_4$
155	sebacic acid*	201.1136	12.4	$[M-H]^-$	1.83	$C_{10}H_{18}O_4$
156	secoisolariciresinol*	327.1613	10.6	$[M+H-2(H_2O)]^+$, $[M+H-H_2O]^+$	0.21	$C_{20}H_{26}O_6$
157	sinapic acid*	207.0668	10.0	$[M+H-H_2O]^+$	-1.29	$C_{11}H_{12}O_5$
158	sphinganine*	302.3067	21.9	$[M+H]^+$	4.3	$C_{18}H_{39}NO_2$
159	stearidonic acid*	275.2022	20.8	$[M-H]^-$	1.99	$C_{18}H_{28}O_2$
160	suberic acid*	173.0819	10.3	$[M-H]^-$	-0.19	$C_8H_{14}O_4$
161	sucrose	365.1050	1.22	$[M+Na]^+$	1.55	$C_{12}H_{22}O_{11}$
162	tachioside*	301.0929	1.68	$[M-H]^-$	0.03	$C_{13}H_{18}O_8$
163	**taxifolin**	303.0400	9.94	$[M-H]^-$	-0.09	$C_{15}H_{12}O_7$
164	trans-EKODE-(E)-Ib*	309.2066	19.6	$[M-H]^-$	-1.72	$C_{18}H_{30}O_4$
165	trans-resveratrol	227.0719	10.9	$[M-H]^-$	2.34	$C_{14}H_{12}O_3$
166	tricin*	329.0664	13.2	$[M-H]^-$	-0.84	$C_{17}H_{14}O_7$

	Compound	*m/z*	RT (min)	Detected Adducts	Δ ppm	Neutral Formula
167	tridecanedioic acid*	243.1610	16.5	$[M-H]^-$	3.36	$C_{13}H_{24}O_4$
168	*L*-tryptophan	188.0713	4.66	$[M-NH_3+H]^+$	3.7	$C_{11}H_{12}N_2O_2$
169	undecanedioic acid*	215.1294	13.6	$[M-H]^-$	2.4	$C_{11}H_{20}O_4$
170	usnic acid*	345.0972	15.7	$[M+H]^+$	0.93	$C_{18}H_{16}O_7$
171	velutin	313.0717	16.0	$[M-H]^-$	-0.2	$C_{17}H_{14}O_6$
172	**vitexin**	431.0997	10.2	$[M-H]^-$	3.08	$C_{21}H_{20}O_{10}$
173	wogonin*	283.0623	16.2	$[M-H]^-$	3.9	$C_{16}H_{12}O_5$

Figure 4. MS/MS spectra of compounds in açaí extracts that were assigned tentatively (L2 annotations) by extensive querying and comparison with spectral libraries. Red lines indicate fragment matches between experimental spectra and library spectra. MS/MS scores are indicated in [ ] and were obtained using either Agilent Qualitative Analysis, GNPS, or SIRIUS for their respective libraries. Numbers shown in the spectra match those corresponding in Table 4.

(R)-2-hydroxycaprylic acid, CID: 5312860, METLIN; [91.77]

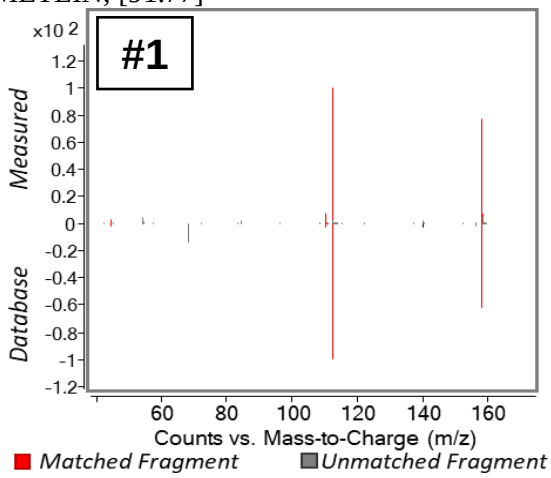

1-(2,4-dihydroxyphenyl)-3-(3,4-dihydroxy phenyl)-1-propanone, CID: 11550826, SIRIUS; [70.04]

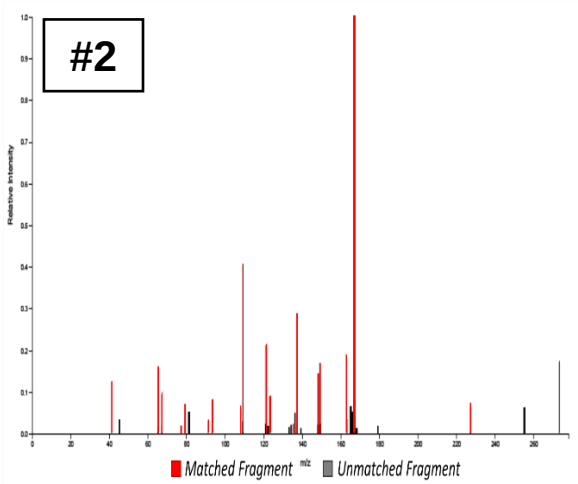

1-monopalmitin CID: 14900, GNPS; [85]

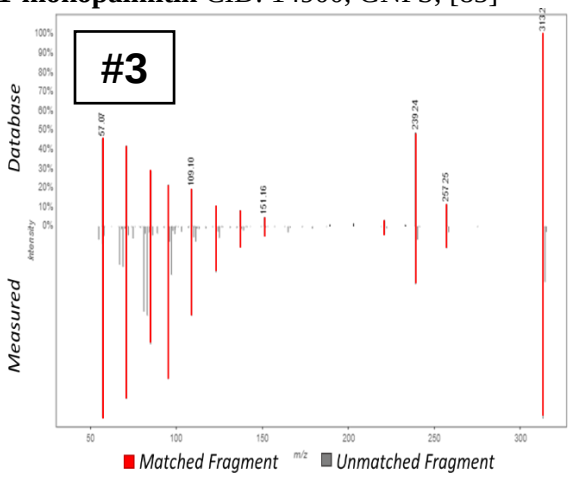

1-oleoyl lysophosphatidic acid, CID: 5311263, METLIN; [94.95]

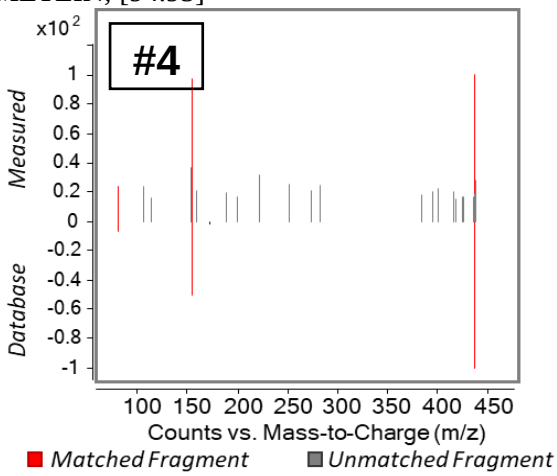

1-palmitoyl lysophosphatidic acid, CID: 89566, METLIN; [91.9]

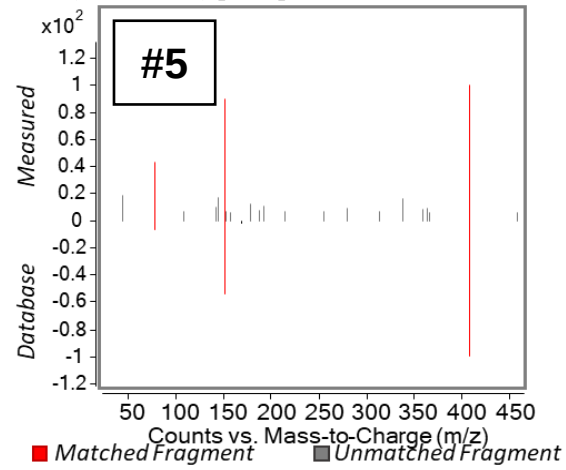

1,1-Dimethylpyrrolidinium-2-carboxylate, CID: 554, SIRIUS; [97.16]

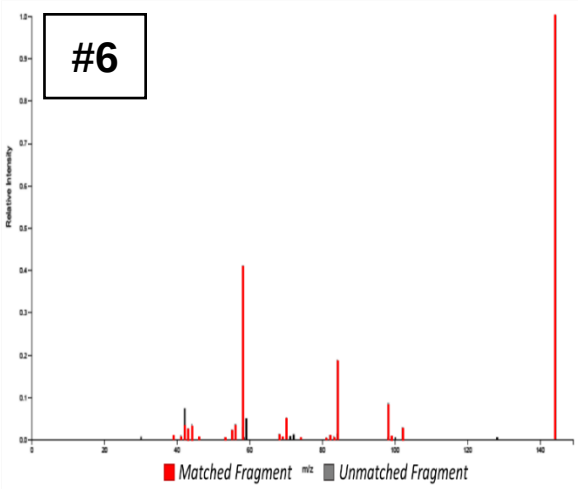

2-ethyl-7-propyloctanedioic acid, CID: 118049839, SIRIUS; [71.21]

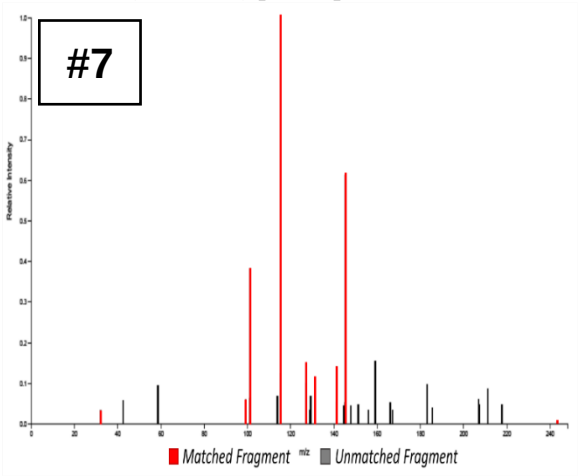

2-hydroxy-4-(methoxycarbonyl)benzoic acid, CID: 15294629, SIRIUS; [76.96]

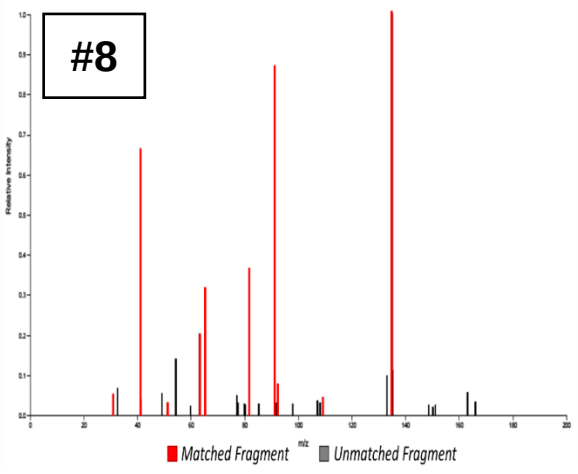

2-hydroxyheptanoic acid, CID: 2750949, SIRIUS; [74.59]

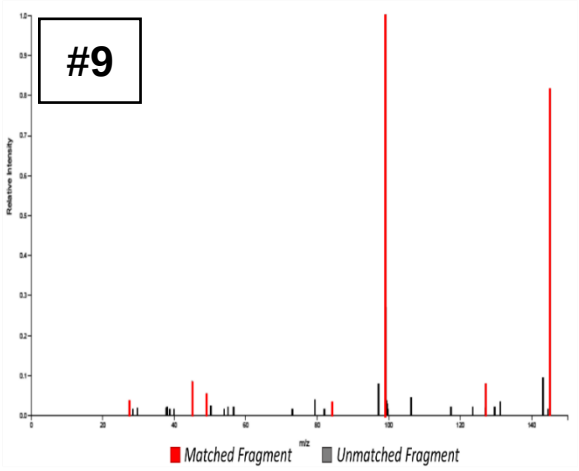

2-hydroxypalmitic acid, CID: 92836, SIRIUS; [90.3]

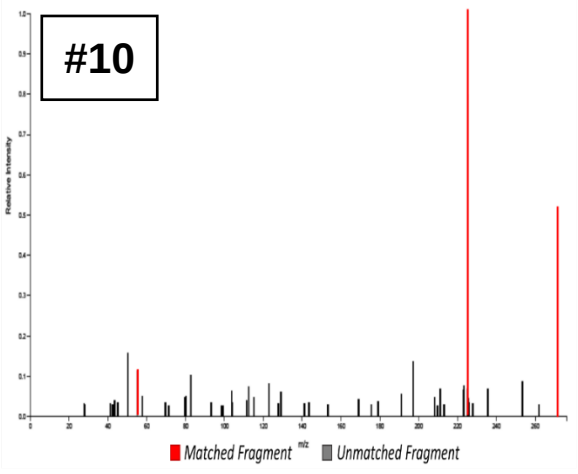

2-hydroxystearic acid, CID: 69417, SIRIUS; [95.95]

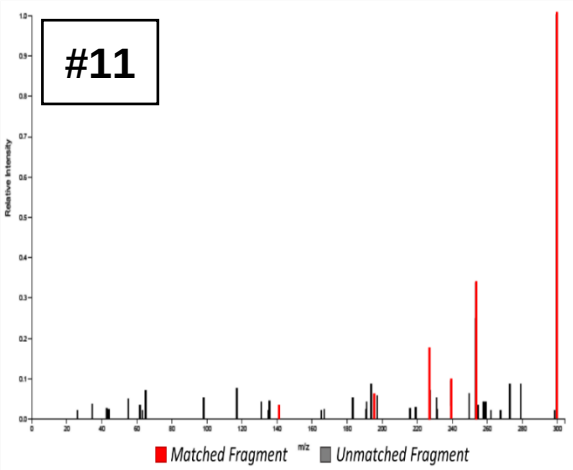

2-methoxy-2-oxoethyltrimethylaminium, CID: 26611, SIRIUS; [79.82]

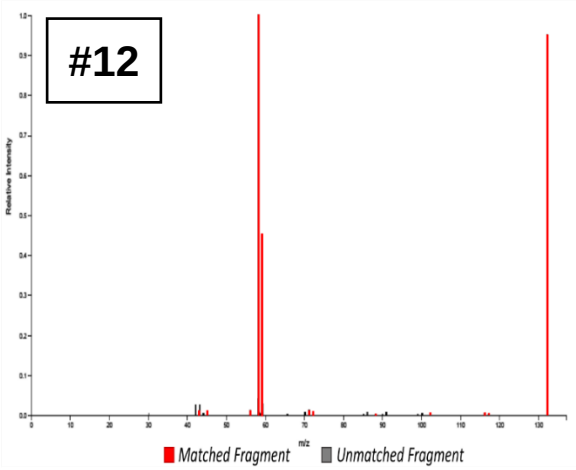

2,3-dihydroxy-3-(3,4,5,6-tetrahydroxy oxan-2-yl)propanoic acid, CID: 76459669, SIRIUS; [77.89]

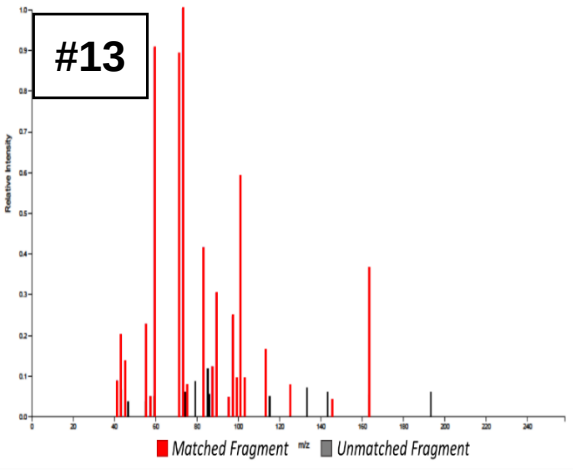

2,9-dihydroxynonanoic acid, CID: 23158568, SIRIUS; [82.68]

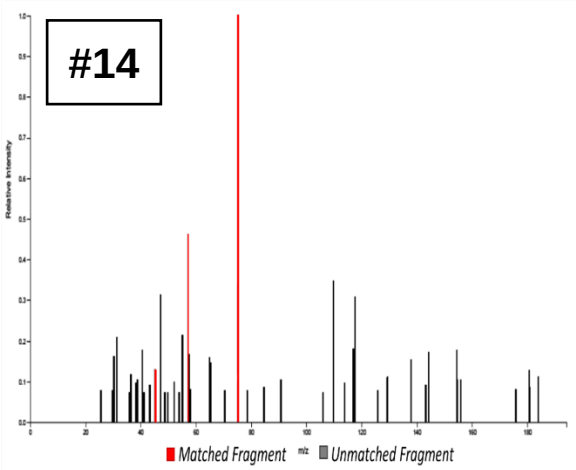

2,11-dihydroxyundecanoic acid, CID: 18981456, SIRIUS; [81.29]

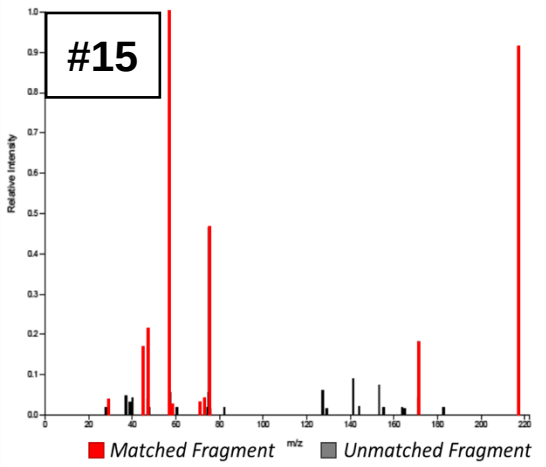

3-furoic acid, CID: 10268, SIRIUS; [90.24]

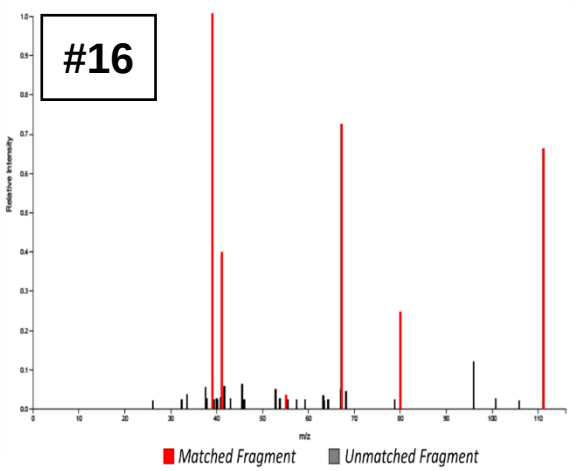

3-hydroxy-3-methyl-glutaric acid, CID: 1662, METLIN; [94.48]

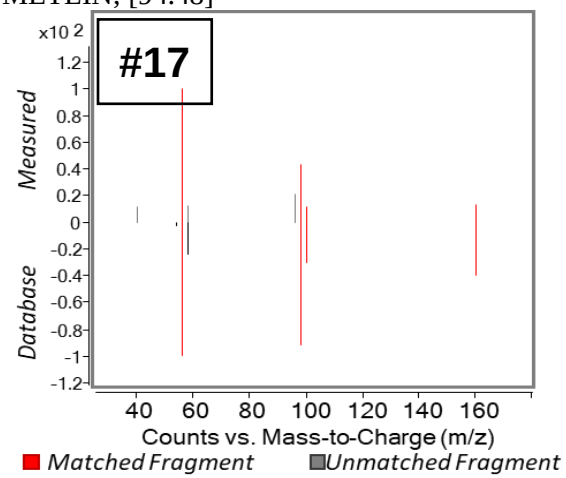

3-hydroxypalmitic acid, CID: 301590, METLIN; [78.55]

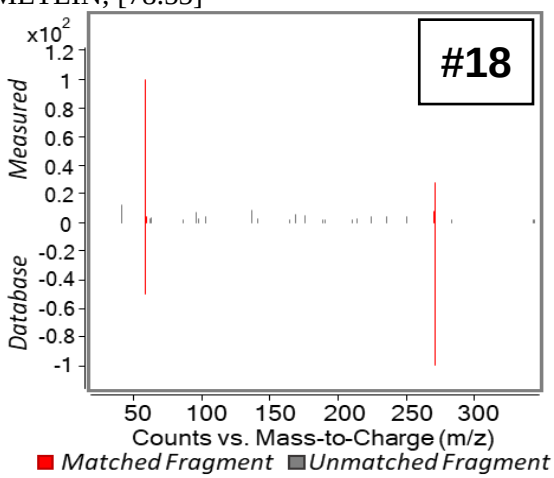

3-methyl-dienelactone, CID: 44123458, SIRIUS; [70.15]

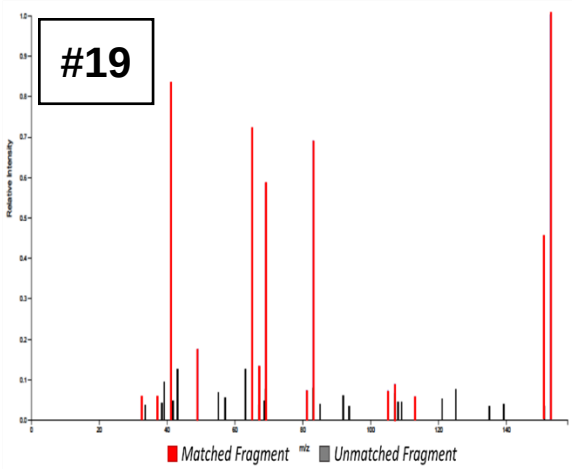

3-O-methylgallic acid, CID: 19829, SIRIUS; [86.36]

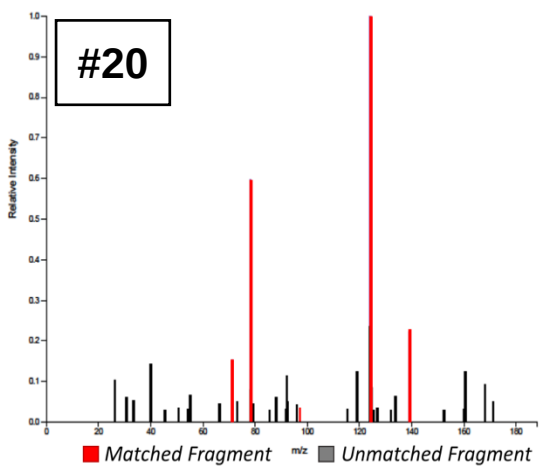

3-phenylpropyl beta-D-glucopyranoside, CID: 13139866, SIRIUS; [70.72]

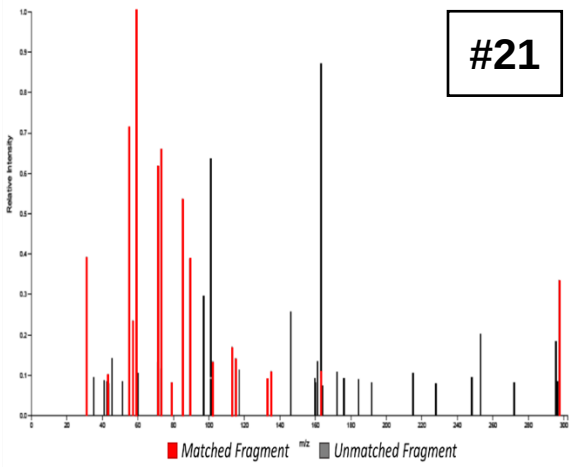

3,10-dihydroxydecanoic acid, CID: 9859090, SIRIUS; [76.69]

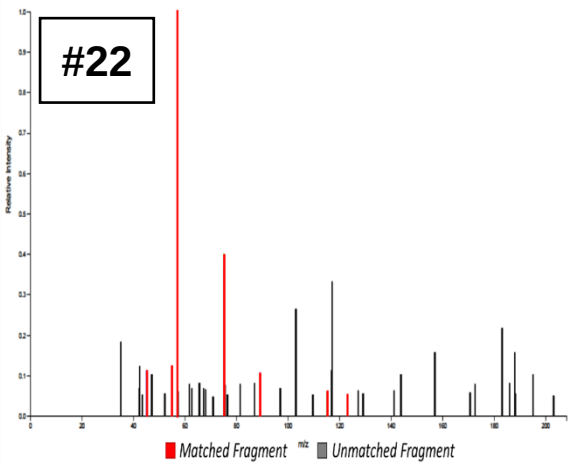

4-hydroxy-6-methylpyran-2-one, CID: 54675757, METLIN; [81.17]

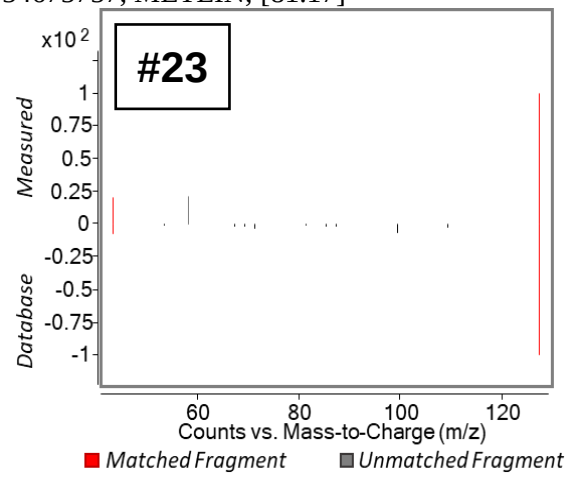

4-hydroxynonenoic acid, CID: 10442150, SIRIUS; [71.24]

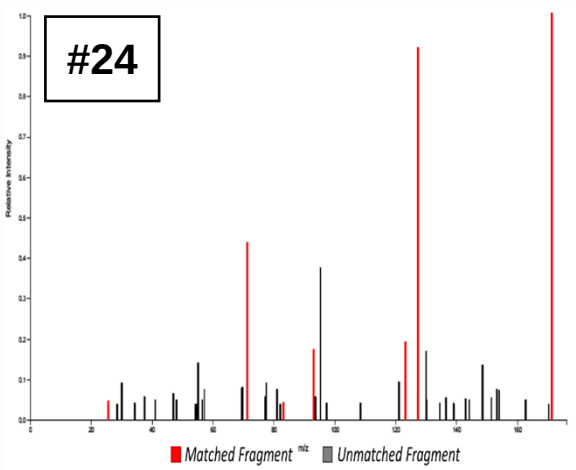

4-methyl itaconate, CID: 81791, SIRIUS; [87.07]

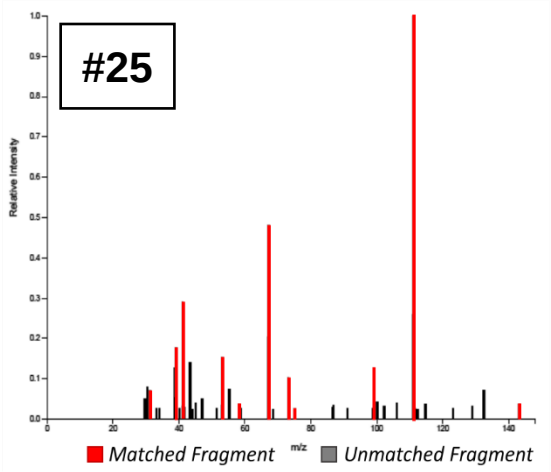

4-oxododecanedioic acid, CID: 13213508, SIRIUS; [100]

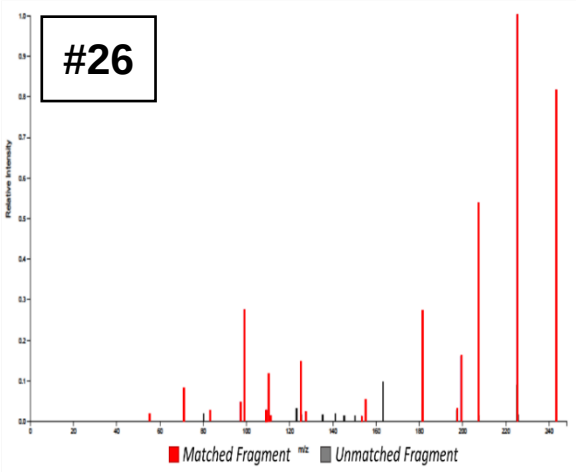

5-keto-D-gluconic acid, CID: 5460352, GNPS; [89]

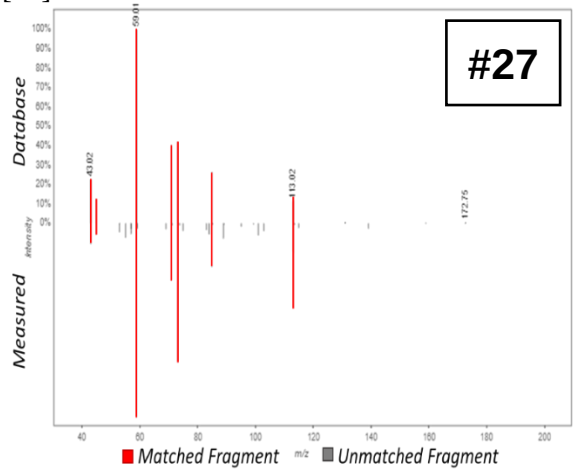

6-gingerol, CID: 442793, GNPS; [88]

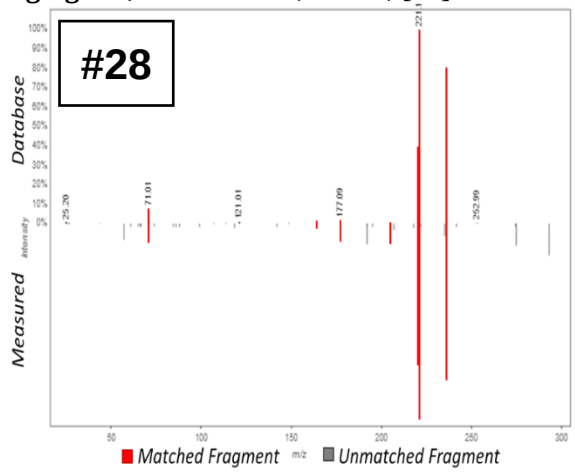

7-(2,3-Dihydroxypropoxy)-7-oxoheptanoic acid, CID: 53823180, SIRIUS; [85.38]

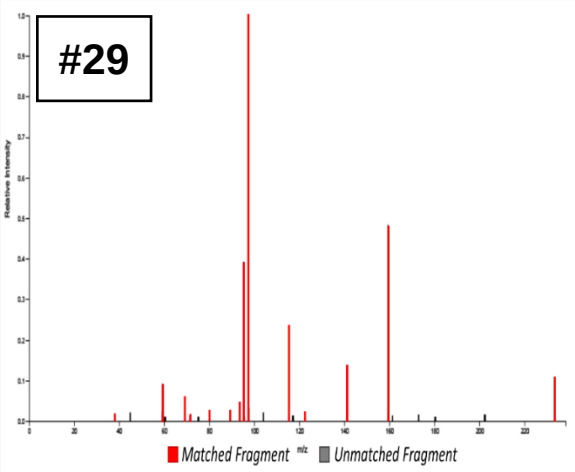

7-keto palmitic acid, CID: 15569760, SIRIUS; [90.76]

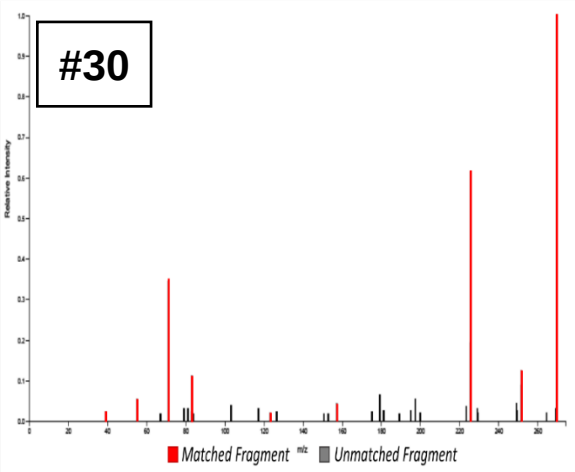

7E-hexadecenoic acid methyl ester, CID: 14029831, METLIN; [70.39]

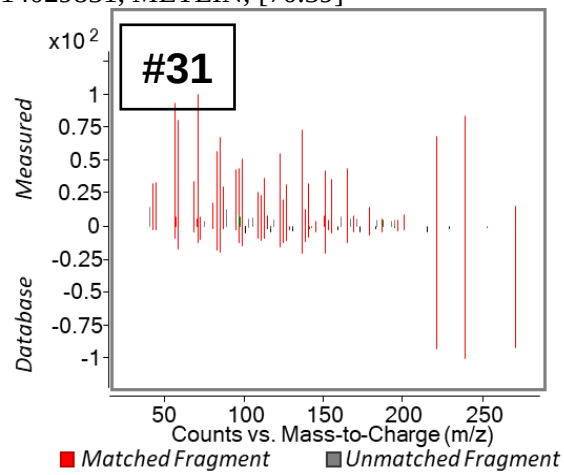

8-methylnonenoic acid, CID: 18188354, SIRIUS; [75.61]

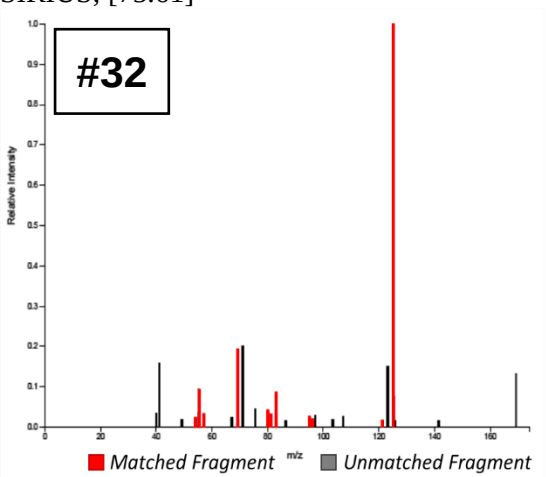

8-oxoxanthosine, CID: 3082183, SIRIUS; [78.19]

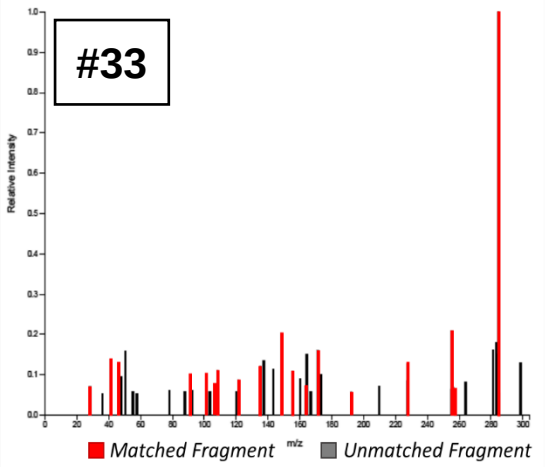

8,11-dihydroxy-9,12-octadecadienoic acid, CID: 76463674, SIRIUS; [93.67]

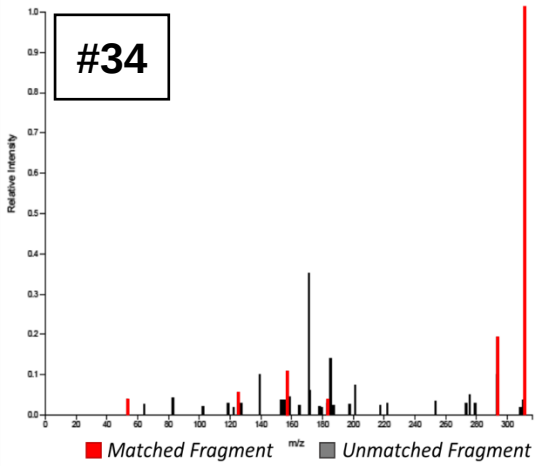

8,9-dihydroxystearic acid, CID: 361946, SIRIUS; [85.52]

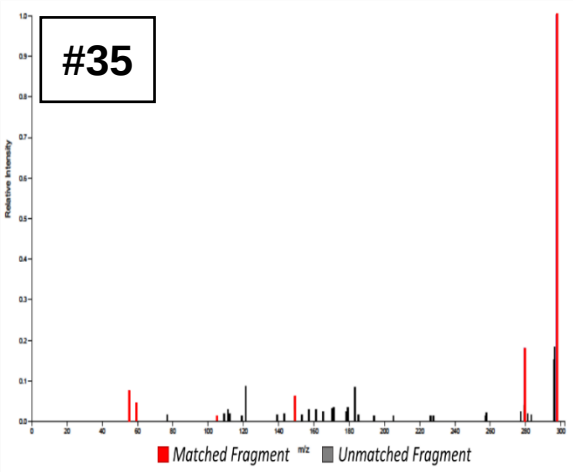

8E-heptadecenoic acid, CID: 5312438, SIRIUS; [96.27]

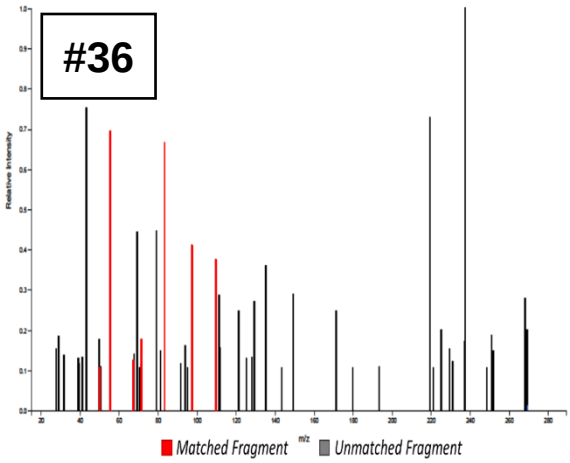

9-(2,3-dihydroxypropoxy)-9-oxononanoic acid, CID: 45783154, GNPS; [94]

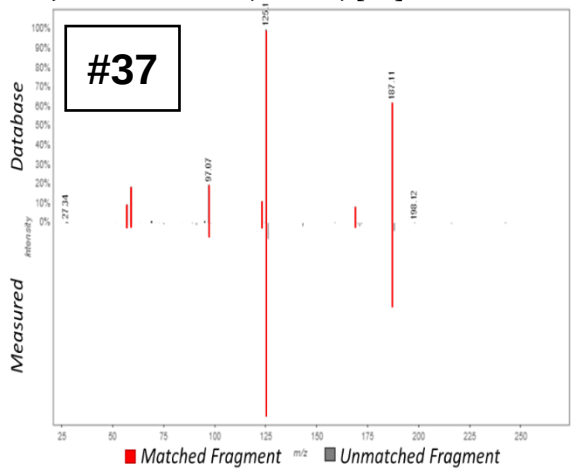

9-HOTrE, CID: 10447175, METLIN; [98.01]

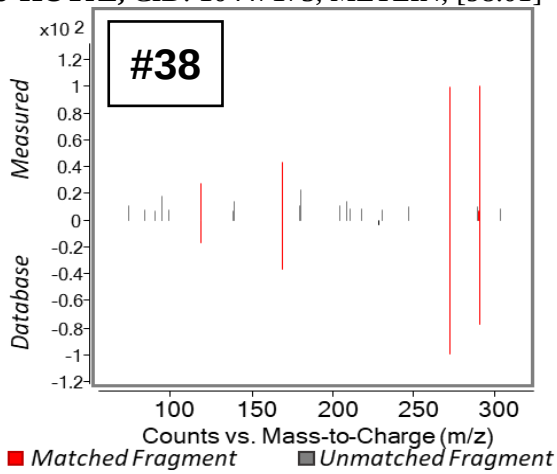

9-Hpode, CID: 5282856, SIRIUS; [86.88]

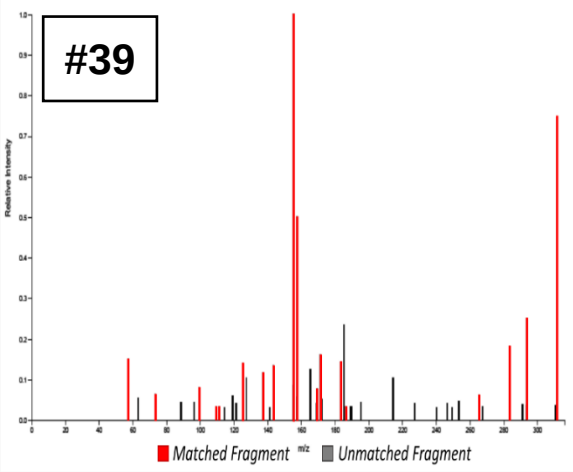

9-HpOTrE, CID: 5282864, GNPS; [74]

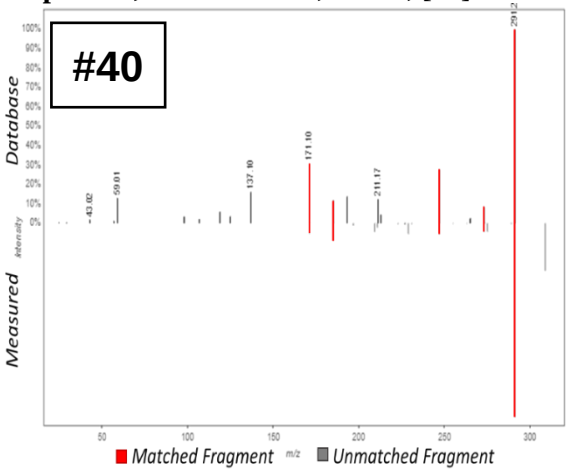

9-Hydroxynonanoic acid, CID: 138052, SIRIUS; [100]

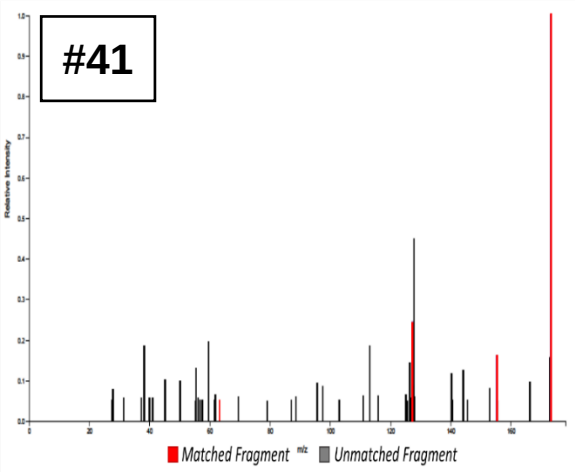

9-oxo-capric acid, CID: 15016, SIRIUS; [78.69]

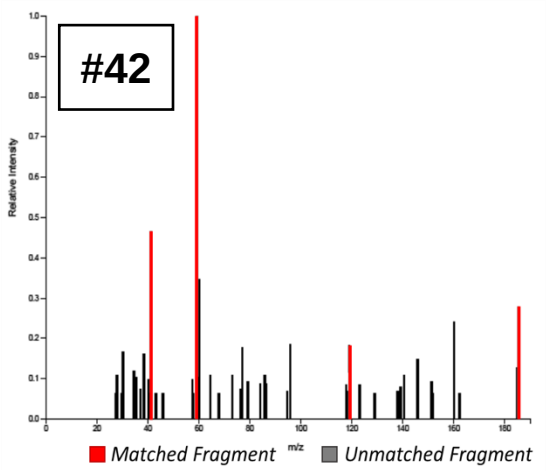

9-OxoODE, CID: 9839084, METLIN; [100]

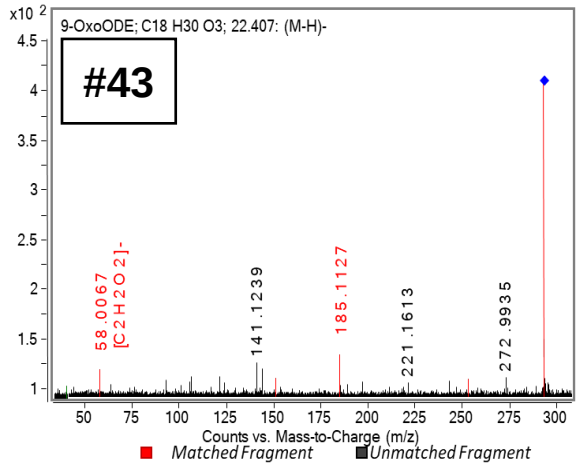

9-OxoOTrE, CID: 11380794, METLIN; [93.03]

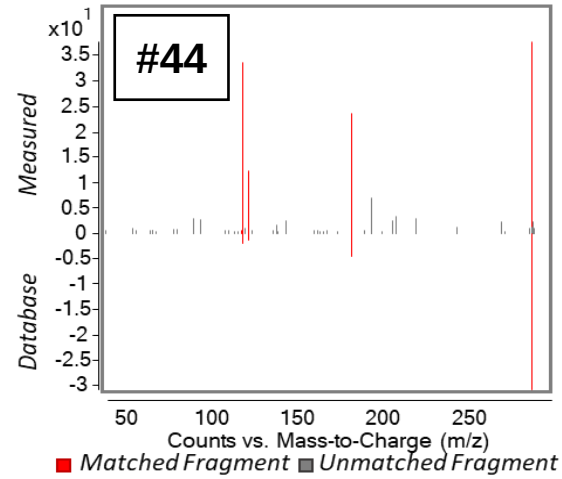

9,10-dihydroxystearic acid, CID: 89377, SIRIUS; [80.25]

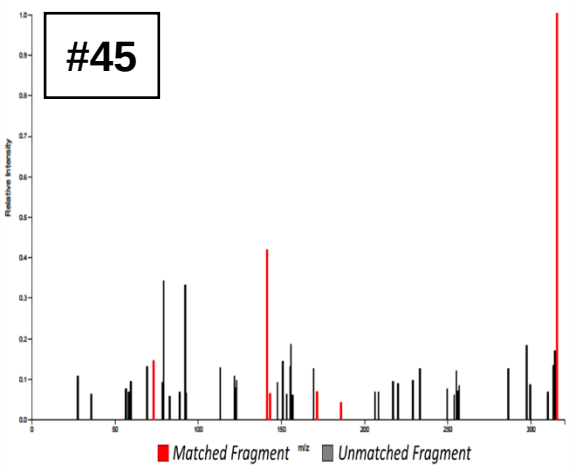

9,10,13-Trihydroxyoctadec-11-enoic acid, CID: 153003, SIRIUS; [91.62]

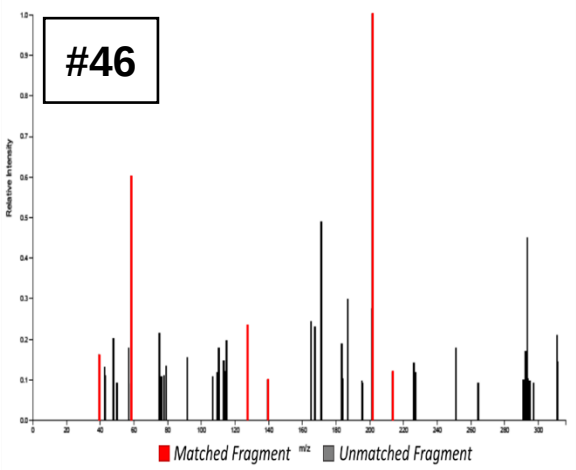

9,12-octadecadiynoic acid, CID: 1931, GNPS; [75]

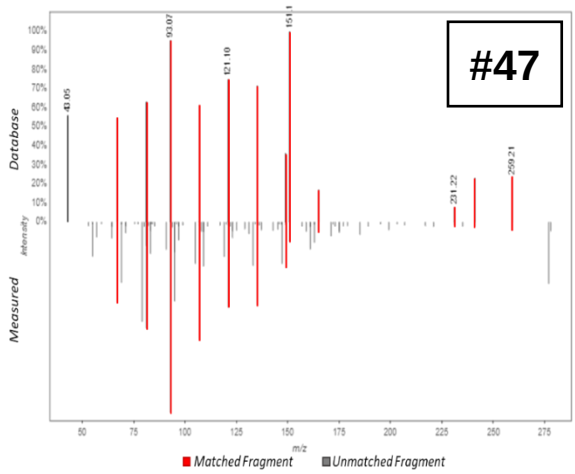

9(10)-EpOME, CID: 6246154, GNPS; [90]

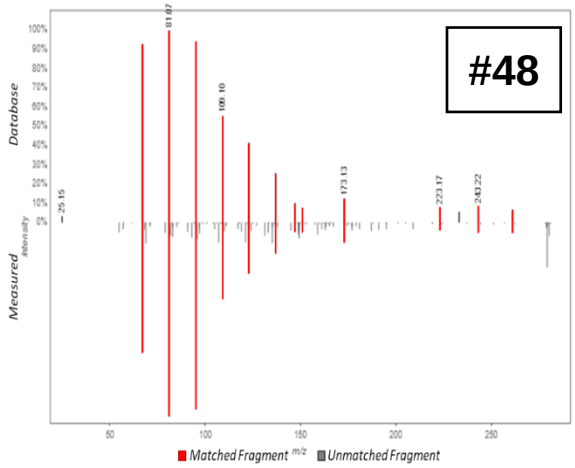

9S,10S,11R-trihydroxy-12Z,15Z-octadecadienoic acid, CID: 16061055, SIRIUS; [94.12]

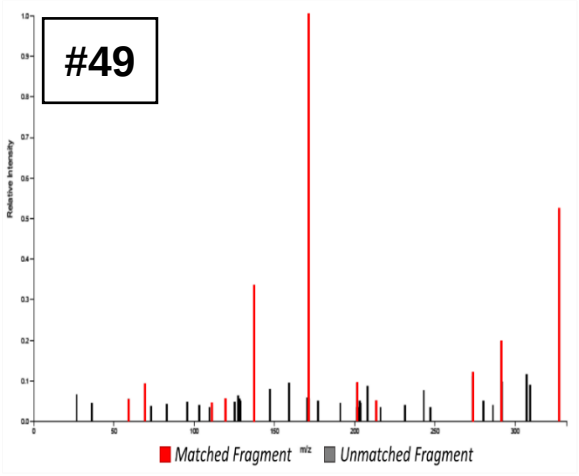

10-hydroxycapric acid, CID: 74300, METLIN; [97.28]

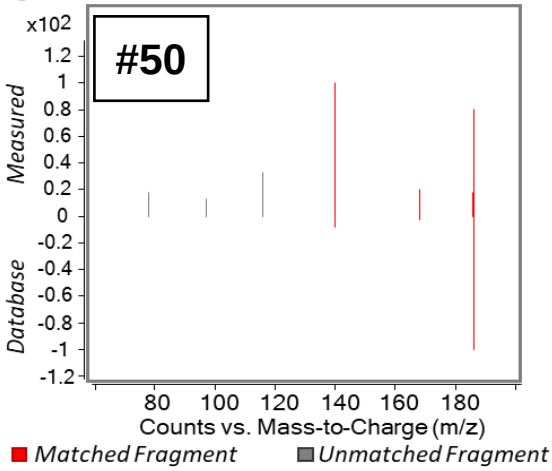

10E-12Z-octadecadienoic acid, CID: 5282944, METLIN; [72.76]

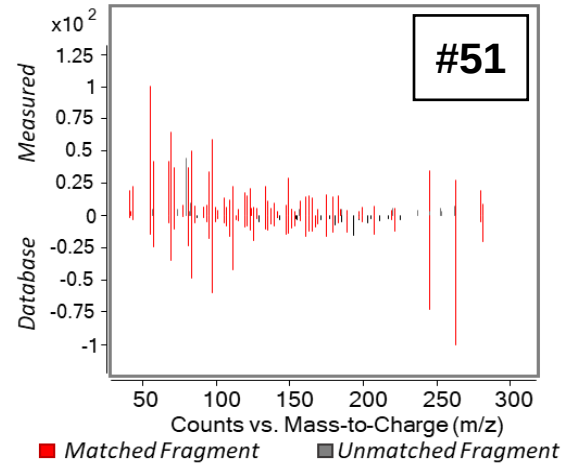

11-hydroxyhexadec-9-enoic acid, CID: 11777937, SIRIUS; [81.94]

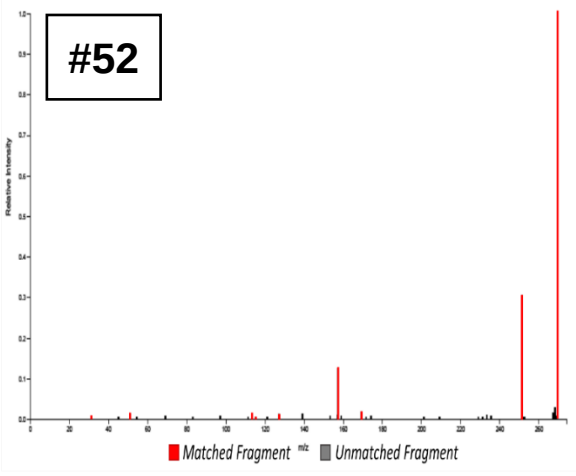

11-oxooctadec-12-enoic acid, CID: 72952636, SIRIUS; [85.99]

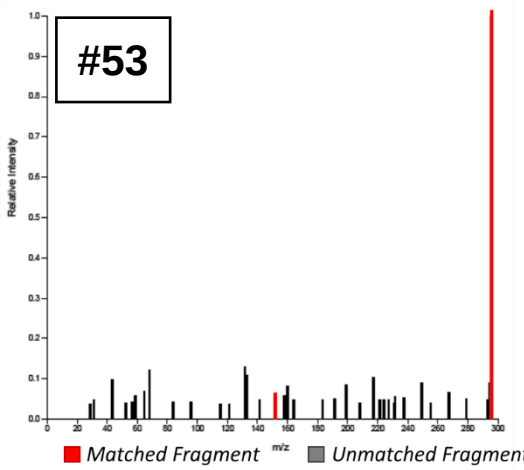

12,13-DiHOME, CID: 10236635, GNPS; [79]

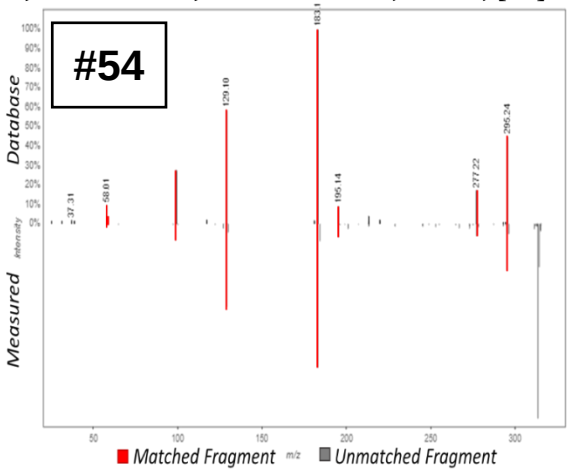

12,13-dihydroxystearic acid, CID: 5282931, SIRIUS; [94.03]

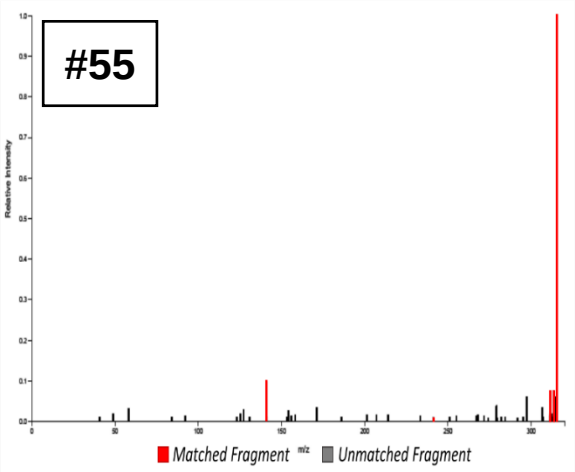

12(13)-EpOME, CID: 5356421, GNPS; [89]

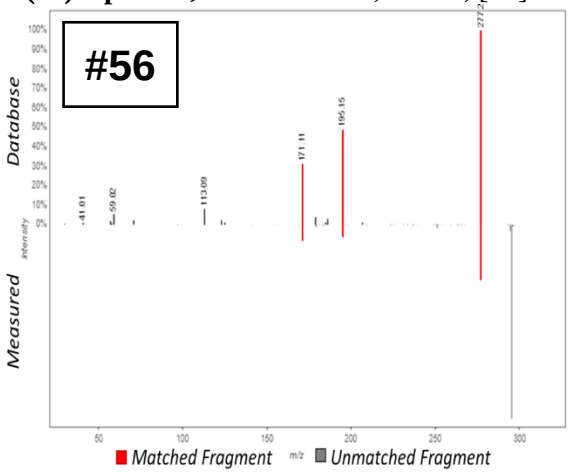

13-amino-13-oxotridecanoic acid, CID: 85711399, SIRIUS; [74.07]

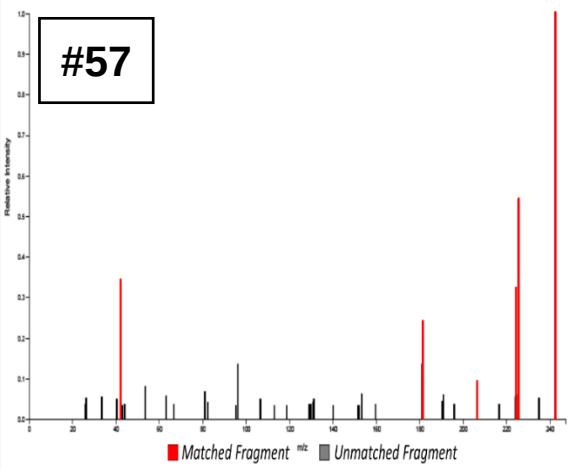

13-docosenamide, CID: 5365371, METLIN; [74.64]

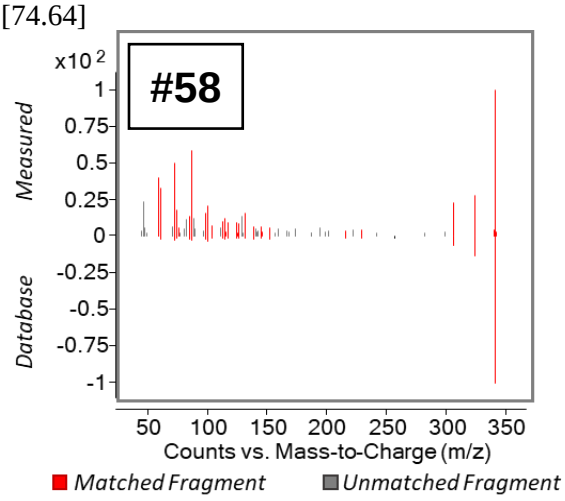

13-HpOTrE, CID: 5282866, METLIN; [70.22]

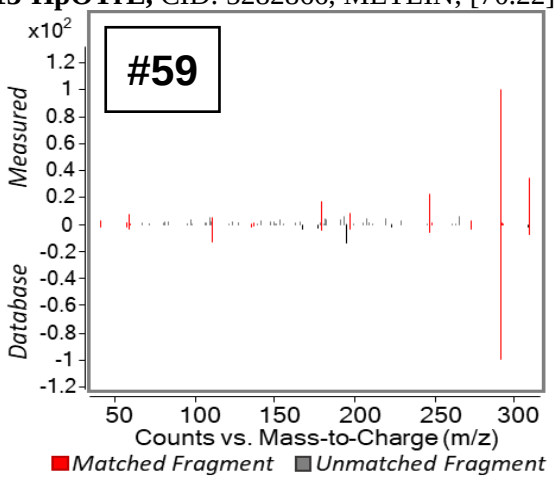

13-OxoODE, CID: 5283012, METLIN; [99.77]

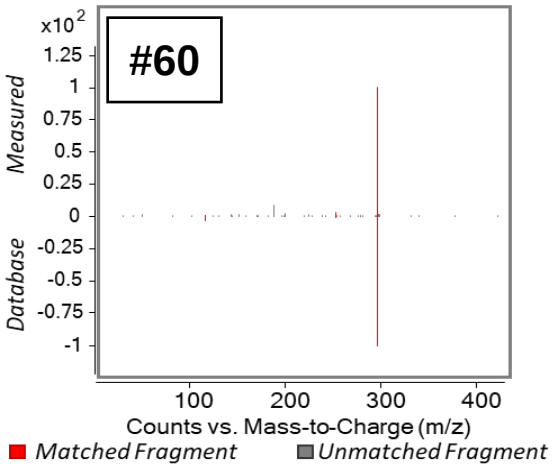

adenine, CID: 190, Agilent LCQTOF Applied Markets; [100]

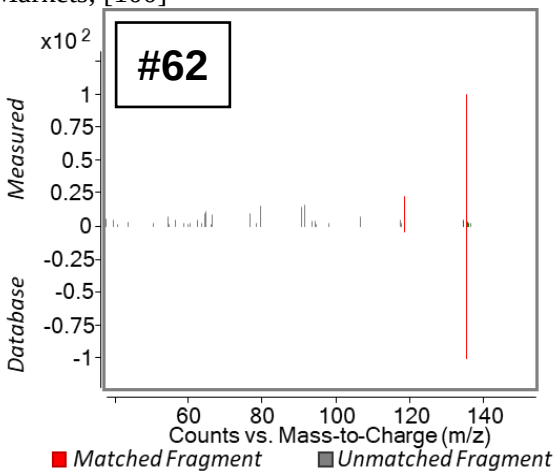

alpha-12,13-DiHODE, CID: 16061067, SIRIUS; [82.94]

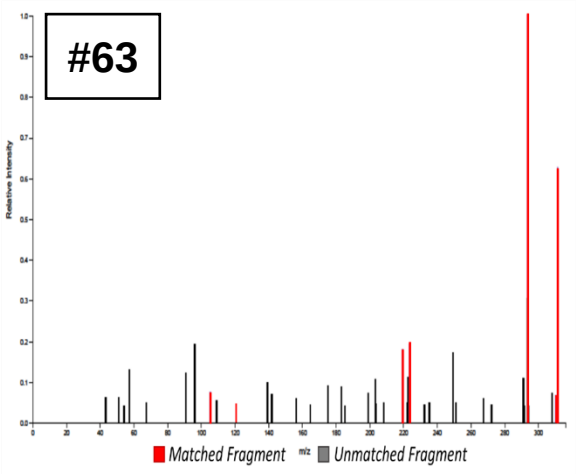

apigenin, CID: 5280443, GNPS; [76]

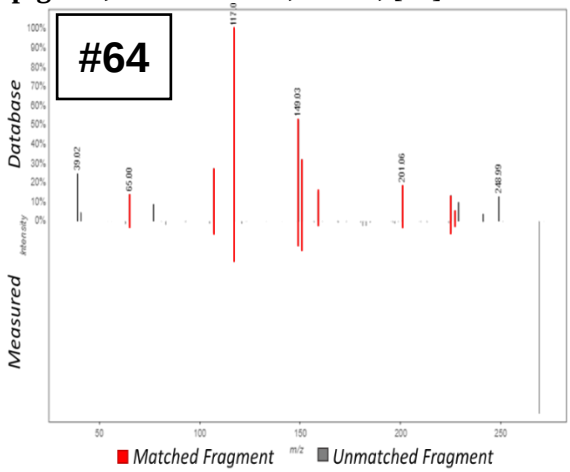

arginine methyl ester, CID: 92932, SIRIUS; [94.08]

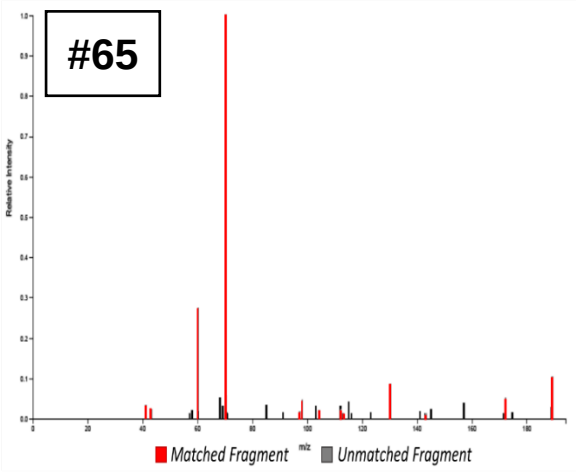

azelaic acid, CID: 2266, GNPS; [97]

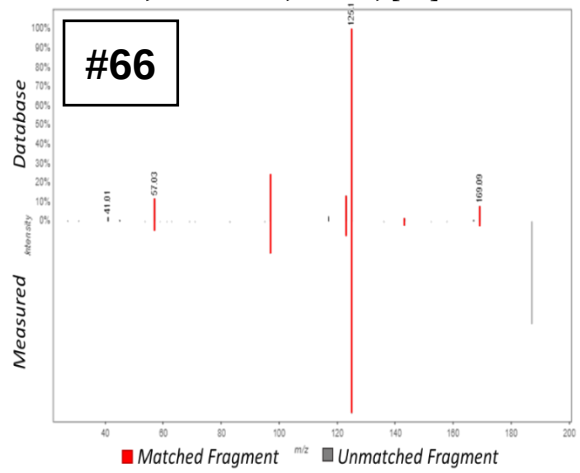

betaine, CID: 247, METLIN, [97.17]

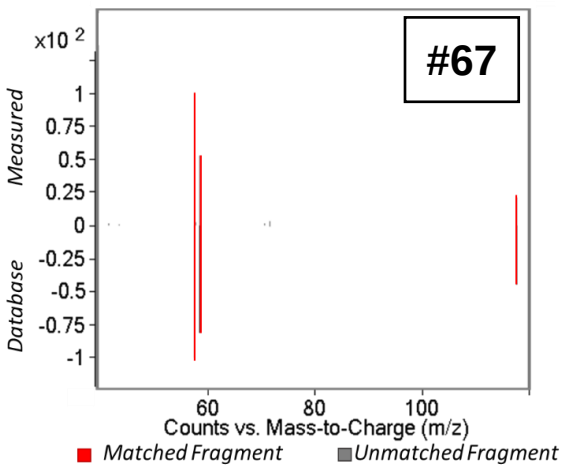

caprylic acid, CID: 379, SIRIUS; [83.02]

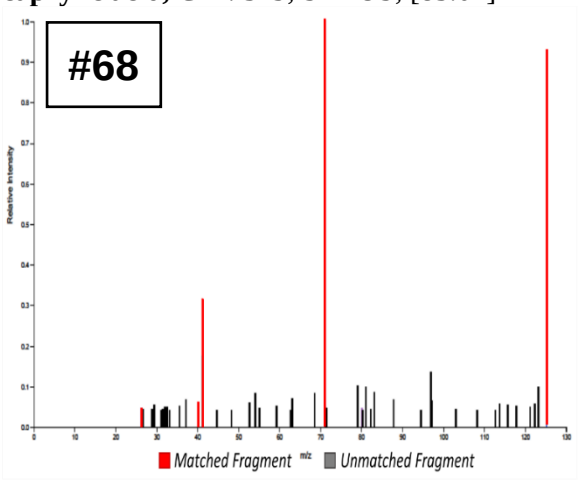

catechol, CID: 289, SIRIUS; [98.86]

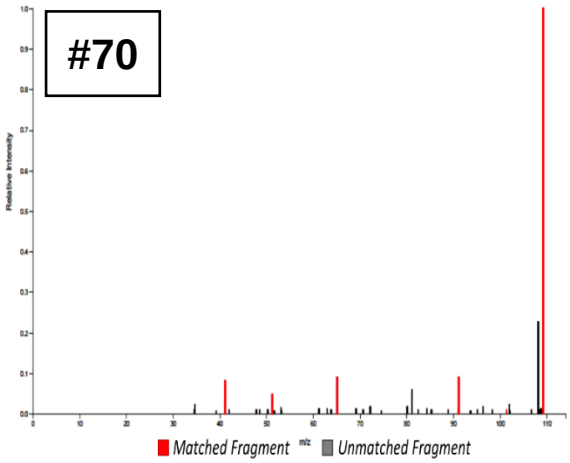

citric acid, CID: 311, GNPS; [97]

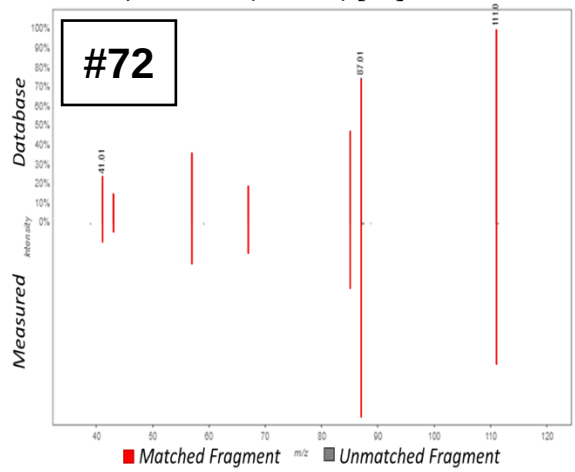

corchorifatty acid D, CID: 85367967, GNPS; [76]

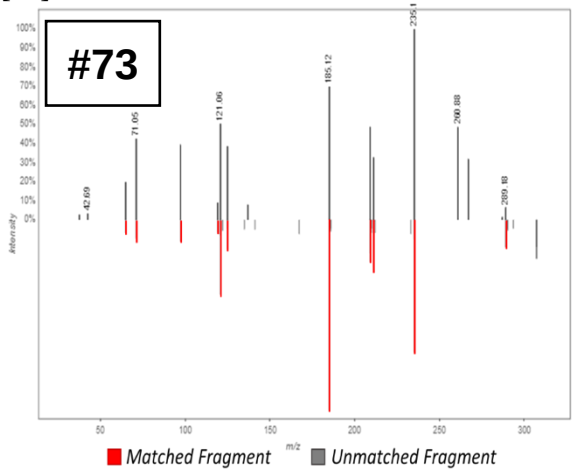

coumaric acid 4-O-glucoside, CID: 9840292, SIRIUS; [98.48]

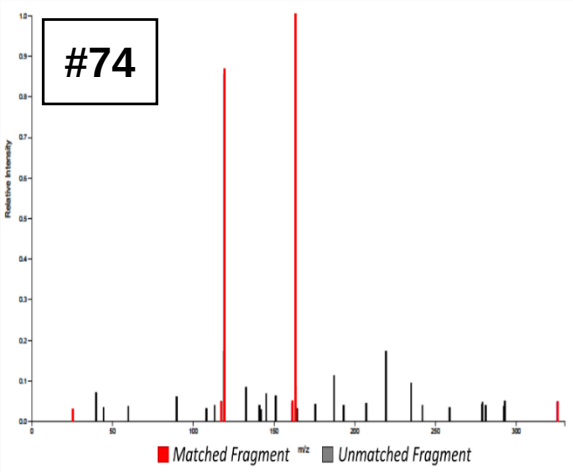

***o*-coumaric acid,** CID: 637540, METLIN; [97.36]

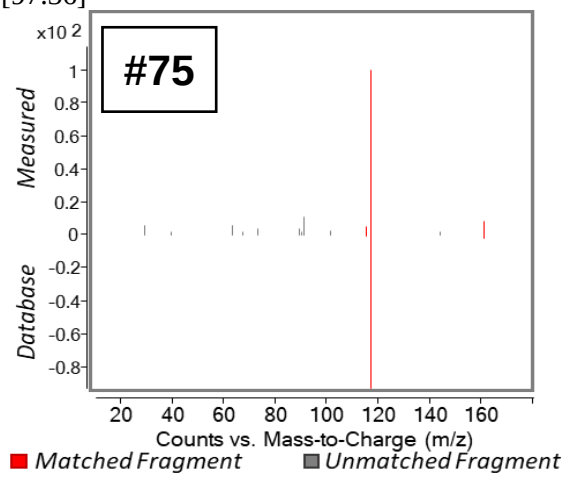

***p*-coumaric acid,** CID: 637542, GNPS; [80]

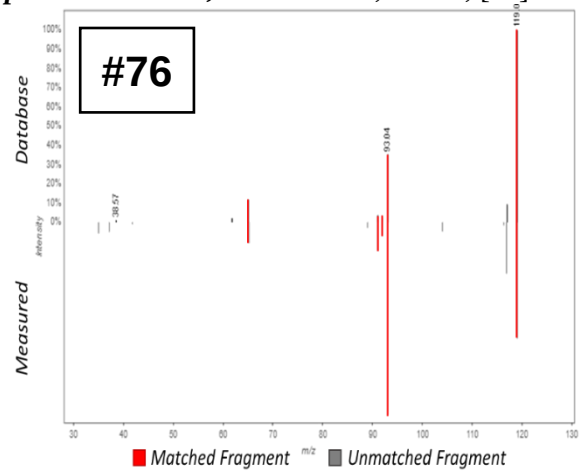

N,N-dimethylpyridin-4-amine, CID: 14284, Agilent LCQTOF Applied Markets; [95.14]

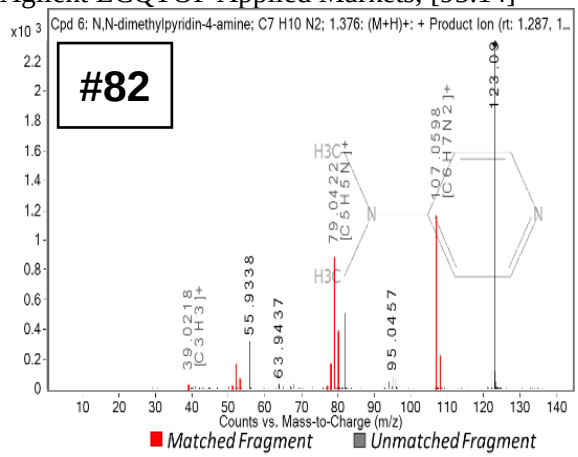

epigallocatechin, CID: 10425234, GNPS; [83]

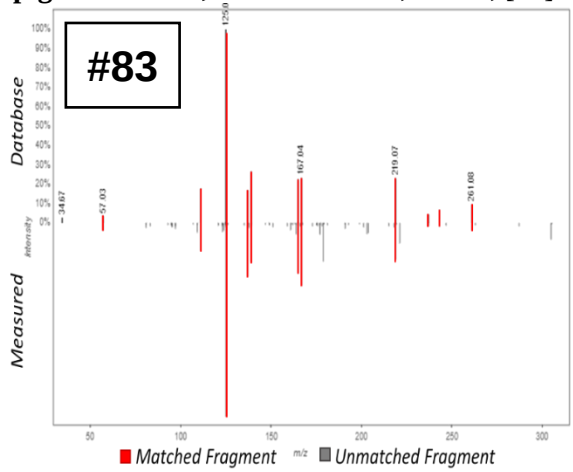

ethyl palmitate, CID: 12366, Agilent LCQTOF Applied Markets; [72.27]

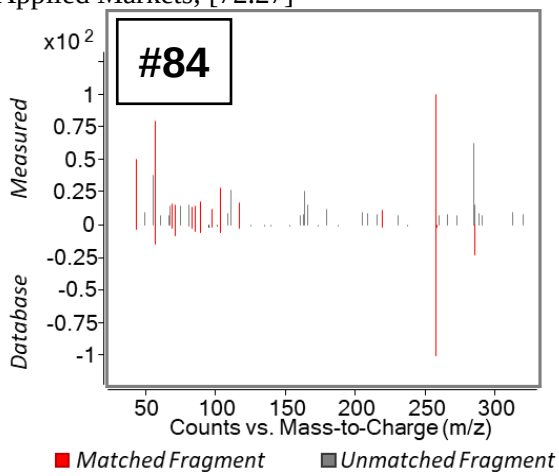

fisetin, CID: 5281614, GNPS; [89]

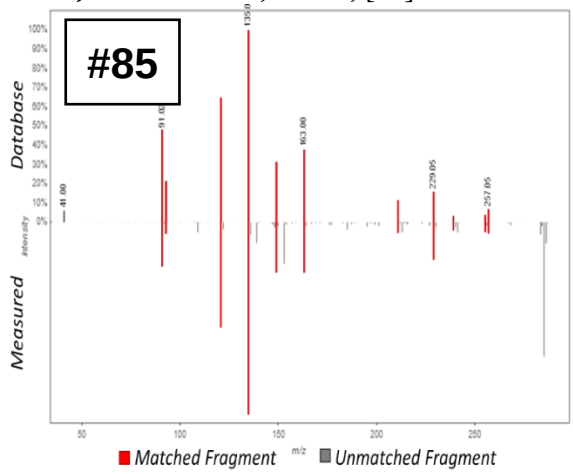

fructosyl leucine, CID: 129689639, GNPS; [85]

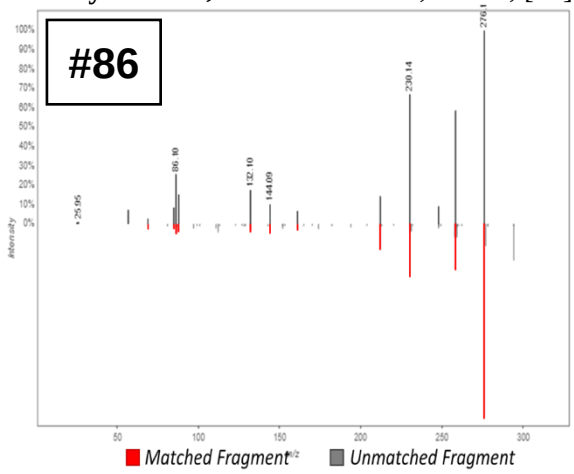

galactaric acid, CID: 3037582, METLIN; [78.87]

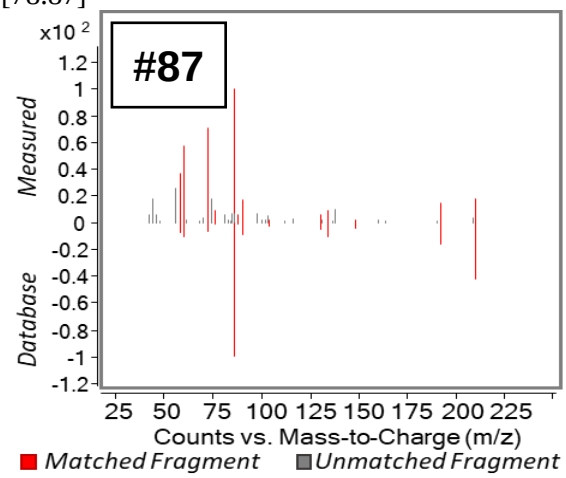

glycerophosphocholine, CID: 657272, METLIN; [78.77]

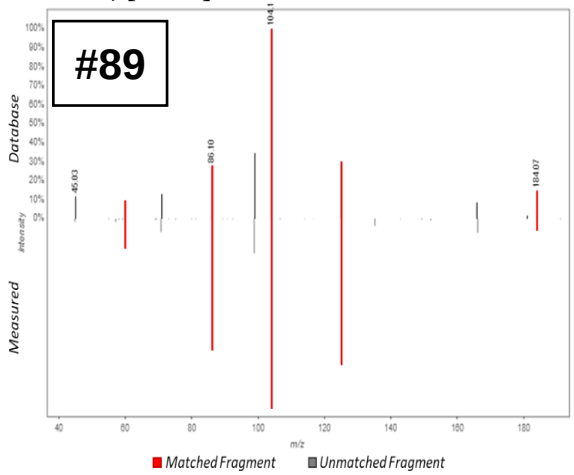

gluconic acid, CID: 152304, GNPS; [85]

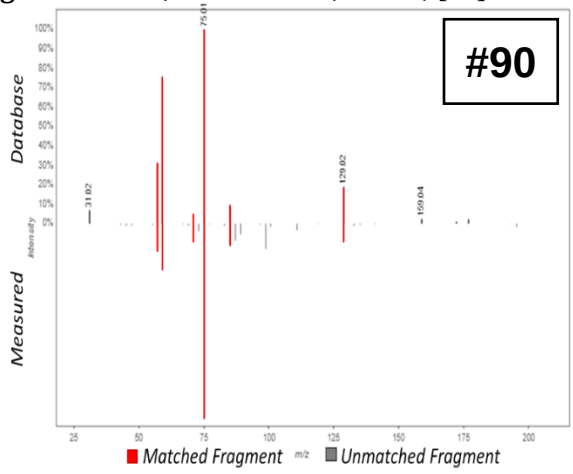

heptanoic acid, CID: 8094, SIRIUS; [82.86]

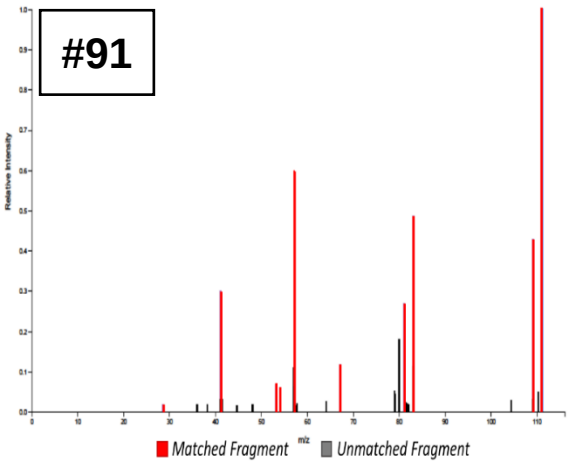

hexadecanedioic acid, CID: 10459, METLIN; [90.85]

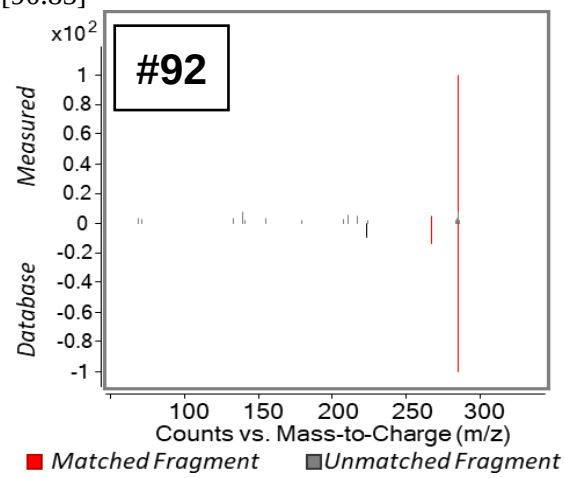

homogentisic acid, CID: 780, SIRIUS; [79.75]

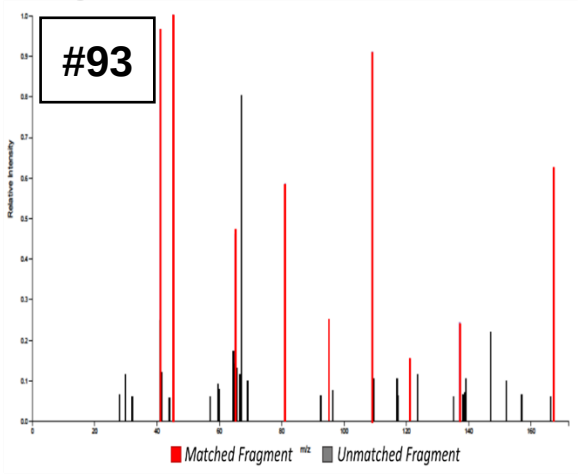

homoveratric acid, CID: 7139, SIRIUS; [89.12]

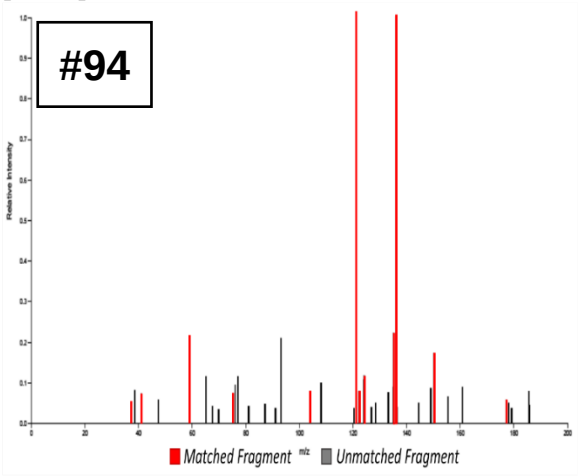

hydroquinone, CID: 785, SIRIUS; [96.34]

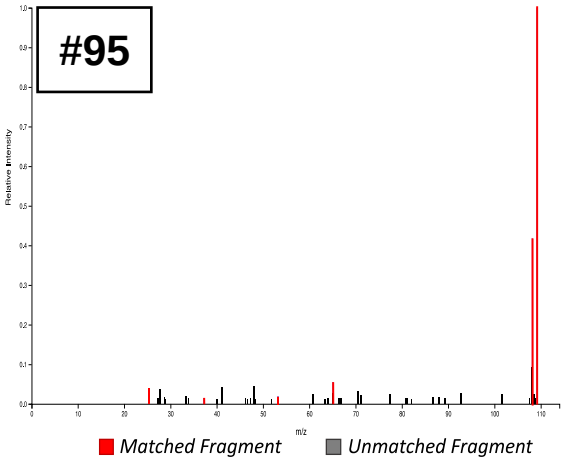

DL-b-hydroxycaprylic acid, CID: 110974, METLIN; [99.68]

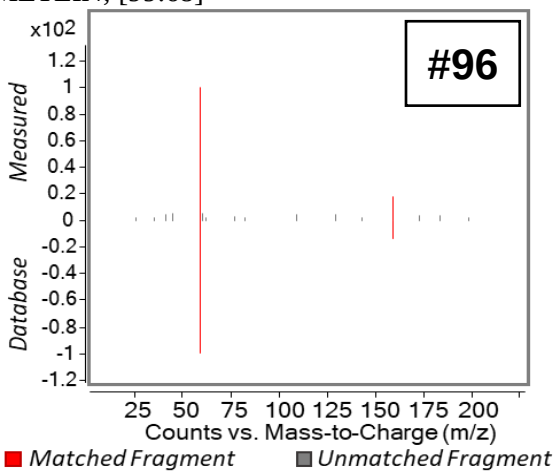

hyperoside, CID: 5281643, GNPS; [74]

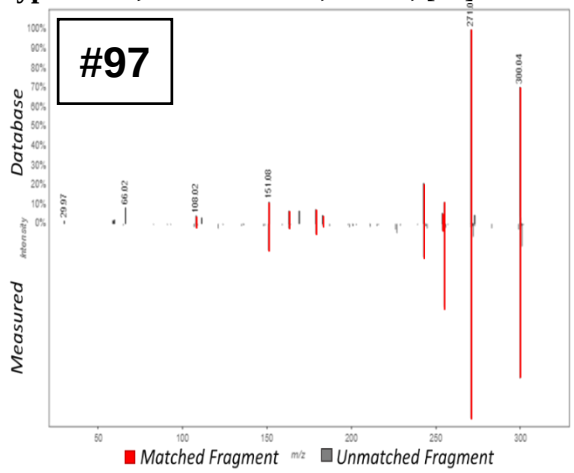

indoline, CID: 10328, SIRIUS; [71.21]

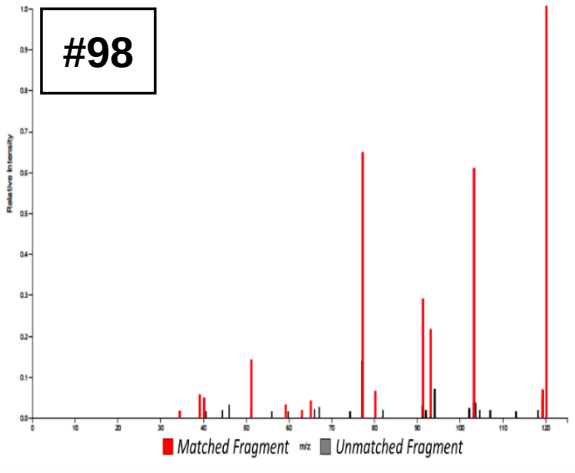

isokaempferide, CID: 5280862, Agilent LCQTOF Applied Markets; [99.21]

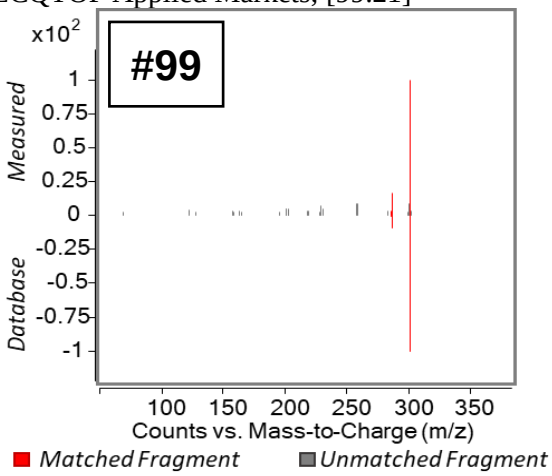

L-isoleucine, CID: 6306, METLIN; [98.71]

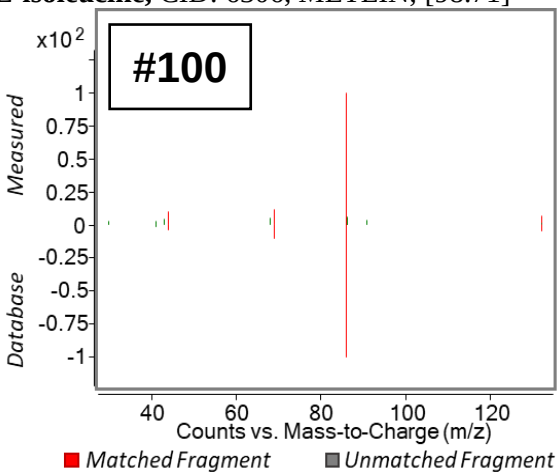

isopalmitic acid, CID: 36247, GNPS; [80]

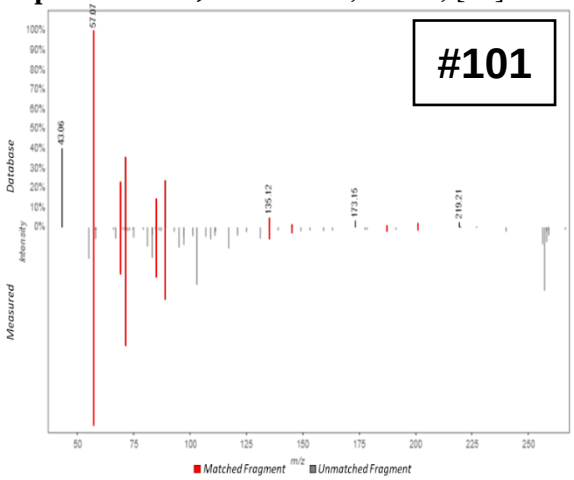

itaconic acid, CID: 811, SIRIUS; [88.42]

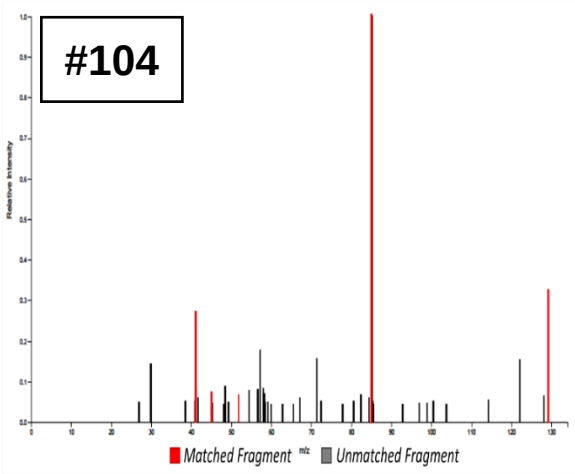

kaempferol 7-O-glucoside, CID: 10095180, Agilent LCQTOF Applied Markets; [81.57]

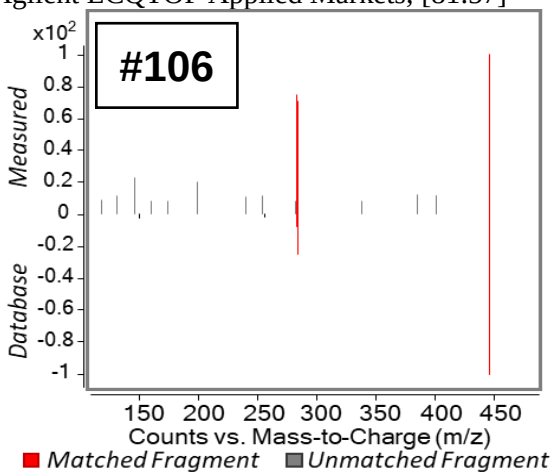

L-leucine, CID: 6106, METLIN; [88.47]

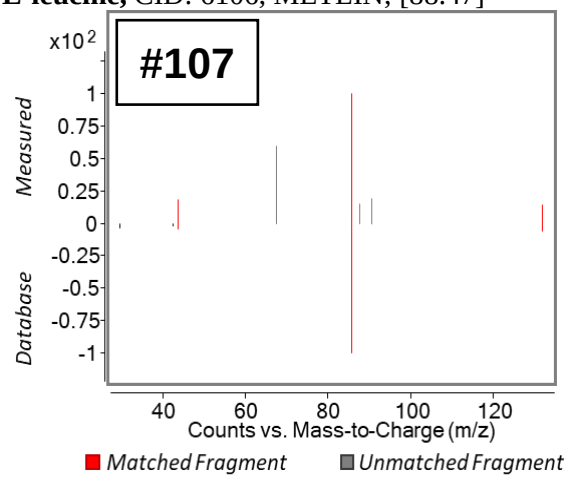

larixinic acid, CID: 8369, METLIN; [85.36]

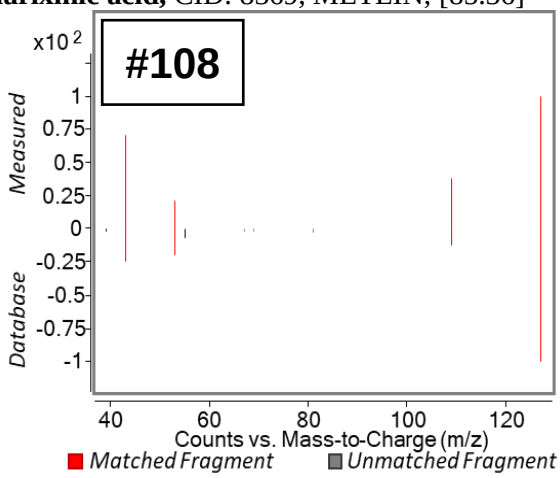

leucyl proline, CID: 80817, METLIN; [94.4]

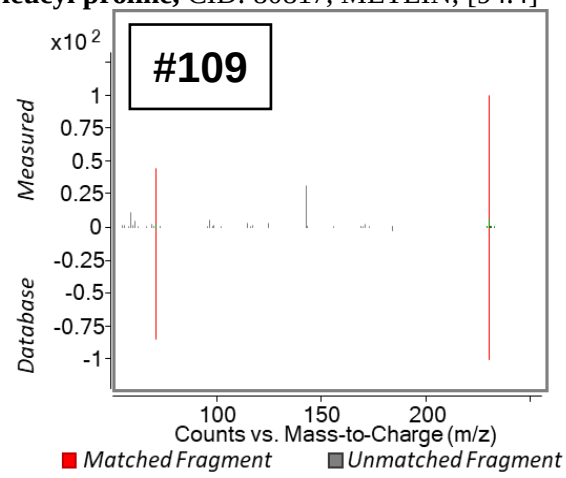

leucyl leucine, CID: 94244, METLIN; [90.06]

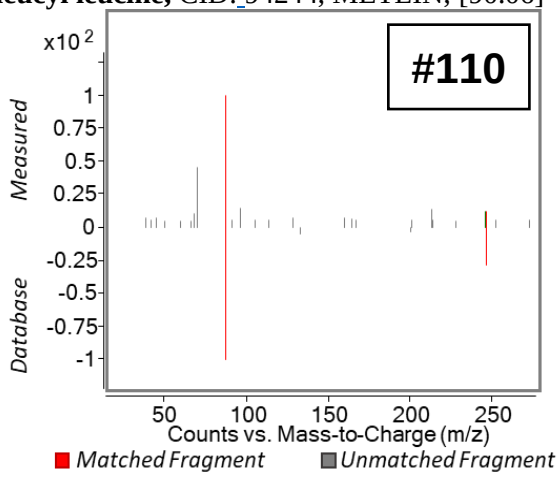

linolenic acid, CID: 5280934, GNPS; [86]

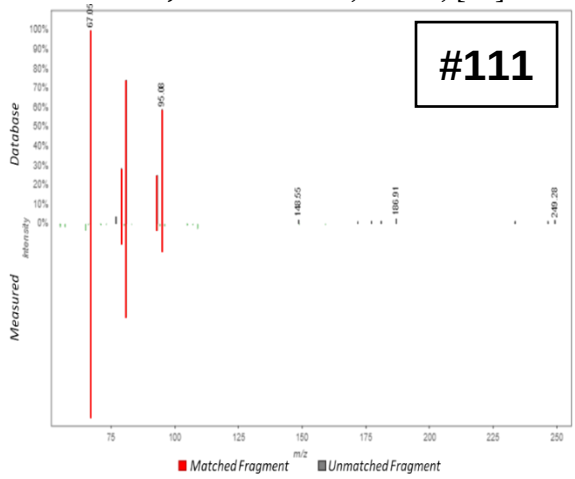

linoleoyl ethanolamide, CID: 5283446, METLIN; [86.46]

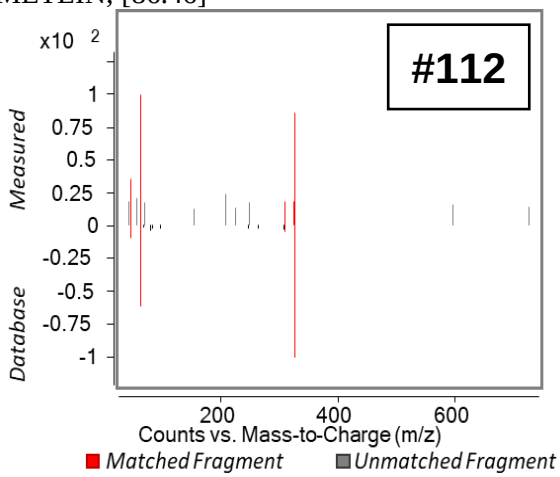

loliolide, CID: 100332, GNPS; [89]

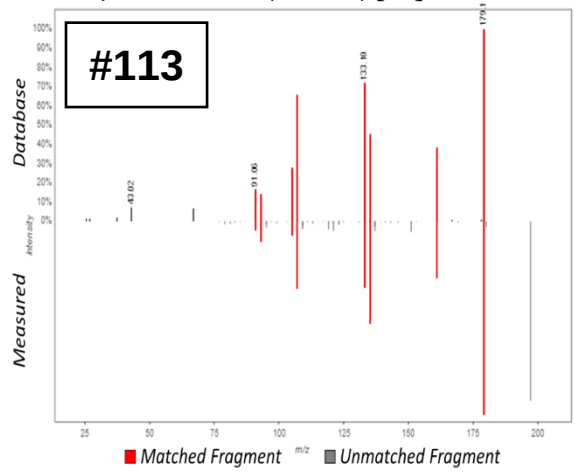

luteolin, CID: 5280445, GNPS; [91]

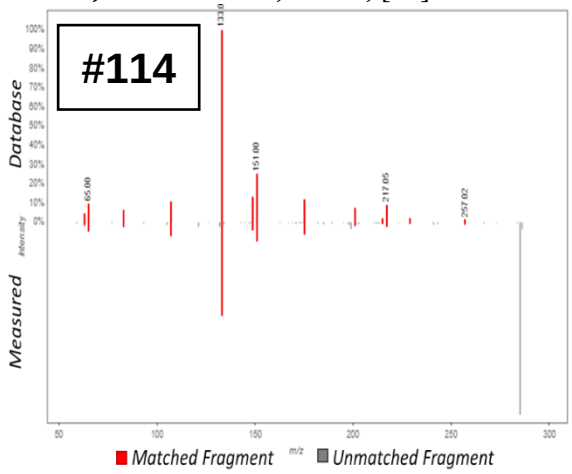

lycaonic acid, CID: 94770, SIRIUS; [75.17]

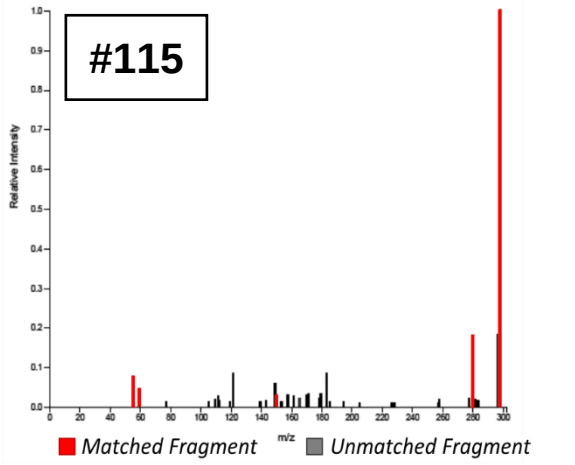

LysoPC(16:0), CID: 10097314, GNPS; [83]

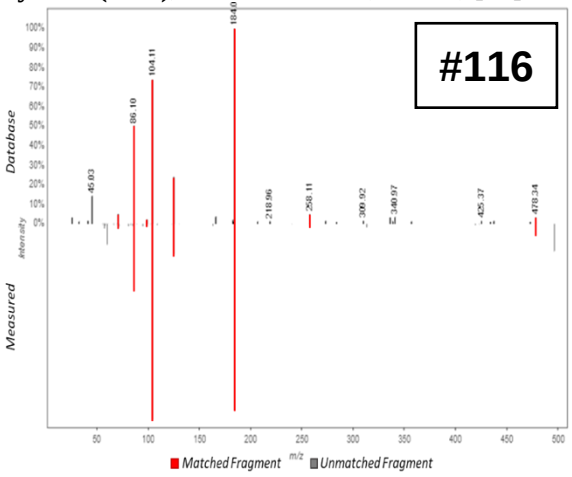

LysoPC(18:1), CID: 16081932, GNPS; [81]

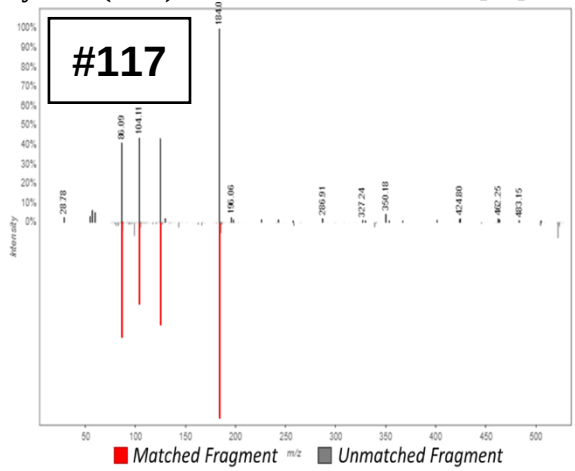

LysoPC(18:2), CID: 24779469, SIRIUS; [94.3]

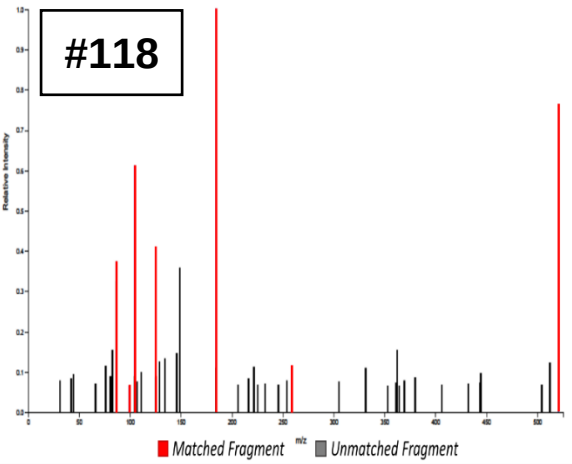

LysoPC (18:3), CID: 11005824, SIRIUS; [86.23]

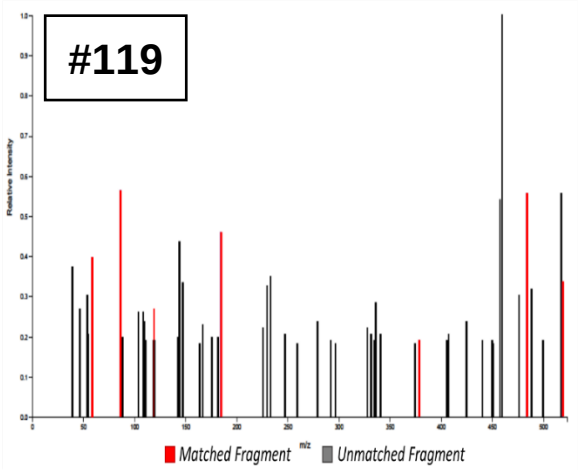

LysoPE(16:0), CID: 9547069, GNPS; [75]

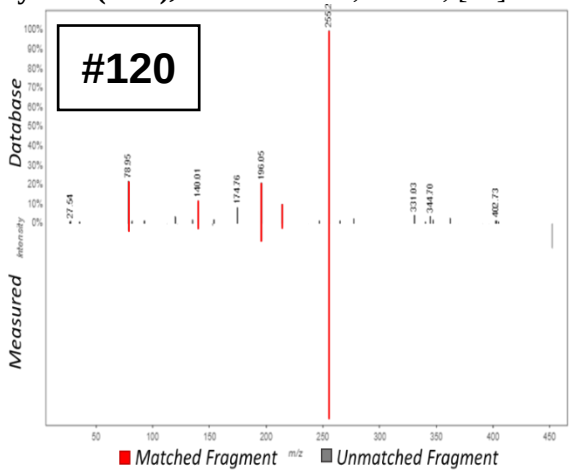

maltose, CID: 6255, GNPS; [82]

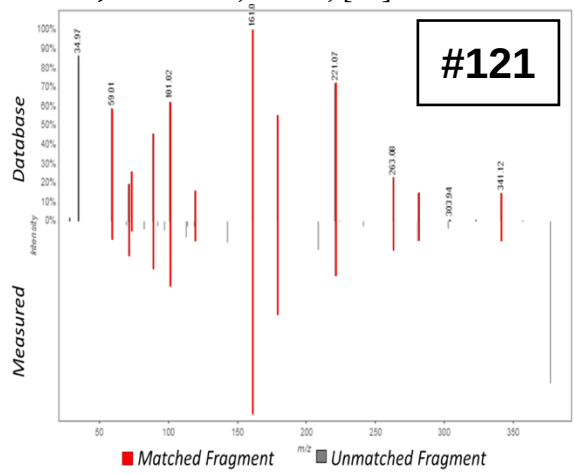

methyl citrate, CID: 12566215, SIRIUS; [95.14]

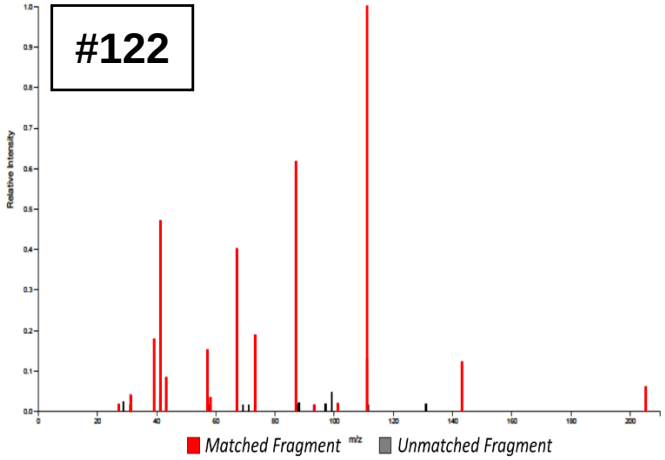

methyl leucine, CID: 6106, SIRIUS; [89.71]

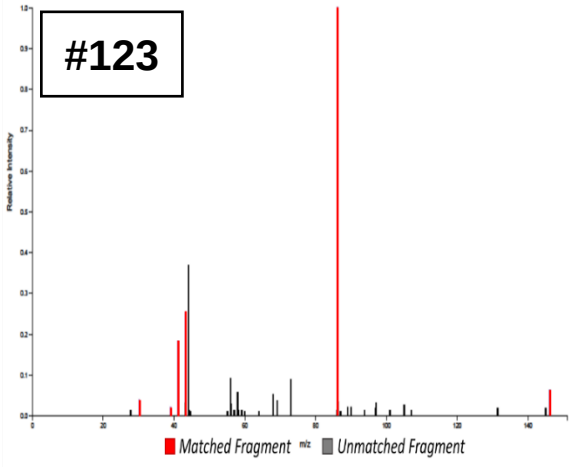

methyl palmitate, CID: 8181, Agilent LCQTOF Applied Markets PCDL; [83.68]

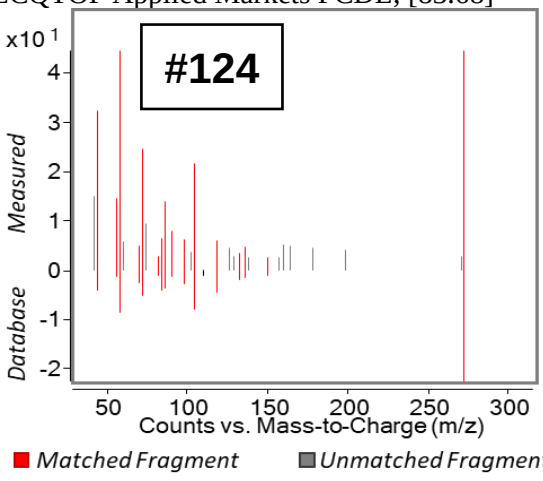

methylgallic acid, CID: 20223962, SIRIUS; [70.74]

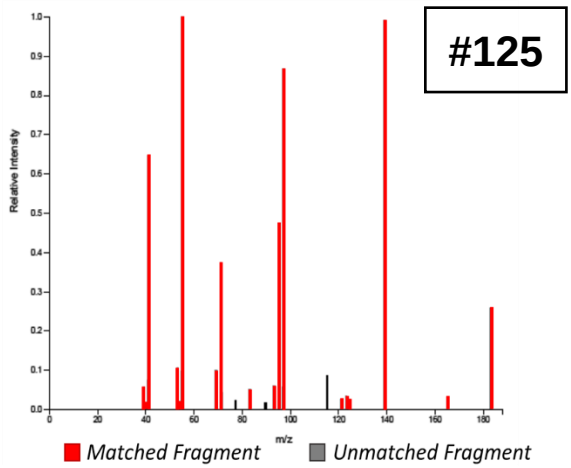

monoolien, CID: 5283468, GNPS; [82]

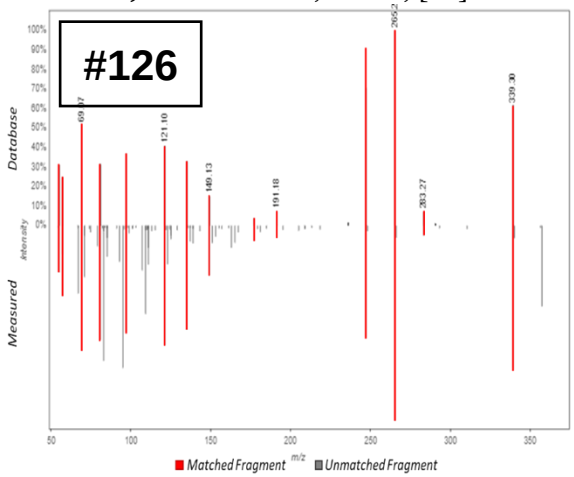

monopalmitin, CID: 14900, SIRIUS; [97.28]

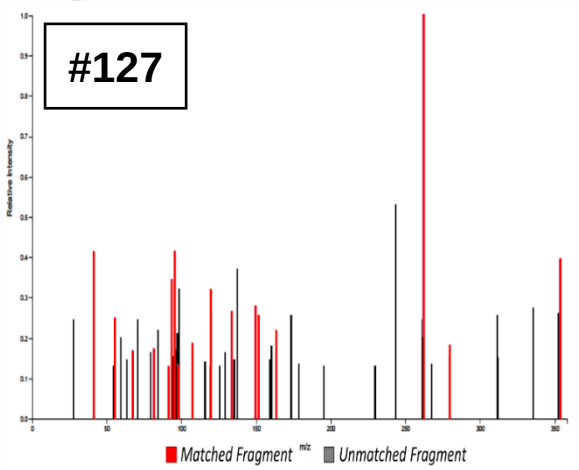

myricetin, CID: 5281672, METLIN; [78.03]

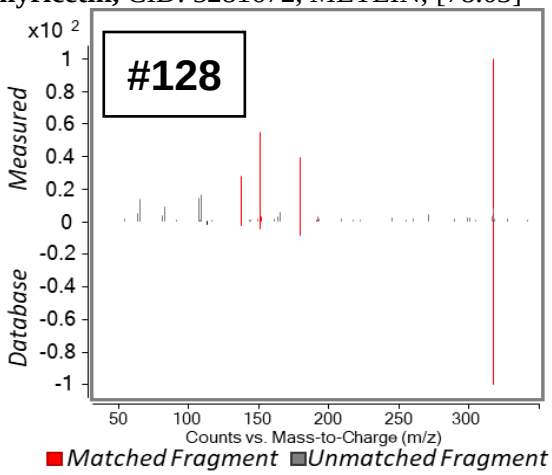

myricetin 3-O-galactoside, CID: 5491408, GNPS; [75]

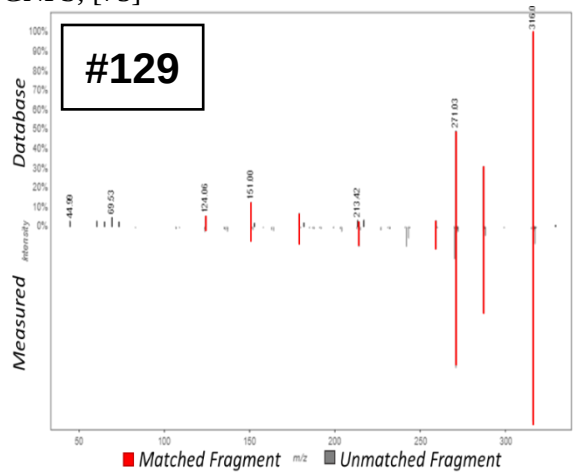

nevadensin, CID: 160921, GNPS; [77]

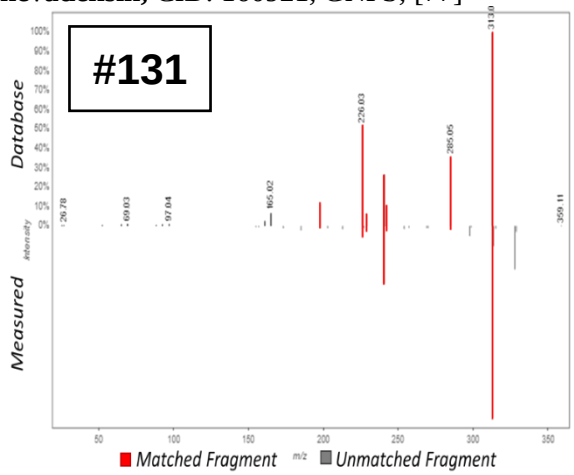

nicotinic acid, CID: 938, METLIN; [91.76]

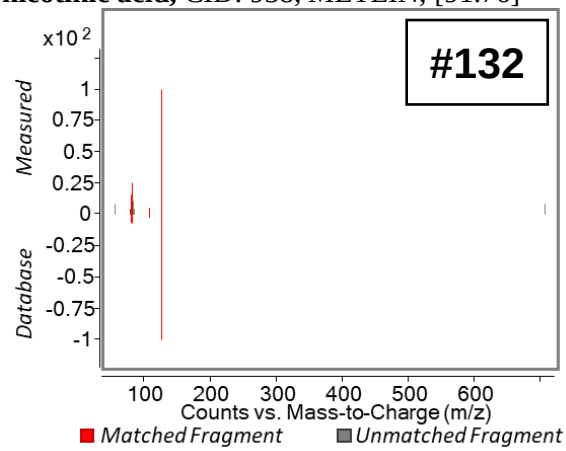

nonanoic acid, CID: 8158, SIRIUS; [86.49]

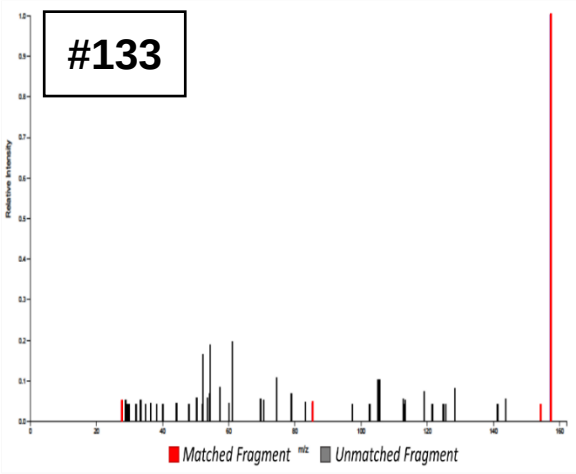

oleoyl ethanolamide, CID: 5283454, METLIN; [87.28]

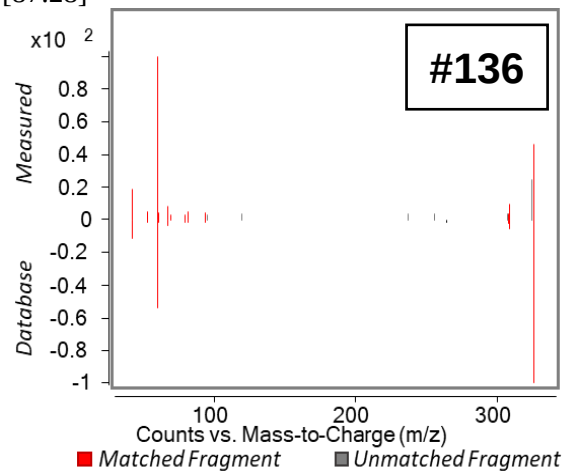

palmitamide, CID: 69421, Agilent QTOF Applied Markets; [98.62]

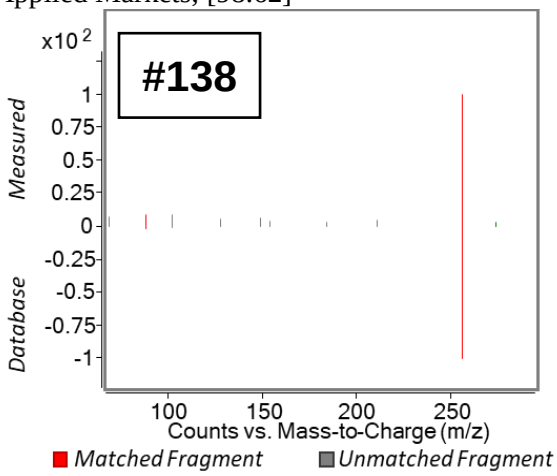

PE(18:1(9Z)/0:0), CID: 9547071, METLIN; [89.84]

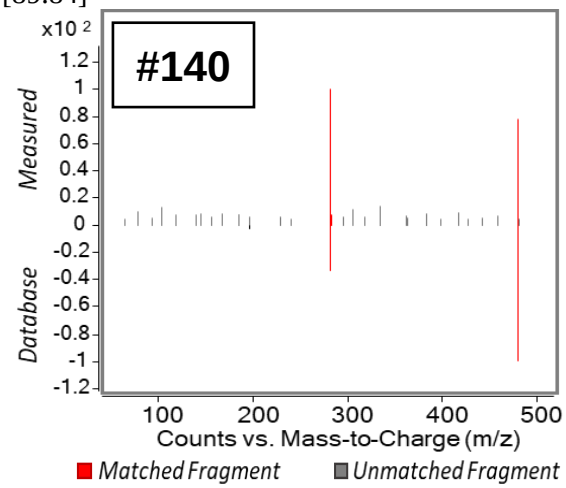

DL-phenylalanine, CID: 994, METLIN; [96.24]

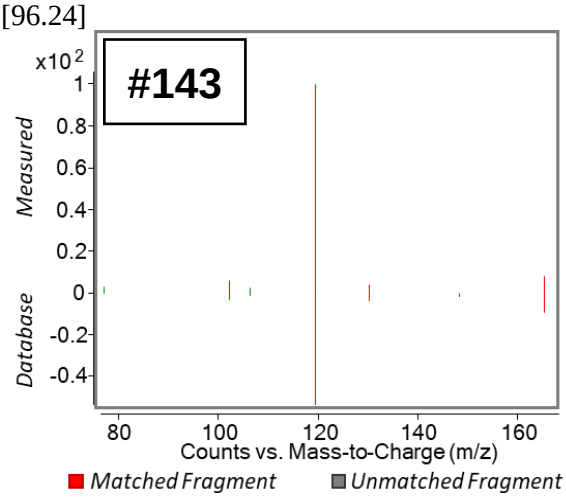

phloridzin, CID: 6072, METLIN; [90.1]

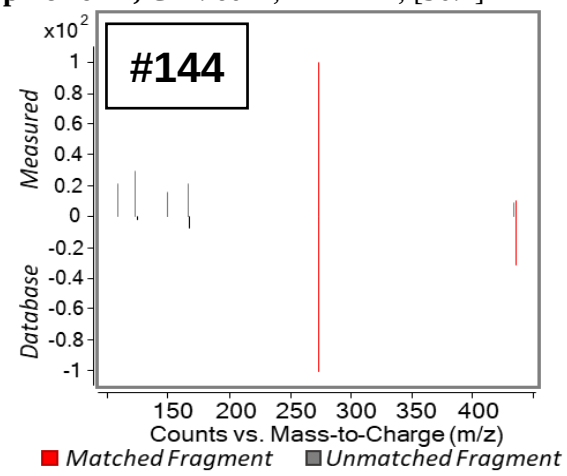

phytosphingosine, CID: 122121, GNPS; [93]

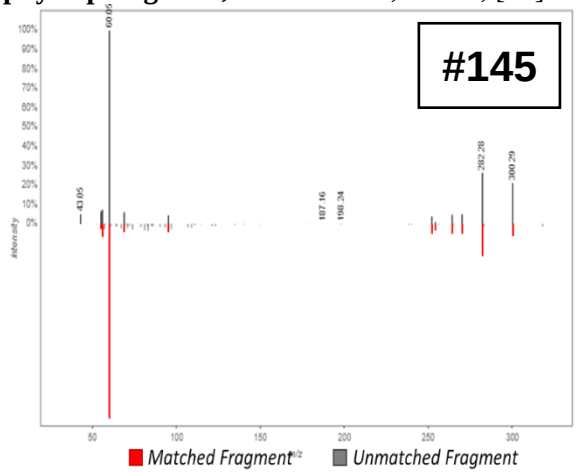

pimelic acid, CID: 385, SIRIUS; [97.75]

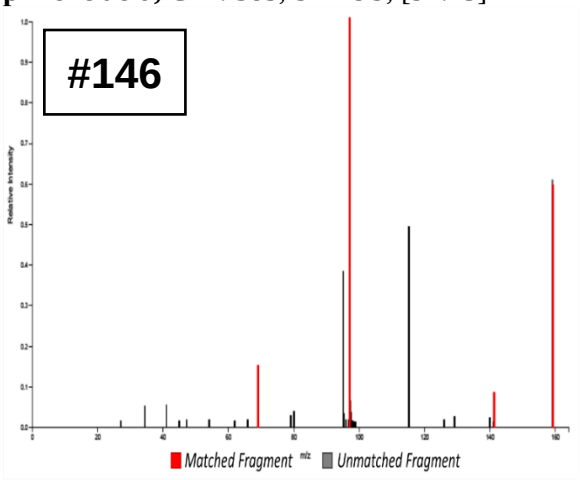

DL-pipecolic acid, CID: 849, METLIN; [96.56]

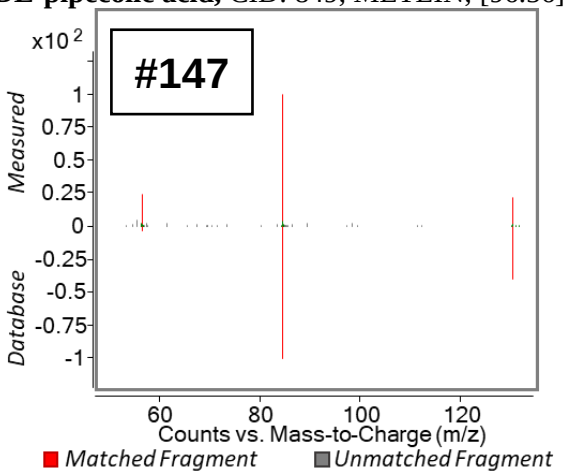

protocatechuic acid, CID: 72, METLIN; [100]

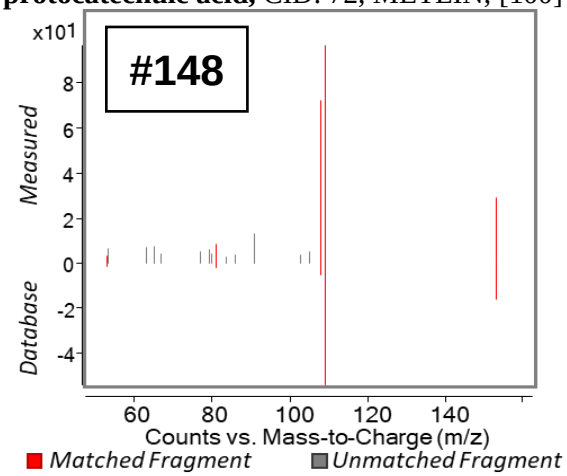

purine, CID: 1044, SIRIUS; [99.3]

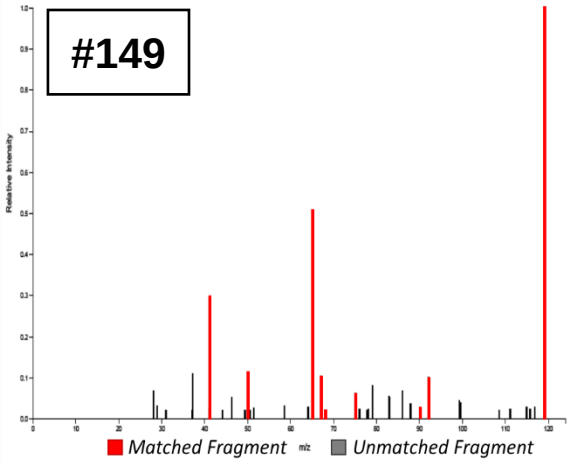

pyrogallol, CID: 1057, SIRIUS; [97.06]

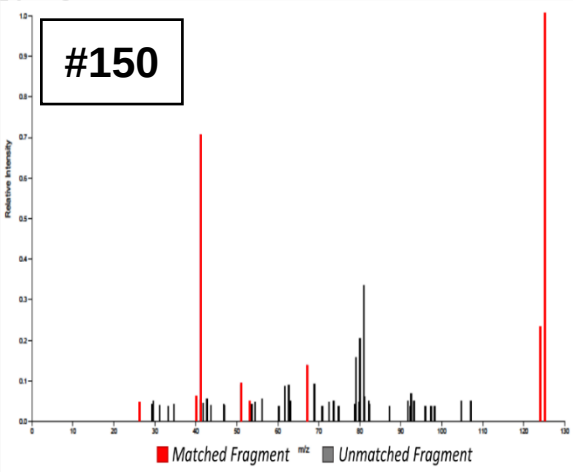

rosilic acid, CID: 9561835, SIRIUS; [99.12]

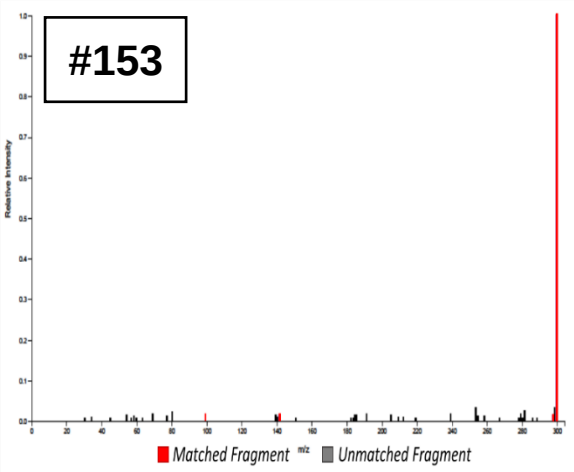

sambucinol, CID: 5459101, Agilent LCQTOF Applied Markets; [89.26]

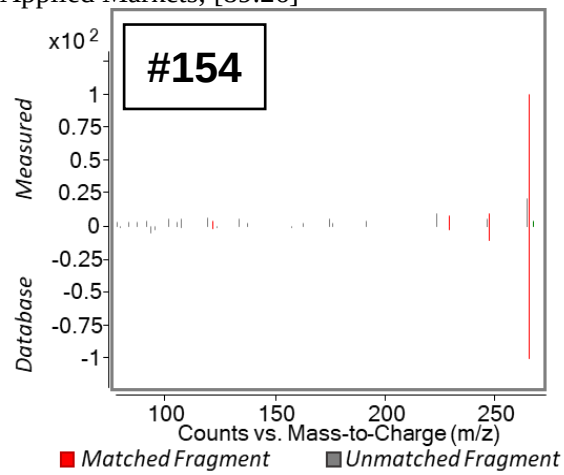

sebacic acid, CID: 5192, GNPS; [93]

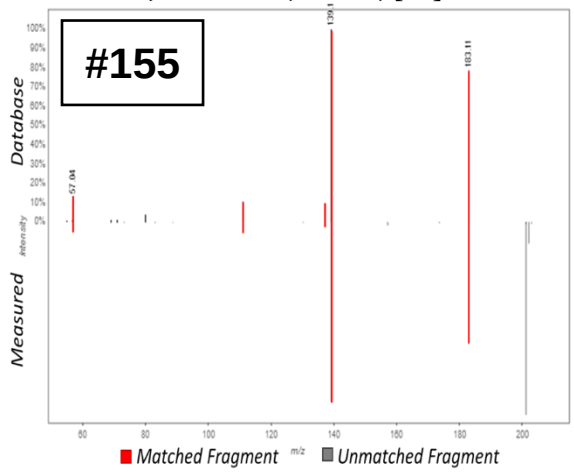

secoisolariciresinol, CID: 65373, GNPS; [91]

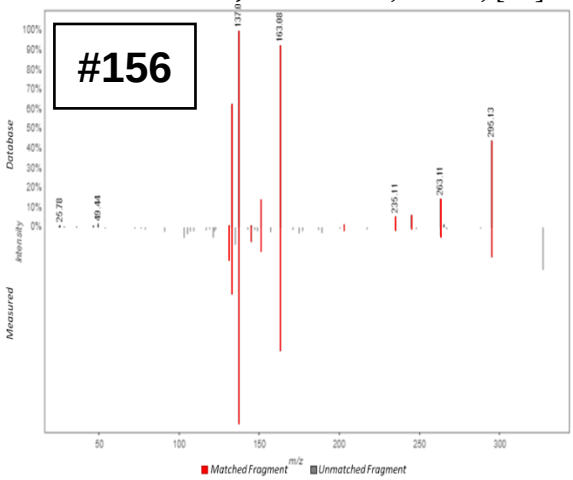

sinapic acid, CID: 637775, GNPS; [74]

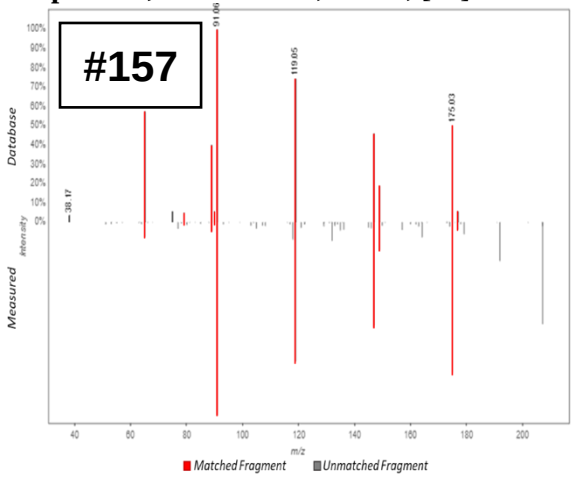

sphinganine, CID: 91486, GNPS; [95]

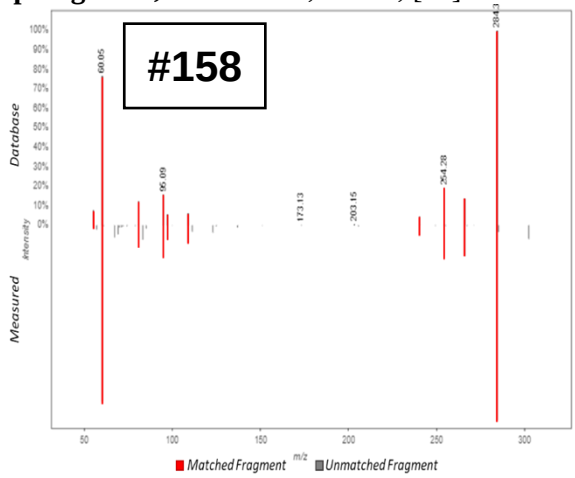

stearidonic acid, CID: 5312508, SIRIUS; [92.31]

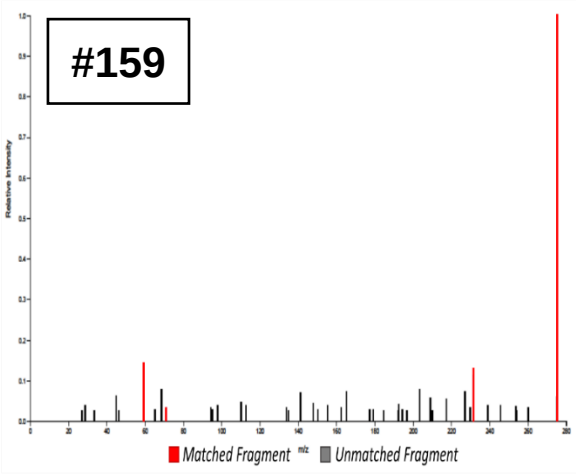

suberic acid, CID: 10457, GNPS; [95]

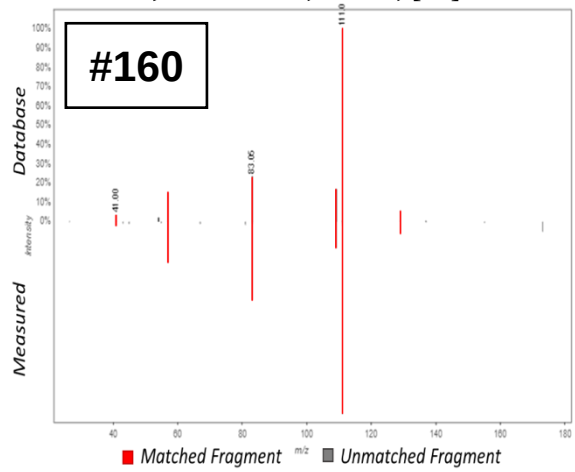

sucrose, CID: 5988, METLIN; [99.7]

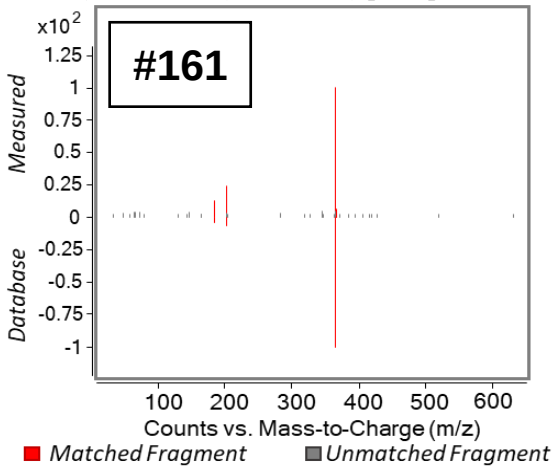

tachioside, CID: 11962143, SIRIUS; [99.16]

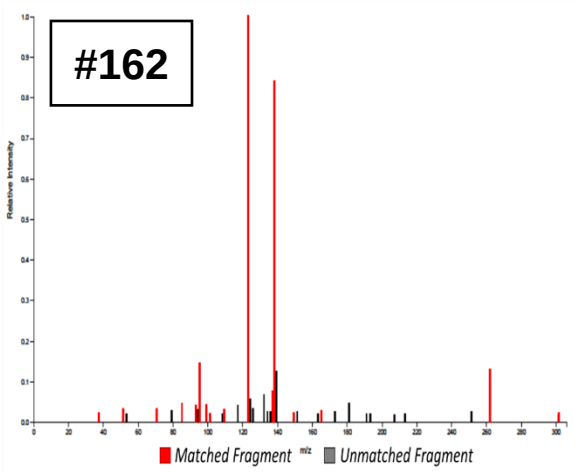

trans-EKODE-(E)-Ib, CID: 5283007, METLIN; [73.47]

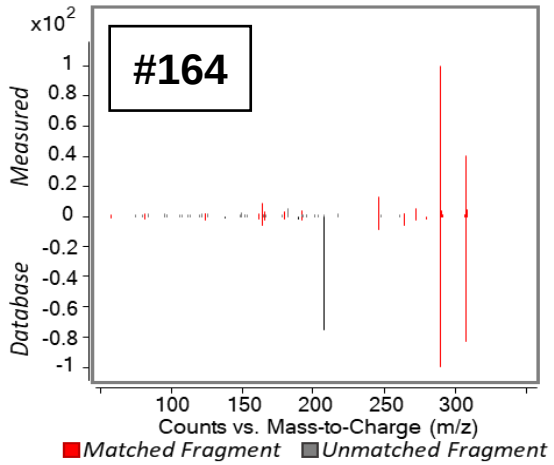

trans-resveratrol, CID: 445154, MoNA HCD Natural Products Library; [70.71]

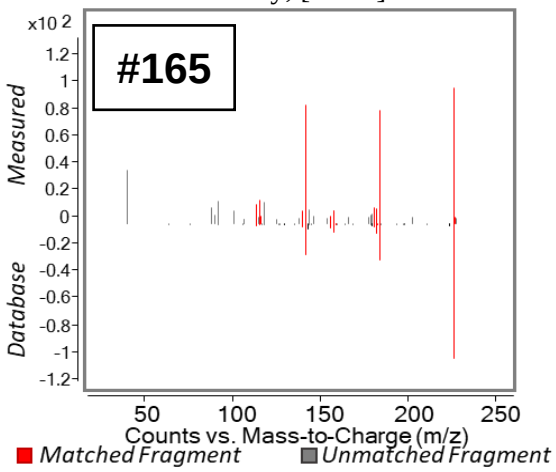

tricin, CID: 5281702, GNPS; [85]

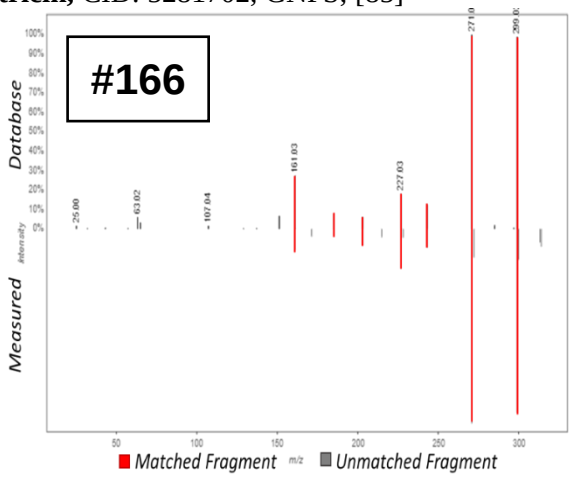

tridecanedioic acid, CID: 10458, Agilent LCQTOF Applied Markets; [86]

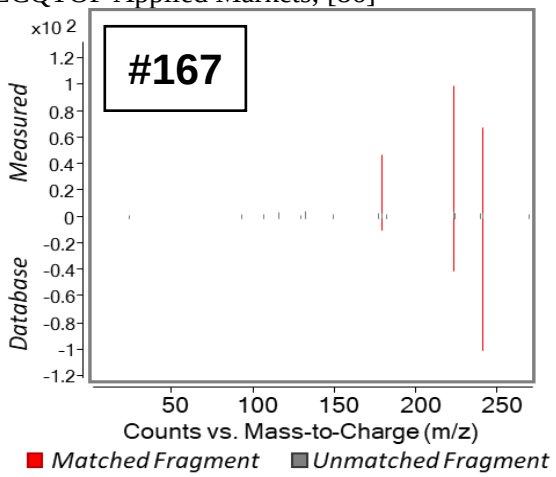

L-tryptophan, CID: 6305, GNPS; [90]

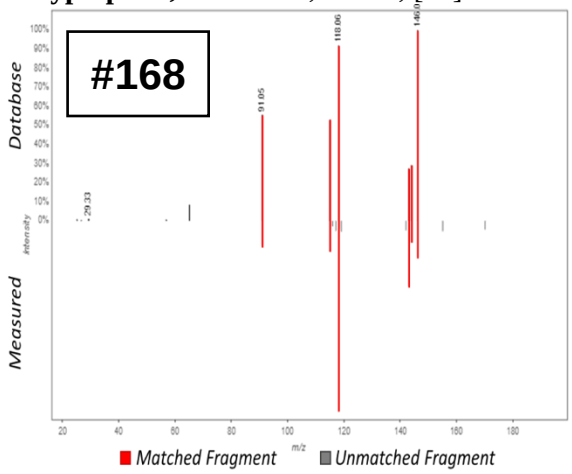

undecanedioic acid, CID: 15816, Agilent LCQTOF Applied Markets; [96.46]

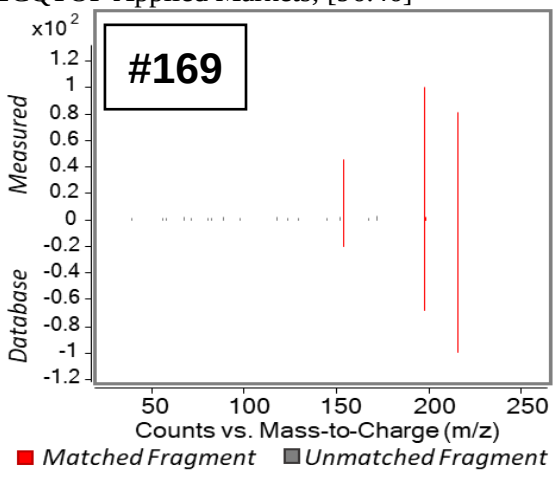

usnic acid, CID: 5646, Agilent LCQTOF Applied Markets; [74.57]

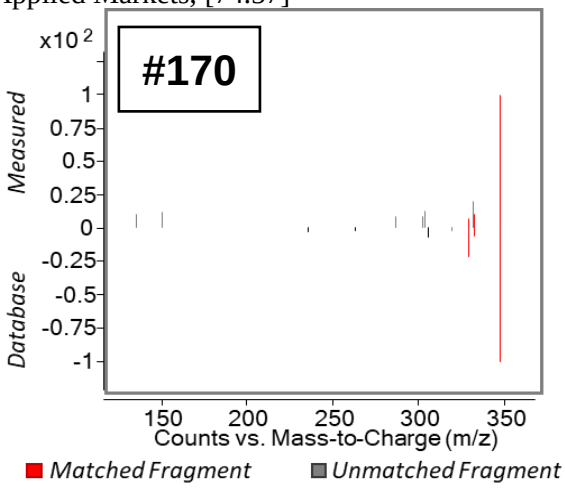

velutin, CID: 6710647, SIRIUS; [97.06]

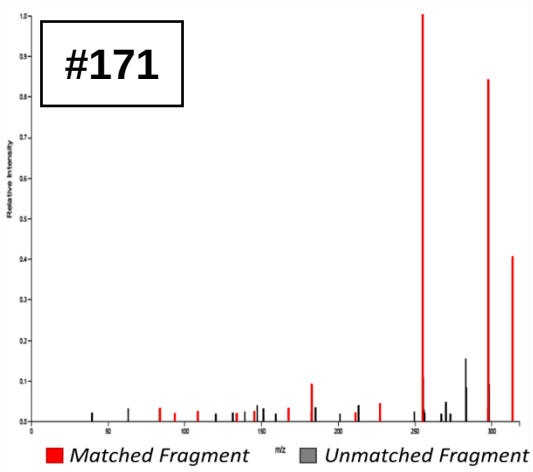

wogonin, CID: 5281703, METLIN; [95.95]

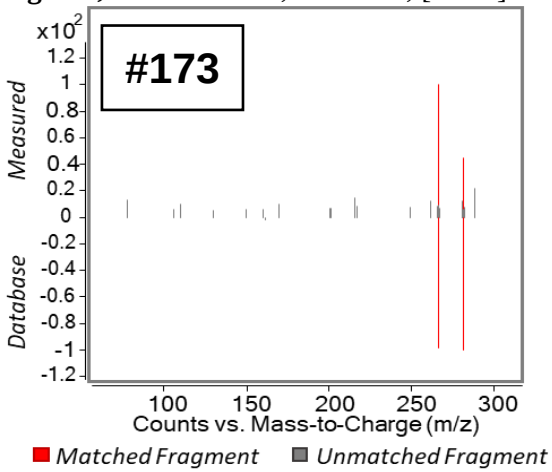

Figure 5. MS/MS spectra for compounds present in açaí extracts that were identified using authentic standards (L1 annotations). MS/MS score is indicated in [ ].

acacetin, CID: 5280442, [89.33]

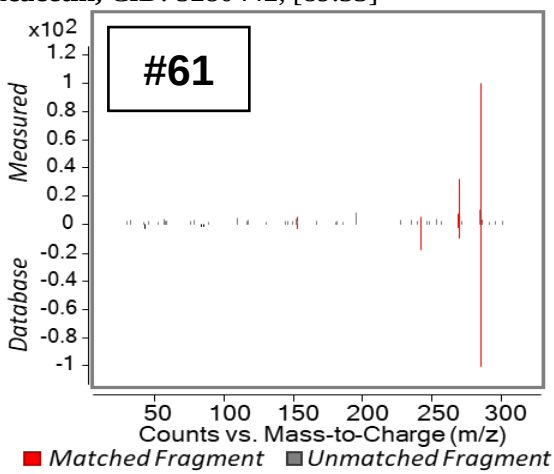

catechin, CID: 9064, [100]

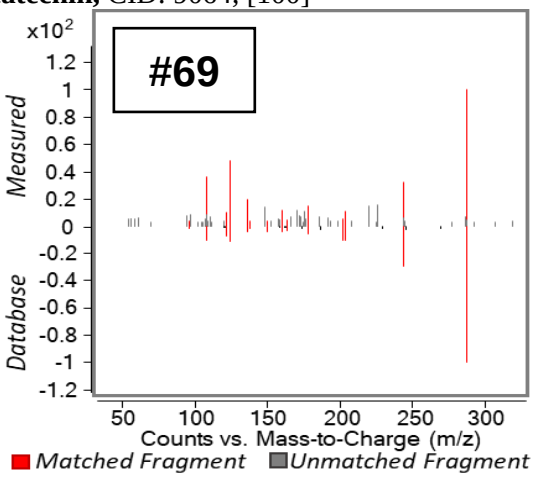

chrysoeriol, CID: 5280666; [97.21]

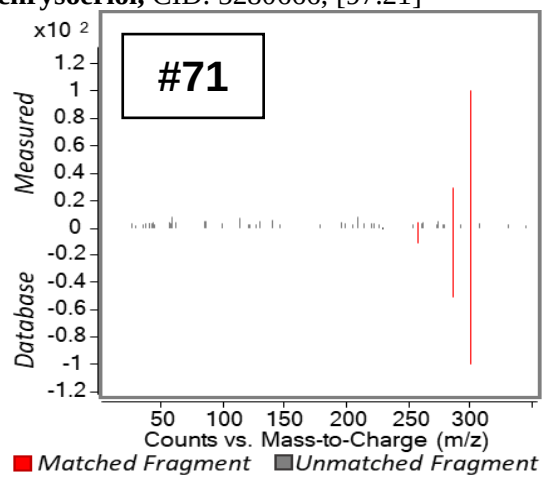

coumarin, CID: 323, [71.21]

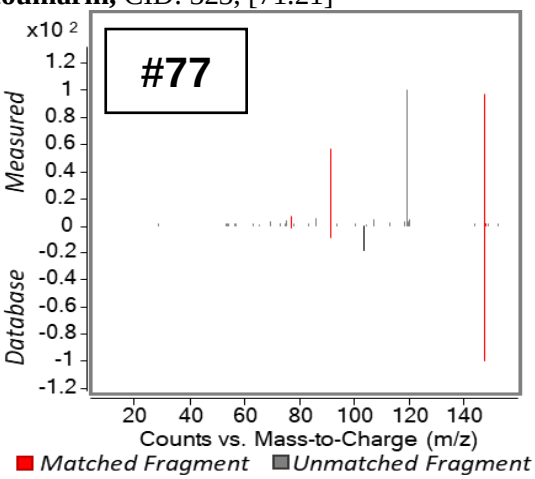

cyanidin 3-*O*-glucoside, CID: 12303220; [97.98]

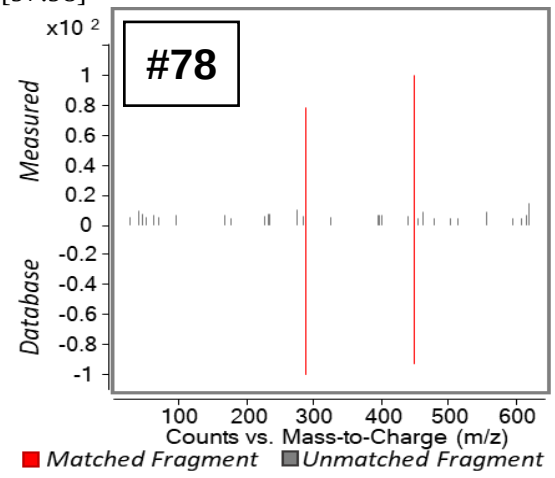

cyanidin 3-*O*-rutinoside, CID: 29231; [97.32]

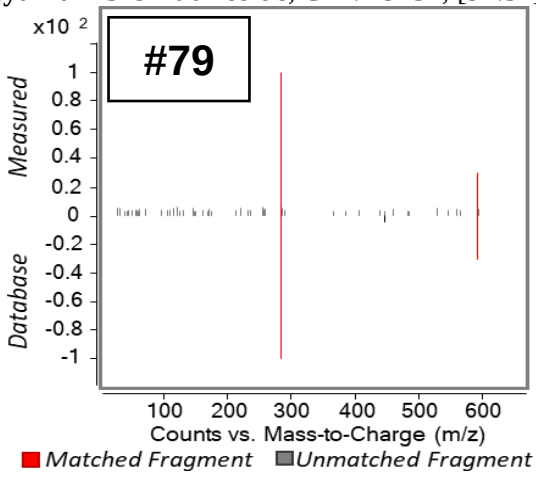

cyanidin 3-*O*-sambubioside, CID: 6602304; [91.73]

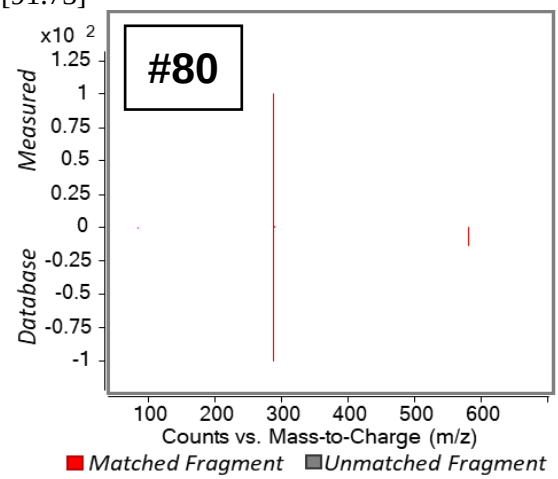

dihydrokaempferol, CID: 122850, [85.01]

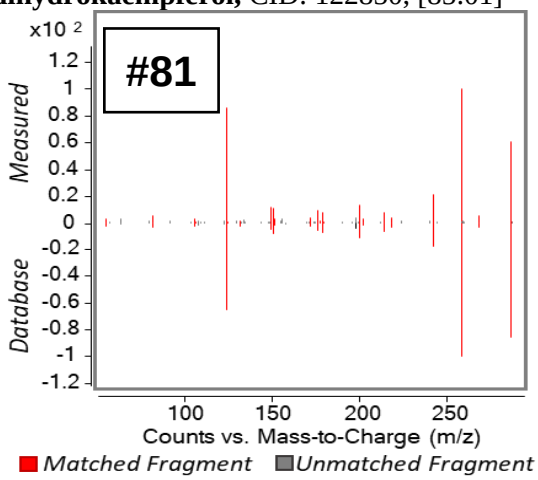

gallic acid, CID: 370; [92.31]

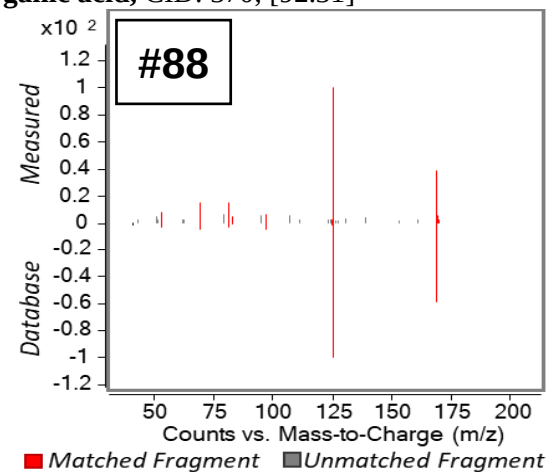

isovanillic acid, CID: 12575; [74.43]

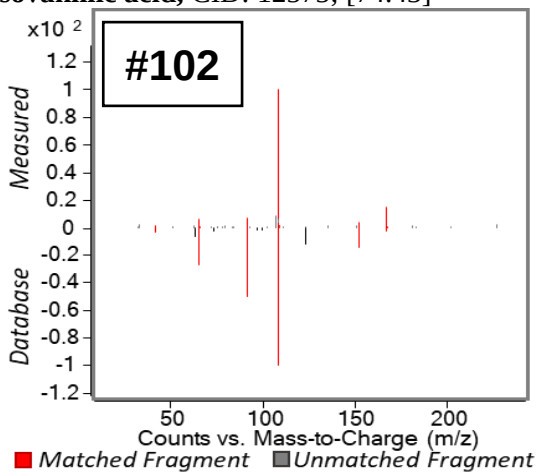

isovitexin, CID: 162350; [94.43]

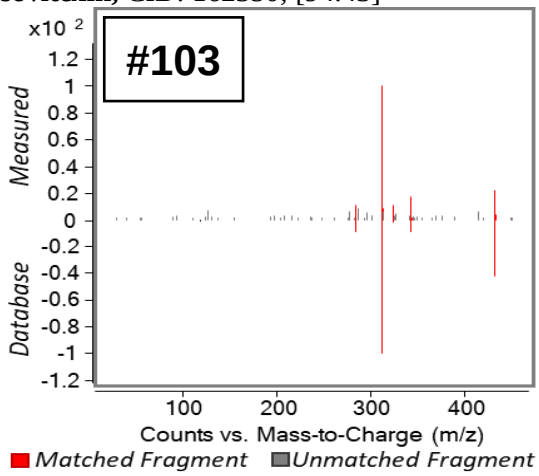

kaempferol, CID: 5280863; [77.95]

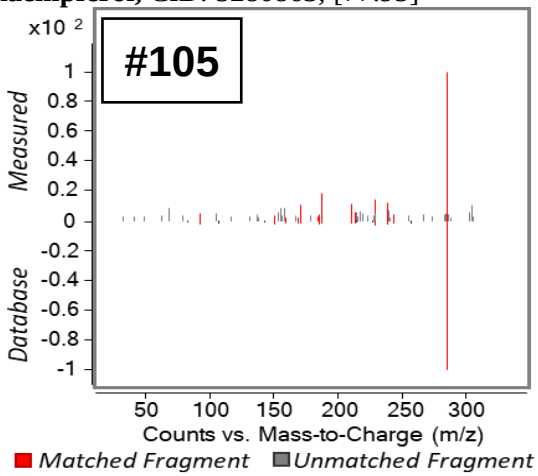

naringenin, CID: 439246; [86.55]

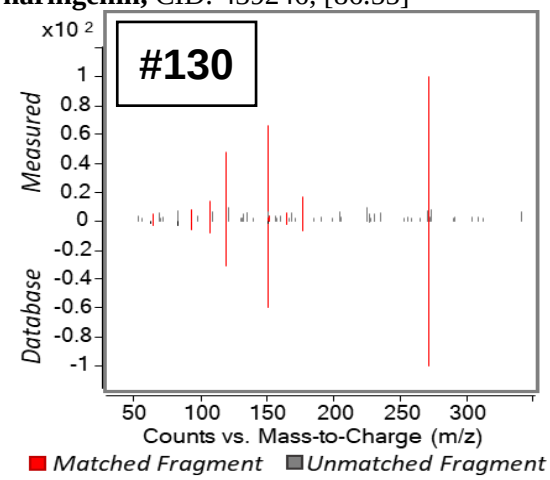

oleamide, CID: 5283387; [80.69]

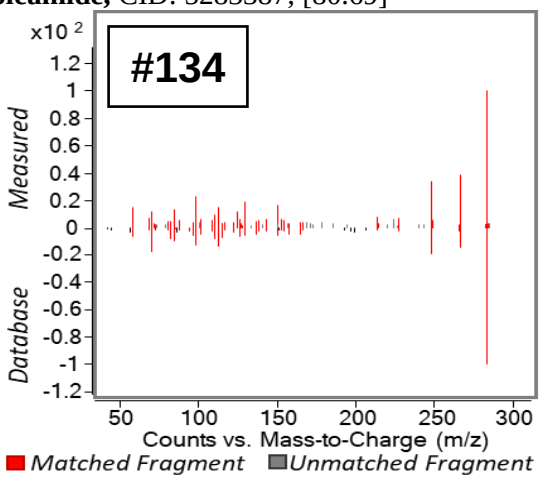

oleic acid, CID: 445639; [84.96]

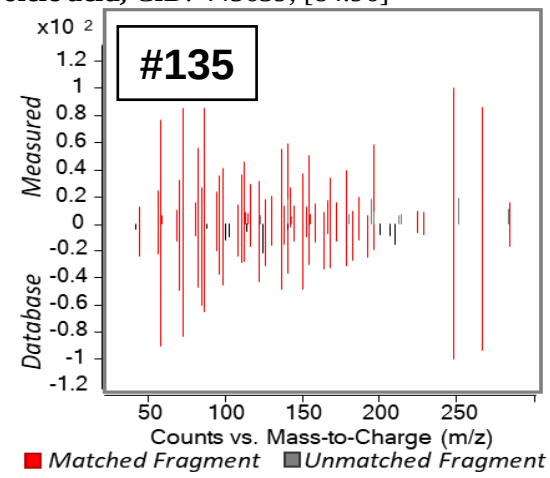

orientin, CID: 5281675; [82.5]

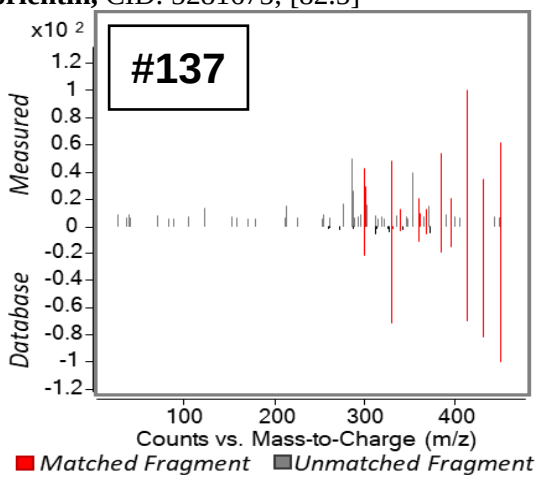

palmitic acid, CID: 985; [99.79]

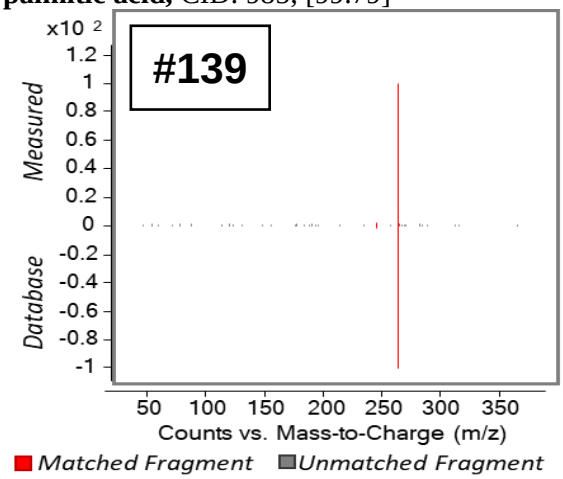

peonidin 3-glucoside, CID: 443654; [97.59]

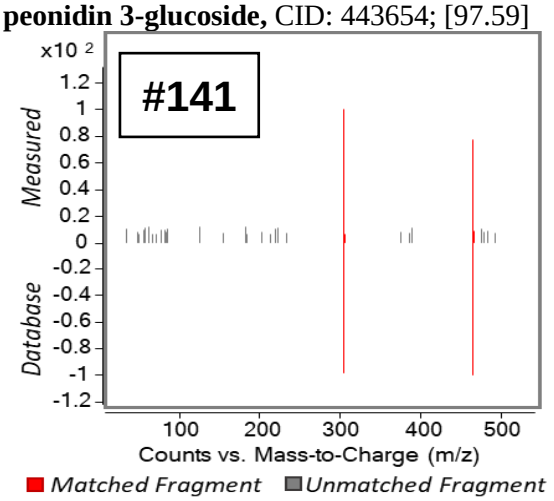

peonidin 3-*O*-rutinoside, CID: 44256842; [84.51]

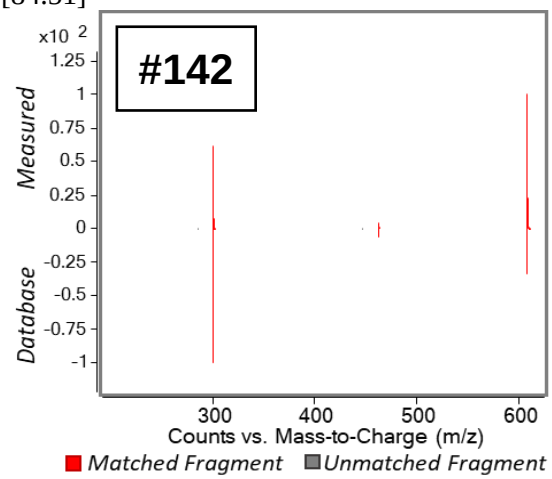

quercetin, CID: 5280343; [83.32]

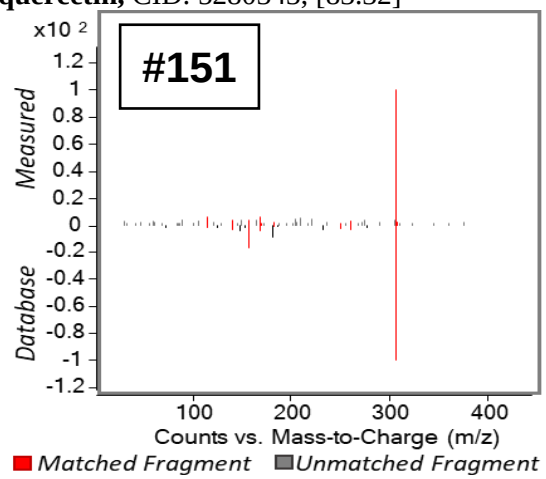

quercetin 3-glucoside, CID: 5280804; [90.72]

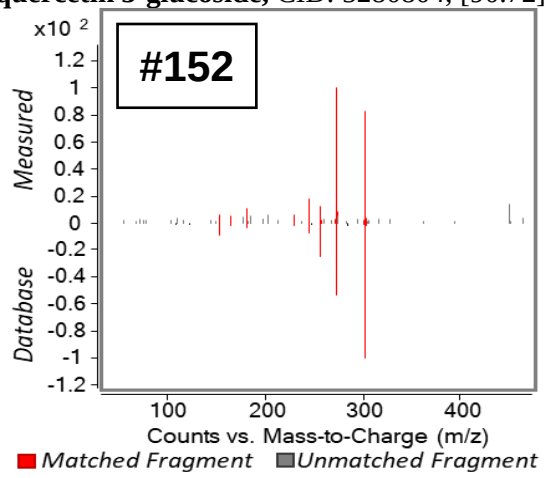

taxifolin, CID: 439533; [73.08]

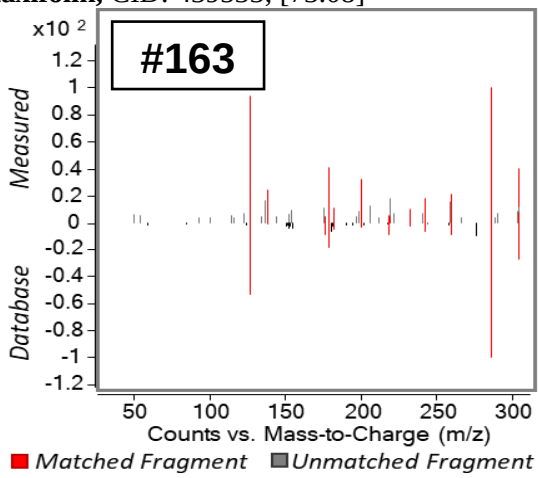

vitexin, CID: 5280441; [97.13]

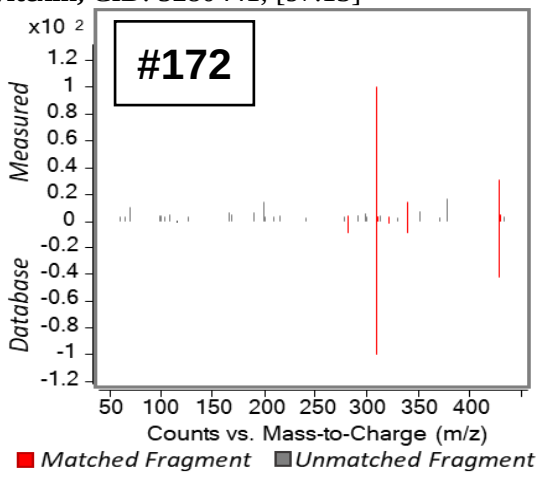

3.1.2 Statistical analyses of açaí extracts

3.1.2.1 Principal component analysis

PCA was used to capture the similarities and differences in the chemical composition of the sixteen açaí extracts using the top 100 mass features observed in full-scan MS using ESI^+ (**Figure 6**). In the PCA plot generated from positive ESI^+ features, significant differences across the açaí extracts based on their polarity and source of origin. This PCA shows distinct separation of extracts generated from BDS extracts on the right of the graph and food product extracts on the left of the plot spanning from 0 to -4. The total variance values of the dataset in ESI^+ were explained by PC1 and PC2 were 29.8% and 17.9%, respectively. In the BDS extracts there are distinct areas which separate the 2019 lot extracts (F1 and F2) from the 2022 lot extracts (F3 and F4). There is also a brand distinction with Nature's Way (F1 and F3) samples showing a distinction from Natrol (F2 and F4) BDS sample extracts. In the food product samples, there are trends of polarity that separate the aqueous food extracts from acMeOH extracts and also organic extracts (MeOH and 95% ethanol). For acMeOH extracts, the Hawaiian fruit (EO) and the Brazillian fruit (MR) extracts have overlapping eclipses indicating that there is a high amount of similarity between the two. For other food product extracts there is separation based on the geographical origin of the fruit. For the PCA plot generated from ESI^- features, most of the same trends are observed as in the ESI^+ PCA plot with the exception that BDS brands cannot be clearly distinguished due to strong similarity between acMeOH and MeOH extracts of the 2019 lot extracts (F1 and F2) (**Figure 7**). Also, rather than the acMeOH food product extracts being together, EOAC shows more similarity with the lipophilic MR extracts (MRME and MRET).

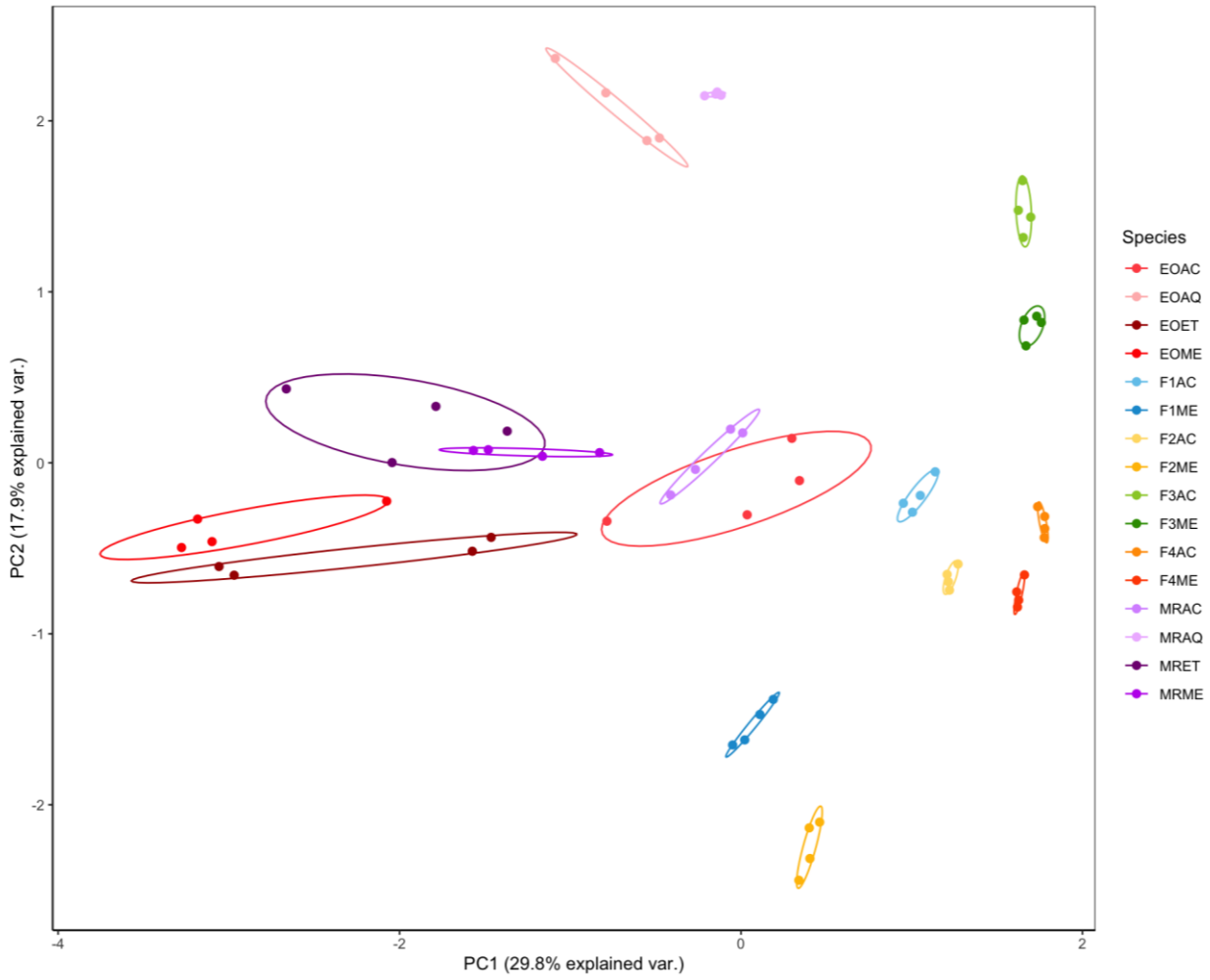

Figure 6. PCA showing similarities between extract types based on features found in ESI^{+}. Each set of dots (technical quadruplicates) represents an açaí extract from 16 different accessions.

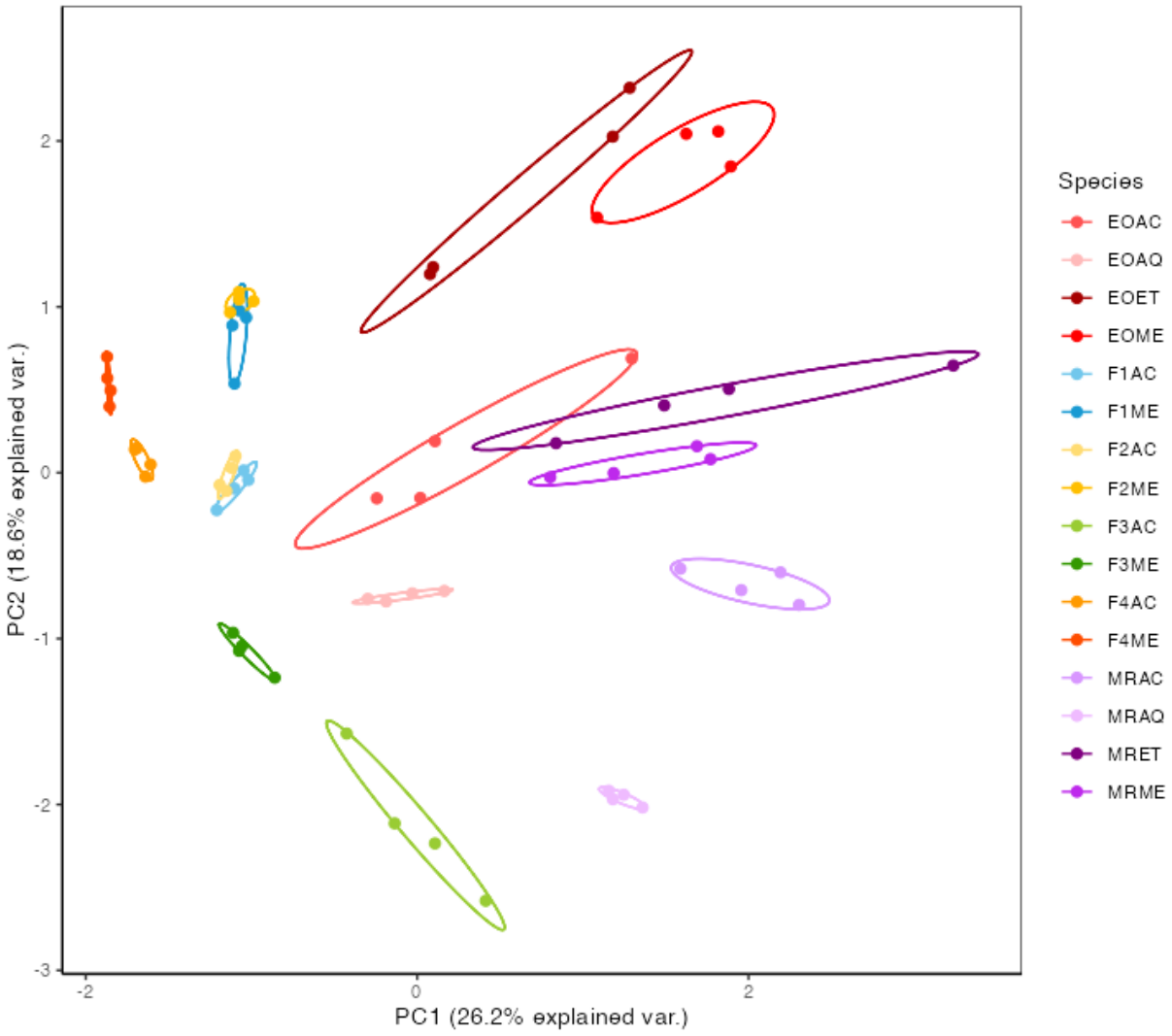

Figure 7. PCA showing similarities between extract types based on features found in ESI$^-$. Each set of dots (technical quadruplicates) represents an açaí extract from 16 different accessions.

3.1.2.2 Correlation matrices

For additional examination of açaí extracts, we used correlation matrix and HCA based on the abundance of features. The correlation matrix uses the correlation score (0-1) to evaluate similarities and dissimilarities of extracts: the higher the score (red) indicates the more similar the extracts are to one another and the lower the score (blue) indicates more dissimilarities between them.

For ESI^+ features, the correlation plot shows mostly areas of low to no correlation with few areas of high correlation (**Figure 8**). For example, the Pearson correlation value calculated between F4AC and F1ME extracts is 0.01, which indicates that there is a small to no linear relationship between these two extracts (small amount of similarity or dissimilar). Other extracts that showed a great amount of dissimilarity include mostly BDS extracts (F) and Hawaiian fruit extracts (EO), specifically: F4AC and F3AC (0.08), F4AC and EOME (0.08), F2ME and EOAQ (0.07), F3ME and EOAQ (0.07), F4ME and EOME (0.07), and F4AC and F3ME (0.07). The Pearson correlation value calculated between methanol Brazilian fruit extract (MRME) and 95% ethanol Hawaiian fruit extract (EOET) extracts is 0.50 which indicates a small linear relationship between extracts MRME and EOET. The Pearson correlation value calculated between EOET and EOME extracts is 0.99 which indicates that these two samples are linearly related, indicating similarities in metabolite contents for the 95% ethanol and MeOH extracts of Hawaiian açaí pulp. Additional extracts with high linear relationships include other samples whose solvents similar in polarity were used to extract the same material, including F3AC and F3ME (0.98), F4AC and F4ME (0.92), and MRET and MRME (0.98). There are two areas of high correlation between extracts coming from different sources including the four MR extracts and EOAC/EOAQ extracts (0.69 – 0.95) and that between F1 and F2 extracts (0.70 – 0.84).

In the ESI^- correlation plot, most extracts were found to be dissimilar and there were no strong correlations between extracts not of the same source material (**Figure 9**). There are some small linear relationships between EO extracts and extracts of F1ME, F2AC and F2ME, except for EOAQ, which appears to have a moderate amount of dissimilarity with all samples outside of EOAQ (0.02 – 0.29). There is also similarity between extracts of F4 with BDS from 2019 lot with correlation values ranging from 0.45 – 0.69 (F1 and F2). While the two BDS lots from 2019 are similar to one another, there is little similarity between BDS extracts from the two different brands of the 2022 lots (F3 and F4 with values from 0.05 – 0.21).

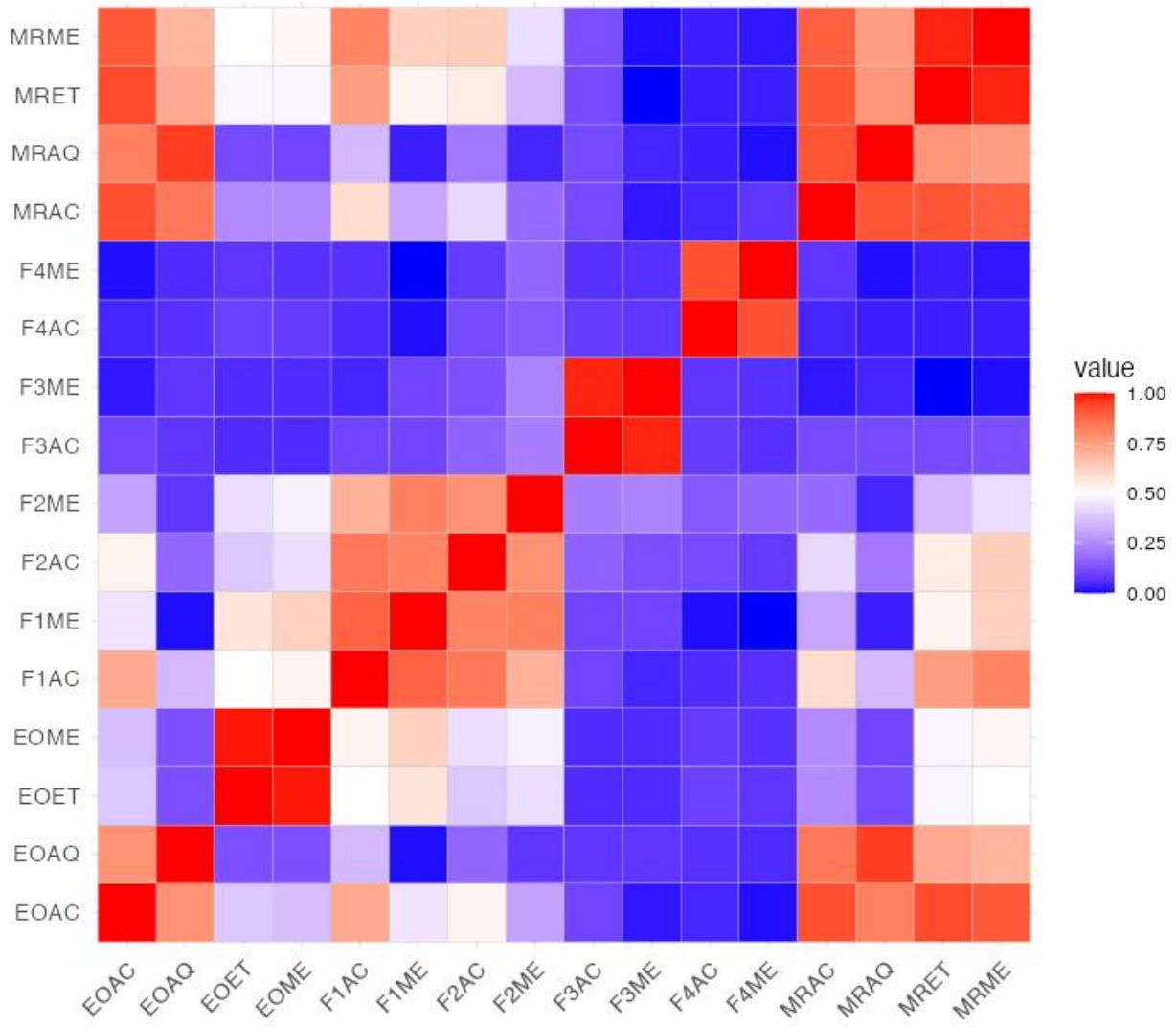

Figure 8. Correlation matrix between the different açaí extracts based on PCA features from ESI^{+}. Each extract is an average of the four replicates.

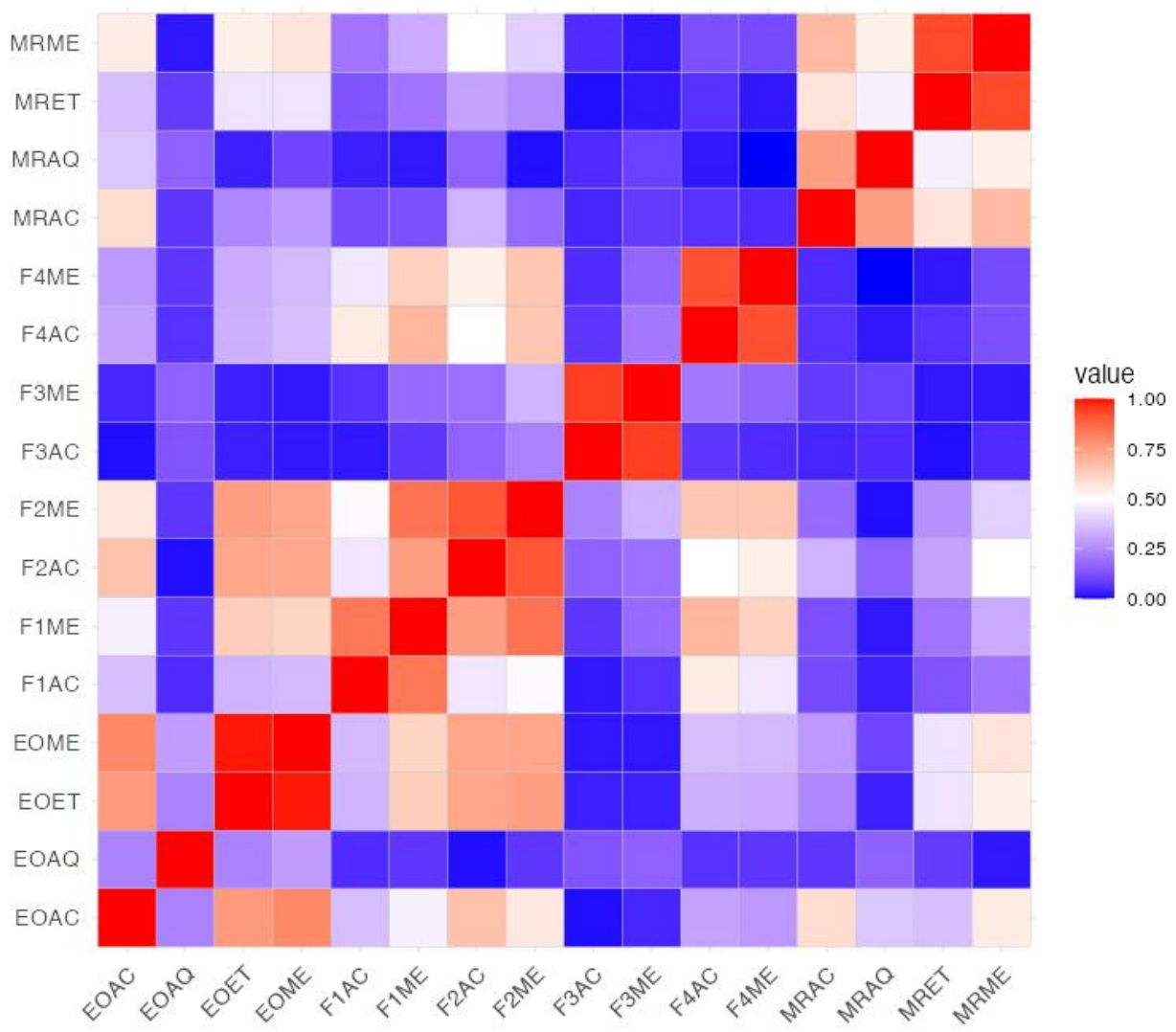

Figure 9. Correlation matrix between the different açaí extracts based on PCA features from ESI$^-$. Each extract is an average of the four replicates.

3.1.2.3 Hierarchical clustering analysis

The heatmap with hierarchical clustering (**Figures 10** and **11**) visualizes mass feature abundances for 100 compounds evaluated in all 16 açaí extracts. The area under the curve has been averaged across the four replicates for each extract. The dendrogram on the y-axis indicates the degree of similarity between the different açaí extract samples and on the x-axis indicates the degree of similarity between the metabolites present. The z-score, shown by the colors in the heatmap, was computed by dividing the standard deviation of a metabolite across all samples by the mean of the peak regions for that metabolite across all 64 samples. The red, white, and blue colors designate a positive score, a zero score, or a negative score, respectively. A larger z-score magnitude indicates a higher color intensity on the scale.

In the ESI^+ HCA, the sample dendrogram (y-axis) shows clear patterns based on the polarity of compounds present and the origin of the extract sample (**Figure 10**). The dendrogram first splits into polar and nonpolar trees, with the nonpolar extracts including methanol and ethanol extracts of the Nature's Way 2019 capsule and both the Brazillian and Hawaiian açaí fruit extracts (F2ME, MRME, MRET, EOME, and EOET). The next branches show the distinctions between BDS extract F2ME and the food product extracts, which are then separated to show different branches for MR and EO extracts. These extracts were classified based on their higher amounts of fatty acids present. Under the polar tree of the dendrogram, there is an additional branch that separates highly water-soluble extracts (F3AC, F3ME, MRAQ, EOAQ) from less water-soluble extracts (F1AC, F2AC, F1ME, F4AC, F4ME, EOAC, and MRAQ). The highly water-soluble extracts were classified based on having high concentrations of organic acids, amino acids, and monosaccharides. The less water-soluble extracts were classified based on having high amounts of anthocyanins and flavonoid glycosides. Both highly and less water-soluble branches go on to

be divided further based on whether the extract was generated from a BDS capsule product or a food product. Under the less water-soluble branch, the BDS extracts are also classified based on if they were from the 2019 or 2022 lots.

In ESI^-, the patterns of branching in the HCA sample dendrogram are not as clearly defined as they are in ESI^+ (**Figure 11**). The branching tends to happen in a more singular manner based on a source of origin rather than in whole groups based on a shared quality such as polarity. However, they do show a more similarity amongst Hawaiian fruit extracts (EO) and BDS samples rather than to Brazillian fruit extracts (MR) as shown in ESI^+. The first branching separates MR extracts from all other extracts, followed by the separation of F3AC and F3ME extracts, F4ME, and EOAQ. The remaining branches show similarity between samples of EOAC, EOET and EOME extracts with various BDS extract samples from F1, F2, and F4AC.

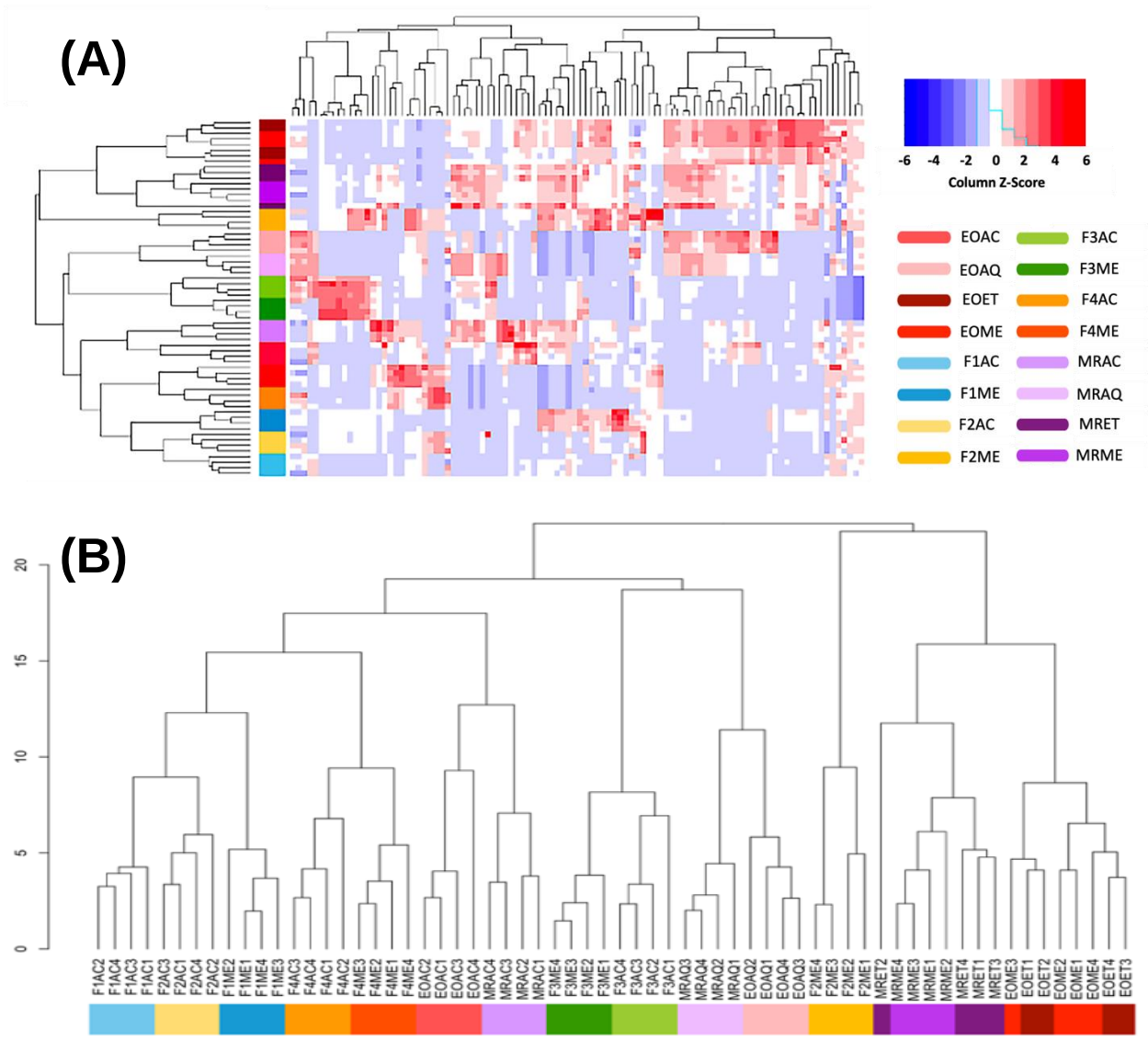

Figure 10. Heatmap visualizing the average area under the curve for 100 compounds used in PCA for ESI$^+$. (A) Heatmap with clustering with metabolite clustering on the x-axis (top) and sample clustering on the y-axis. (B) Close-up examination of sample dendrogram for positive features showing extract similarities.

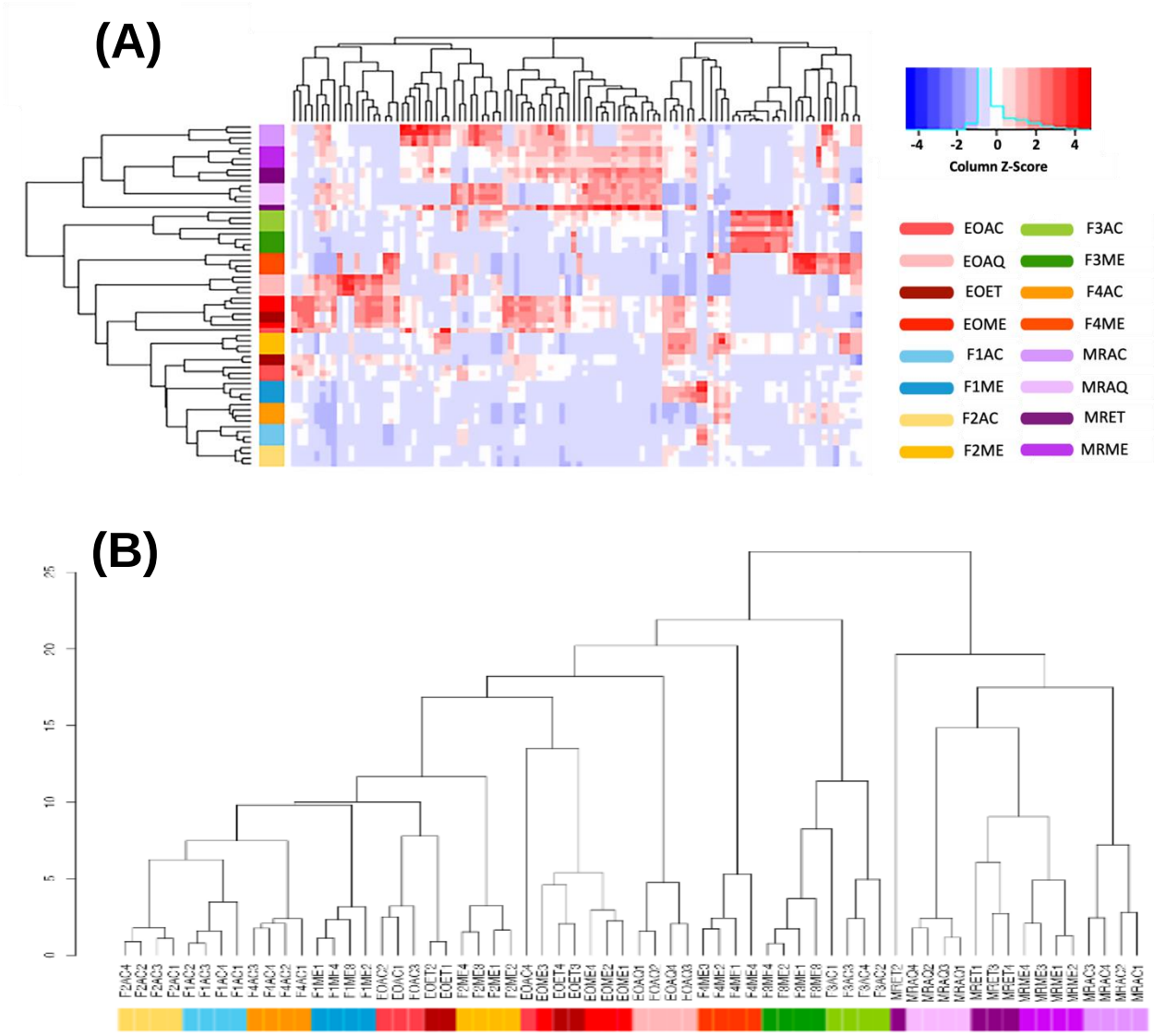

Figure 11. Heatmap visualizing the average area under the curve for 100 compounds used in PCA for ESI$^-$. (A) Heatmap with clustering with metabolite clustering on the x-axis (top) and sample clustering on the y-axis. (B) Close-up examination of sample dendrogram for positive features showing extract similarities.

3.2 Anthocyanin quantitation

3.2.1 Quantitation method development

3.2.1.1 Optimization of separation parameters

Our initial goal was to develop a method quantifying anthocyanins with faster runtimes yet still accurate and reproducible. Method development began by using our previously published method. However, the previous column was a 1.8 µm ZORBAX Eclipse plus C18 column which we found quickly reached maximum pressure using a 400barr HPLC system. We decided to change from this fully porous particle stationary phase to a superficially porous column (2.7 µm Poroshell 120 SB-C18 column) of larger particle size and diameter. This change greatly reduced the column backpressure and allowed for a greater variety of flow rates and mobile phase conditions. Once the new column was in place, an optimal chromatographic resolution was achieved by evaluating several chromatographic gradients and flow rates while using the same mobile phase as our previously optimized method [including alternative mobile phases [e.g., aqueous phase (A): water with added FA; organic phase (B): MeOH:ACN (50:50) with added FA]. The chromatographic method which showed the best chromatographic separation and peak shape was the Poroshell 120 SB-C18 (Agilent Technologies) with a binary mobile phase consisting of 0.1% FA in water and 0.1% FA in a MeOH:ACN (50:50) mixture at a flow rate of 0.35 mL/min. A method was developed capable of the quantification of anthocyanins in complex açaí extracts from a variety of starting materials and with multiple extraction solvents.

Anthocyanins **1**, **2**, **3**, and **4**, eluted at 5.605, 5.538, 5.605, and 5.755 min, respectively (**Figure 12**). The IS reserpine eluted at 6.989 min. While isotopically labeled standards can be used to increase the accuracy of quantitative analysis, there are no commercially available stable

isotopically labeled standards for anthocyanins. Reserpine was used because of its ease of ionization in the ESI^+, which has made it a popular standard for positive ionization using ESI-MS. It was decided not to use another anthocyanin as an IS due to the potential for other anthocyanins not normally present in açaí that may be present in the case of adulteration. Adulteration of açaí materials has been reported by both addition or substitution of different plant species of lesser monetary value and by the addition of chemical standards to increase the yield of bioactive constituents or for enhancement of color [19, 128]. This methodology benefits greatly from the column used which has not previously been used for the separation and identification of anthocyanins or characterization of any açaí extracts, but has been used to separate different analytes from natural product mixtures such as phloroglucinol derivatives [130], flavonoids [131, 132], saponins [133-135], and alkaloids [136, 137]. The use of this column allowed us to achieve an optimal separation at a shorter run time while using a 400barr HPLC system. This enhanced separation without the requirement of a UPLC system makes this method easily transferable to academic or industrial lab settings.

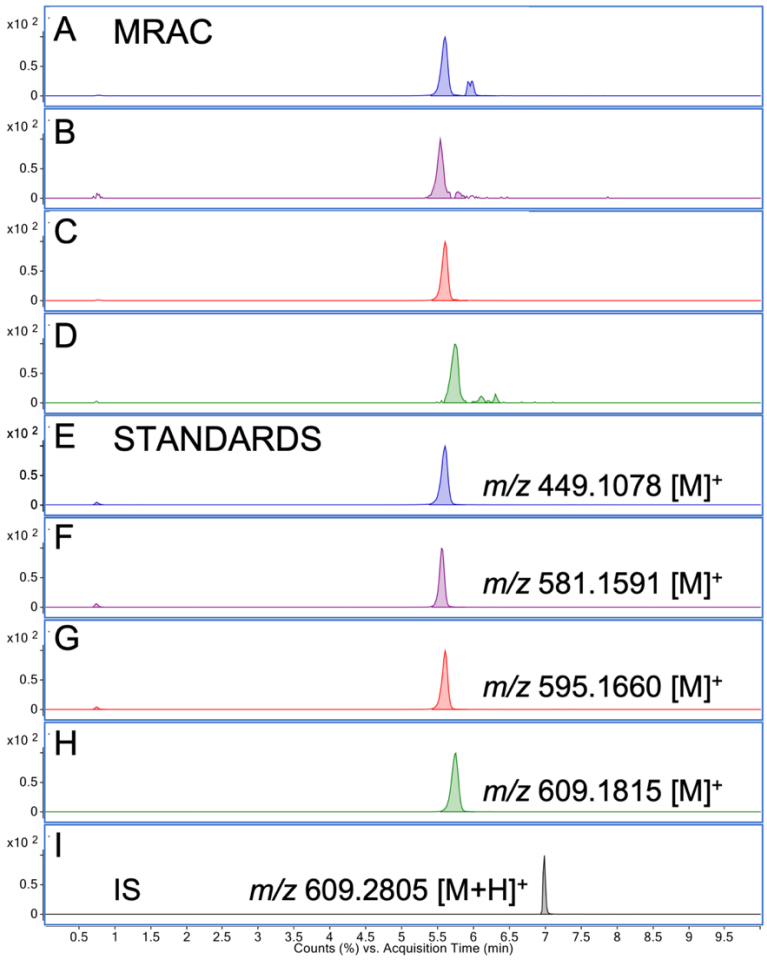

Figure 12. Extracted ion chromatogram of anthocyanins **1** (**A**), **2** (**B**), **3** (**C**), and **4** (**D**) present in acMeOH extracts of açaí raw materials (MRAC), anthocyanin standards (**E**-**H**), and internal standard (IS) reserpine (**I**).

The MS conditions reported previously by our group remained optimal for this application [85]. Some papers which have quantified anthocyanins from açaí materials have described them as protonated ions, $[M+H]^+$, however, our mass spectrometer failed to detect an added proton. Rather, they should be described at $[M]^+$ ions due to the three bonds to the anthocyanin oxygen [138]. The anthocyanins **1**, **2**, **3**, and **4** showed $[M]^+$ molecular ions at m/z 449.1078, 595.1660, 581. 1510, and 609.1815, respectively (**Table 5**). The protonated molecular ion $[M+H]^+$ of the IS reserpine was detected at m/z 609.2805. All analytes could be detected within a range of 5 ppm.

Table 5. LC-ESI-MS data of anthocyanins present in MRAC extract and IS reserpine.

Analyte	RT[a] (min)	Ion formula $[M]^+$	$[M]^+$ *m/z*	Dif (ppm)	DBE[b]
1	5.605	$C_{21}H_{21}O_{11}$	449.1078	-0.02	12
2	5.538	$C_{26}H_{29}O_{15}$	581.1591	1.33	13
3	5.605	$C_{27}H_{31}O_{15}$	595.1660	0.17	13
4	5.755	$C_{28}H_{33}O_{15}$	609.1815	-3.87	13
IS	6.989	$C_{33}H_{41}N_2O_9$[c]	609.2805[c]	-0.27	13

[a]Retention time

[b]Double bond equivalence

[c]Reserpine ion formula and *m/z* are $[M+H]^+$ ions.

3.2.1.2 Calibration curve

The analytical method was then validated for linearity, sensitivity, accuracy, repeatability, and intermediate precision. The quantitation of anthocyanins present in various açaí samples was performed by preparing a calibration curve of 12 concentrations containing all four anthocyanin standards. Whereas our previous linearity ranges were 0.24 – 31.25, 0.49 – 15.62, 0.12 –15.62, and 0.06 – 15.62 µg/mL for anthocyanins **1**, **2**, **3**, and **4**, our new linearity ranges for this method are more sensitive now due to enhancement of chromatographic conditions [85]. The new linearity ranges were determined to be 0.0044 – 1.12 µg/mL for **1**, 0.0116 – 1.148 µg/mL for **2**, 0.0113 – 2.97 µg/mL for **3**, and 0.0059 – 1.52 µg/mL for **4**. With the enhancement of chromatographic conditions, our LLOD's are at least a full order of magnitude lower than in our previous method: **1** from 0.03 to 0.0014 µg/mL, **2** from 0.12 to 0.0043 µg/mL, **3** from 0.03 to 0.0028 µg/mL, and **4** from 0.01 to 0.0027 µg/mL. All correlation coefficients are greater than 0.99 (**Table 6**).

Table 6. Regression equation, correlation coefficient, lower limit of detection (LLOD), lower limit of quantitation (LLOQ), and linearity range for anthocyanins by high resolution LC-ESI-MS.

Analyte		Calibration curve	Correlation coefficient (r^2)	LLOD (µg/mL)	LLOQ (µg/mL)	Linearity range (µg/mL)
Modified Method	**1**	y = 0.170x – 0.035	0.9977	0.0014	0.0044	0.0044 – 1.120
	2	y = 0.123x – 0.050	0.9972	0.0043	0.0116	0.0116 – 1.148
	3	y = 0.158x – 0.177	0.9929	0.0028	0.0113	0.0113 – 2.970
	4	y = 0.076x – 0.016	0.9981	0.0027	0.0059	0.0059 – 1.520
Previously Reported	**1**	y = 1.835x + 0.527	0.9986	0.03	0.24	0.24 – 31.25
	2	y = 1.948x + 1.519	0.9952	0.12	0.49	0.49 – 15.62
	3	y = 2.898x + 0.721	0.9955	0.03	0.12	0.12 – 15.62
	4	y = 2.933x + 1.412	0.9930	0.01	0.06	0.06 – 15.62

3.2.1.3 Validation

Accuracy of the method was assessed through recovery experiments in which samples were quantified before and after spiking with 0.1 µM of all four anthocyanin standards (**Table 7**). The samples were analyzed twice in the same day to assess intraday accuracy (repeatability) and analyzed two and four days after to assess interday accuracy (intermediate precision). The method was found to be accurate as all samples were between 80 – 120% accurate, with the range of intraday accuracy being 92.88 – 104.17%. The range of interday (2 and 4 day) accuracy was found to be 92.72 – 107.50%, which also falls between 80 and 120%. Relative standard deviation (RSD) percentages were very consistent across intraday and interday assessments, indicating that the method is also robust. For intraday (day 0), %RSDs remained under 4.59%, with 3.48 being the average %RSD. For interday assessment of the method, all measurements were between 2 – 4%, with 3.50% being the largest %RSD. All %RSD values were below the acceptable cutoff value of 20%.

Table 7. Intraday (0 day) and interday (2 and 4 day) accuracy for anthocyanins **1**, **2**, **3**, and **4** in MRAC, EOAC, and F2AC extracts.

		Intraday (n=3)			Interday (n=3)		
Sample	Analyte	Found (ug/mL)	% RSD	Accuracy (%)	Found (ug/mL)	% RSD	Accuracy (%)
MRAC	**1**	0.6962 ± 0.032	4.59	97.27	0.7209 ± 0.024	3.28	100.72
	2	0.1103 ± 0.003	3.11	104.17	0.1139 ± 0.003	2.57	107.50
	3	1.6984 ± 0.066	3.93	95.57	1.7243 ± 0.055	3.24	97.03
	4	0.1054 ± 0.004	3.54	101.04	0.1108 ± 0.004	3.50	106.24
EOAC	**1**	0.1787 ± 0.006	3.81	100.37	0.1805 ± 0.006	3.40	101.38
	2	0.0871 ± 0.003	3.52	100.92	0.0881 ± 0.003	2.85	102.05
	3	0.3940 ± 0.008	2.74	98.28	0.3904 ± 0.010	2.62	97.36
	4	0.0803 ± 0.002	2.01	92.88	0.0802 ± 0.002	2.43	92.72
F2AC	**1**	0.1348 ± 0.006	4.35	100.41	0.1399 ± 0.004	3.16	104.22
	2	0.0852 ± 0.004	4.14	101.10	0.0870 ± 0.002	2.54	103.29
	3	0.9970 ± 0.027	2.68	96.48	1.0175 ± 0.026	2.60	98.46
	4	0.0767 ± 0.003	3.43	94.32	0.0782 ± 0.002	3.05	96.20

MRAC and EOAC were diluted 10X to avoid saturation of detector. Diluted samples were spiked and compared to diluted sample concentrations from strict quantitation the same day.

3.2.2 Anthocyanins in various açaí materials

LC-ESI-MS analysis revealed that all four anthocyanins were present and quantifiable in all extracts at the concentration of 1 mg/ml (**Figure 13**, **Table 8**). For MR extracts, **3** was the most abundant anthocyanin (0.472 ± 0.009 – 15.1 ± 0.0 mg/g dry extract), followed by **1** (0.308 ± 0.006 – 8.95 ± 0.01 mg/g dry extract), **4** (0.0631 ± 0.0011 – 1.01 ± 0.01 mg/g dry extract), and **2** (0.0291 ± 0.0008 – 0.470 ± 0.002 mg/g dry extract). This trend holds true for fruit extracts as well except for the aqueous extract (EOAQ), in which **3** is followed by **2**, **4**, and lastly **1**. For EO extracts, **3** was also the most abundant (0.608 ± 0.001 – 3.34 ± 0.01 mg/g dry extract), followed by **1** (0.144 ± 0.001 – 1.58 ± 0.01 mg/g dry extract), **4** (0.193 ± 0.001 – 0.569 ± 0.002 mg/g dry extract), and **2** (0.0723 ± 0.0012 – 0.319 ± 0.001 mg/g dry extract). For both F1AC and F1ME extracts, **4** (0.0522 ± 0.0017 – 0.0699 ± 0.0034 mg/g dry extract) was the least abundant anthocyanin rather than **2** (0.114 ± 0.004 – 0.119 ± 0.003 mg/g dry extract). While **3** was still the most abundant anthocyanin in all F1 and F2 extracts (0.380 ± 0.006 – 1.09 ± 0.02 mg/g dry extract), it was followed by **1** in F1AC extracts and **2** in F1ME extracts. For F2, both F2AC and F2ME extracts follow an order of abundance in alignment with the majority of extracts (**3** > **1** > **4** > **2**).

MRAC contained the most total anthocyanins out of all extracts (25.5 ± 0.1 mg/g dry extract) followed by MRAQ (12.5 ± 0.1 mg/g dry extract), MRME (3.88 ± 0.01 mg/g dry extract), and MRET (0.872 ± 0.011 mg/g dry extract). For EO extracts, EOME had the most anthocyanin content (5.82 ± 0.01 mg/g dry extract), followed by EOAC (4.70 ± 0.01 mg/g dry extract), EOET (2.51 ± 0.01 mg/g dry extract), and EOAQ (1.16 ± 0.01 mg/g dry extract). F2 had a higher concentration of anthocyanins overall than F1 for both AC and ME extracts. Out of the formulation extracts, F2ME contained the greatest anthocyanin content (1.27 ± 0.02 mg/g dry extract),

followed by F2AC (1.23 ± 0.02 mg/g dry extract), F1AC (0.924 ± 0.010 mg/g dry extract), and F1ME (0.650 ± 0.011 mg/g dry extract).

These findings are in agreement with the literature which describes **3** being the most abundant anthocyanin followed by **1** [19, 85, 96, 98]. The third and fourth most prominent anthocyanins found in açaí materials are interchangeably **2** and **4** [85, 98]. One limitation to this study was that we were not able to analyze açaí fruits cultivated from Brazil. This limitation arises from the fact that açaí fruits cannot be exported from Brazil where the plant is endemic due to the country's regulations from their Biodiversity Law (Law 13.123) [139]. The law was put into place to protect the biological diversity of Brazil's endemic species and prevent practices such as biopiracy [140].

We did not expect the anthocyanin concentration to be the lowest in EOAQ in comparison to other EO extracts when MRAQ was almost as concentrated as MRAC. The difference here could be the pH of the materials before extraction with plain deionized water. The MR materials were preserved with the addition of citric acid (lime juice) to enhance the stability of the chemical constituents whereas the EO fruits did not have this procedure performed in our laboratory. In contrast to other fruits such as blackberries which have a natural pH that is appropriate for anthocyanin stability (pH 2.6 – 3.9), açaí fruits have a higher pH at approximately 5.0 [141, 142]. Future extractions of our açaí fruits should include various amounts of acid modifiers to aqueous cleaning or extraction solvents to test if this improves anthocyanin stability and recovery.

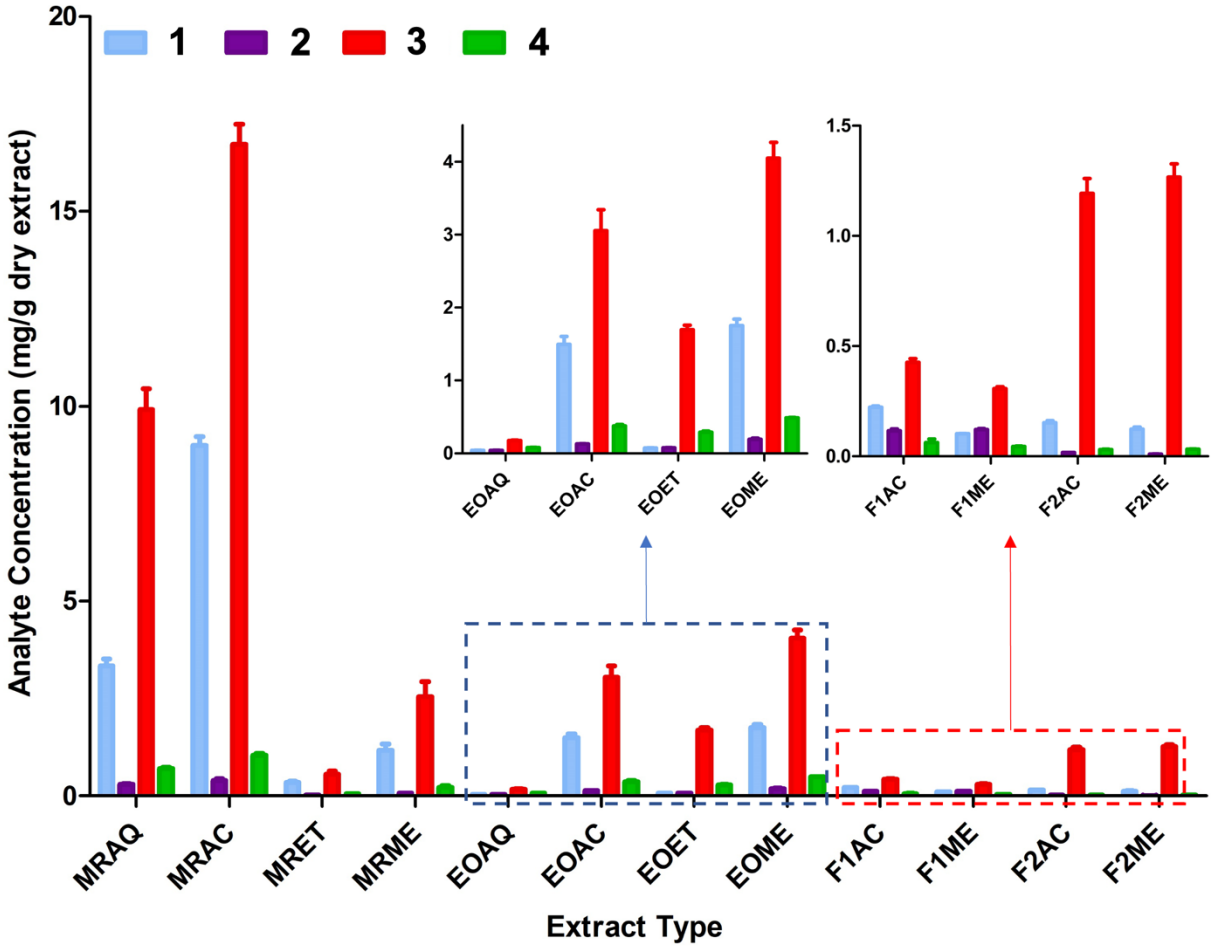

Figure 13. Illustration of anthocyanin contents in various açaí extracts. AC, acidic methanol extract; AQ, aqueous extract; EO, *Euterpe oleracea* Mart. fruits; ET, ethanol extract; F1, BDS formulation 1; F2, BDS formulation 2; ME, methanol extract; MR, Mountain Rose powder (raw material)

Table 8. Anthocyanin content in various extracts of açaí purée, raw material, and dietary supplement capsules.

Extract	**1**	%RSD	**2**	%RSD	**3**	%RSD	**4**	%RSD	Total
0-Day Quantitation									
MRAQ	3.0780 ± 0.004	1.23	0.3675 ± 0.001	3.46	8.3702 ± 0.025	2.94	0.7223 ± 0.002	2.52	12.5380 ± 0.030
MRAC	8.9525 ± 0.009	1.03	0.4703 ± 0.002	4.2	15.1336 ± 0.016	1.04	1.0108 ± 0.003	2.94	25.5399 ± 0.008
MRET	0.3083 ± 0.006	2.01	0.0291 ± 0.001	2.71	0.4718 ± 0.009	1.85	0.0631 ± 0.001	1.76	0.8723 ± 0.004
MRME	1.0504 ± 0.002	1.74	0.2504 ± 0.001	3.5	2.2596 ± 0.002	0.69	0.3220 ± 0.001	3.43	3.8824 ± 0.006
EOAQ	0.1437 ± 0.001	4.23	0.2121 ± 0.001	1.94	0.6081 ± 0.001	1.02	0.1930 ± 0.001	4.73	1.1569 ± 0.001
EOAC	1.3665 ± 0.001	1.04	0.2783 ± 0.001	3.15	2.6251 ± 0.004	1.37	0.4324 ± 0.001	1.16	4.7023 ± 0.002
EOET	0.6989 ± 0.006	0.86	0.0723 ± 0.001	1.73	1.4737 ± 0.013	0.89	0.2667 ± 0.007	2.57	2.5116 ± 0.007
EOME	1.5845 ± 0.003	1.78	0.3194 ± 0.001	2.35	3.3456 ± 0.004	1.23	0.5687 ± 0.002	3.2	5.8182 ± 0.002
F1AC	0.2014 ± 0.003	1.7	0.1142 ± 0.004	3.44	0.5390 ± 0.008	1.53	0.0700 ± 0.003	4.88	0.9246 ± 0.004
F1ME	0.0988 ± 0.003	2.72	0.1189 ± 0.003	2.92	0.3804 ± 0.006	1.52	0.0522 ± 0.002	3.3	0.6503 ± 0.004
F2AC	0.1392 ± 0.003	2.37	0.0320 ± 0.001	3.16	1.0247 ± 0.015	1.45	0.0390 ± 0.001	1.48	1.2349 ± 0.005
F2ME	0.1129 ± 0.001	1.74	0.0297 ± 0.001	3.95	1.0964 ± 0.016	1.43	0.0405 ± 0.001	3.2	1.2795 ± 0.005
30-Day Quantitation									
MRAQ	2.5322 ± 0.004	1.45	0.3762 ± 0.001	0.79	8.2645 ± 0.009	1.11	0.7172 ± 0.001	1.73	11.8901 ± 0.004

MRAC	7.1106 ± 0.006	0.65	0.4257 ± 0.001	2.43	14.6167 ± 0.013	0.9	1.0319 ± 0.002	1.47	23.1849 ± 0.006
MRET	0.2648 ± 0.007	2.74	0.0329 ± 0.001	3.95	0.4906 ± 0.004	0.92	0.0543 ± 0.002	4.23	0.8426 ± 0.004
MRME	0.9276 ± 0.002	1.89	0.2723 ± 0.001	2.12	2.1577 ± 0.001	0.65	0.2504 ± 0.001	4.21	3.6081 ± 0.001
EOAQ	0.1694 ± 0.001	1.87	0.2414 ± 0.001	1.18	0.6022 ± 0.001	0.99	0.1013 ± 0.001	4.83	1.1143 ± 0.001
EOAC	1.1413 ± 0.002	1.8	0.2860 ± 0.001	2.25	2.5864 ± 0.002	0.72	0.3753 ± 0.001	2.75	4.3890 ± 0.002
EOET	0.5561 ± 0.009	1.55	0.0678 ± 0.002	2.75	1.4478 ± 0.020	1.37	0.2743 ± 0.005	1.69	2.9562 ± 0.009
EOME	1.3090 ± 0.002	1.48	0.3332 ± 0.001	3.93	3.2681 ± 0.003	0.98	0.4976 ± 0.001	1.76	5.4079 ± 0.002
F1AC	0.1598 ± 0.002	1.6	0.0963 ± 0.002	2.19	0.4334 ± 0.007	1.7	< LLOD	n.d.	0.6895 ± 0.003
F1ME	0.0846 ± 0.003	3.3	0.1049 ± 0.004	3.49	0.3351 ± 0.014	4.17	< LLOD	n.d.	0.5246 ± 0.005
F2AC	0.1160 ± 0.001	1.31	0.0324 ± 0.001	3.17	1.0252 ± 0.013	1.27	0.0320 ± 0.001	2.86	1.2056 ± 0.004
F2ME	0.0979 ± 0.002	2.07	0.0311 ± 0.001	1.93	1.1128 ± 0.012	1.06	0.0306 ± 0.001	4.55	1.2724 ± 0.007

LLOD, lower limit of detection

n.d., not described

3.2.3 Anthocyanin stability testing

Strict quantitation of extracts was performed again after extracts had been stored in acMeOH solution for 30 days at -80°C. The amount of anthocyanin content was lower at the 30-day period than when quantified on the 0-day for **1** and **4** (**Figure 14**). Across all samples tested, the average recovery of **1** compared to 0-Day was 86.2%. The average recovery of 4 was similar at 71.0%. 3 had a slightly higher average recovery than **1** and **4**, with an average of 96.5% of the analyte was measured at day 30 compared to day 0. 2 had the highest average percent recovery at 100.6%. However, when 1 mg/mL extract solution was made from the lyophilized extract material that had been stored at -20°C, the concentration of anthocyanins was very similar to that of results of the previous 0-day quantitation that had been performed (data not shown). All %RSD values for quantitation of anthocyanins on 0-Day and 30-Day were less than 5% (**Table 8**).

The stability of anthocyanins was also looked at from a matrix perspective (Figure 15). All extracts had nearly 100% average anthocyanin recovery except for extracts of F1, both AC and ME extracts. The average recovery of these two extracts was lower than the rest because of the instability of **4** in the two extracts, as it was not quantifiable after storage for 30 days (**Table 8**).

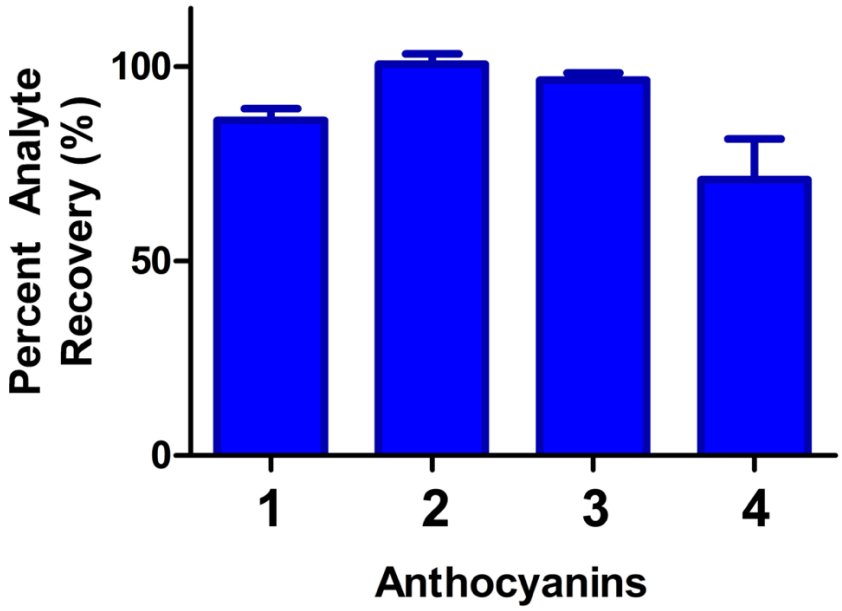

Figure 14. Depiction of average anthocyanin stability in acMeOH for 30 days at -80°C. Data shows is percent analyte recovery calculated by dividing the anthocyanin concentration on day 30 by the anthocyanin concentration on day 0 and multiplying by 100.

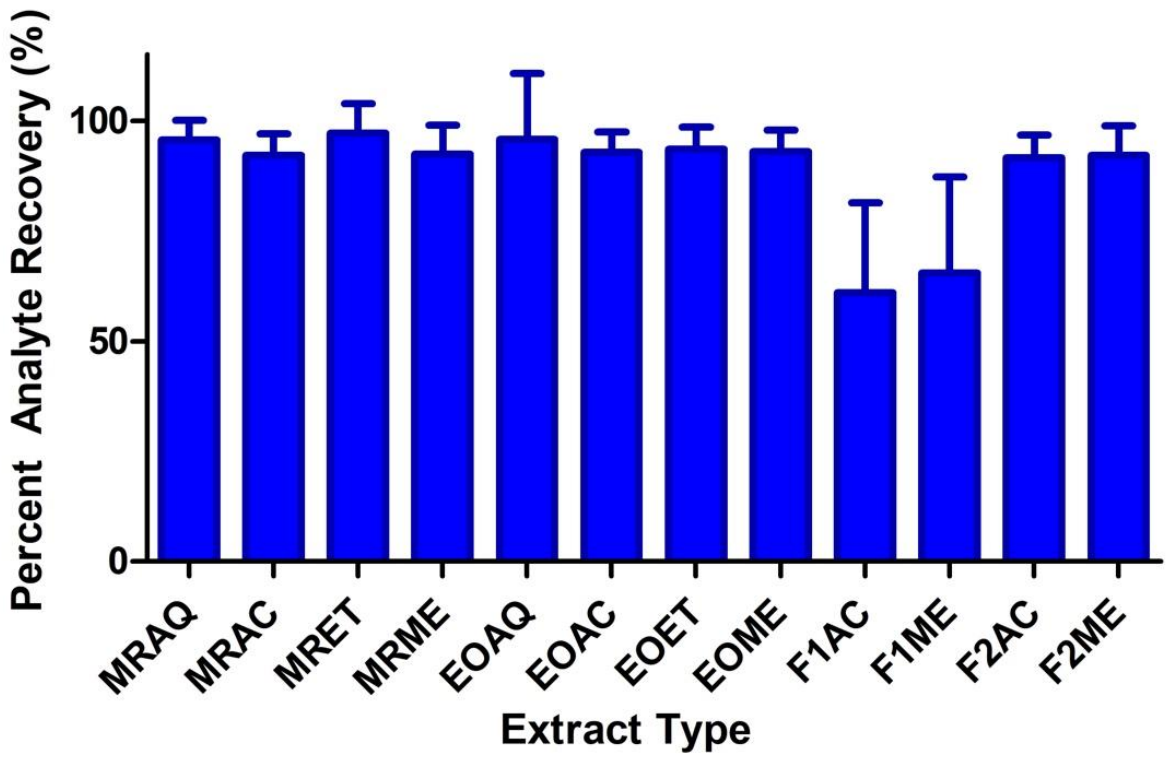

Figure 15. Illustration of differences in average anthocyanin stability for various extract types stored in acMeOH for 30 days in -80°C. Data shows is percent analyte recovery calculated by dividing the anthocyanin concentration on day 30 by the anthocyanin concentration on day 0 and multiplying by 100.

3.3 CYP3A4

3.3.1 Inhibition potential of BDS extracts on CYP3A4

A CYP3A4 inhibition assay was performed on genotyped CYP3A5*3/*3 HLM (homozygous non-expressors of CYP3A5) to examine the inhibition potential of F1 and F2 extracts without the interference of CYP3A5. To avoid overestimating the effects of BDIs *in-vitro*, the absorption profiles of botanicals should be considered since several components of BDS, such as polyphenols, are poorly bioavailable [143]. A robust way to forecast transcellular passive absorption from the gastrointestinal tract is the PAMPA. Furthermore, due to PAMPA's high throughput capabilities and correlation with *in-vivo* absorption data, it has been utilized to assess the permeability of natural products from complex mixtures during bioavailability screening [144]. Instead of evaluating the entire extract for CYP3A4 inhibition, we have used the PAMPA in this instance to investigate components of açaí BDS that either have or have not passively diffused across the artificial membrane to mimic physiological conditions better. Inhibition curves are displayed in **Figure 16** for both passively and non-passively diffused compounds of F1 and F2 extracts. For F1AC, passively and non-passively diffused compounds displayed 50% CYP3A4 inhibition at the donor compartment concentrations 1,253 and 15.58 ng/mL CG, respectively. F1ME extracts inhibited CYP3A4 at 1,486 and 5.764 ng/mL CG for both passively and non-passively diffused constituents. While no inhibitory effects were observed in the presence of F2ME passively or non-passively diffused constituents, the non-passively diffused constituents of F2AC inhibited CYP3A4 with a predicted IC_{50} value of 1,158 ng/mL CG. This value was predicted due to the inhibition not reaching 50% within the human-relevant concentration ranges administered. The non-passively diffused compounds in F1ME extract exhibited the highest inhibitory activities at concentrations less than the manufacturer's recommended dose at 2 capsules per intestinal fluid

volume (equivalent to 256.7 ng/mL CG or 2% of the daily dose). F1 extracts generally displayed higher inhibition potential than extracts of F2.

In contrast to our previous work, the passively diffused constituents did not inhibit CYP3A4 at a significantly relevant concentration. This indicates that BDS containing açaí may not inhibit CYP3A4, at least not through passively diffused compounds. Compounds from açaí BDS that inhibit CYP3A4 may be absorbed through other mechanisms, such as transporters. IC_{50} values reported for passively diffused F1 and F2 extracts constituents in the acceptor compartments for CYP3A4 inhibitory activity were calculated based on the concentrations of the extracts applied on the donor compartments of the PAMPA plates at time 0. These values do not reflect the concentration in the acceptor compartment.

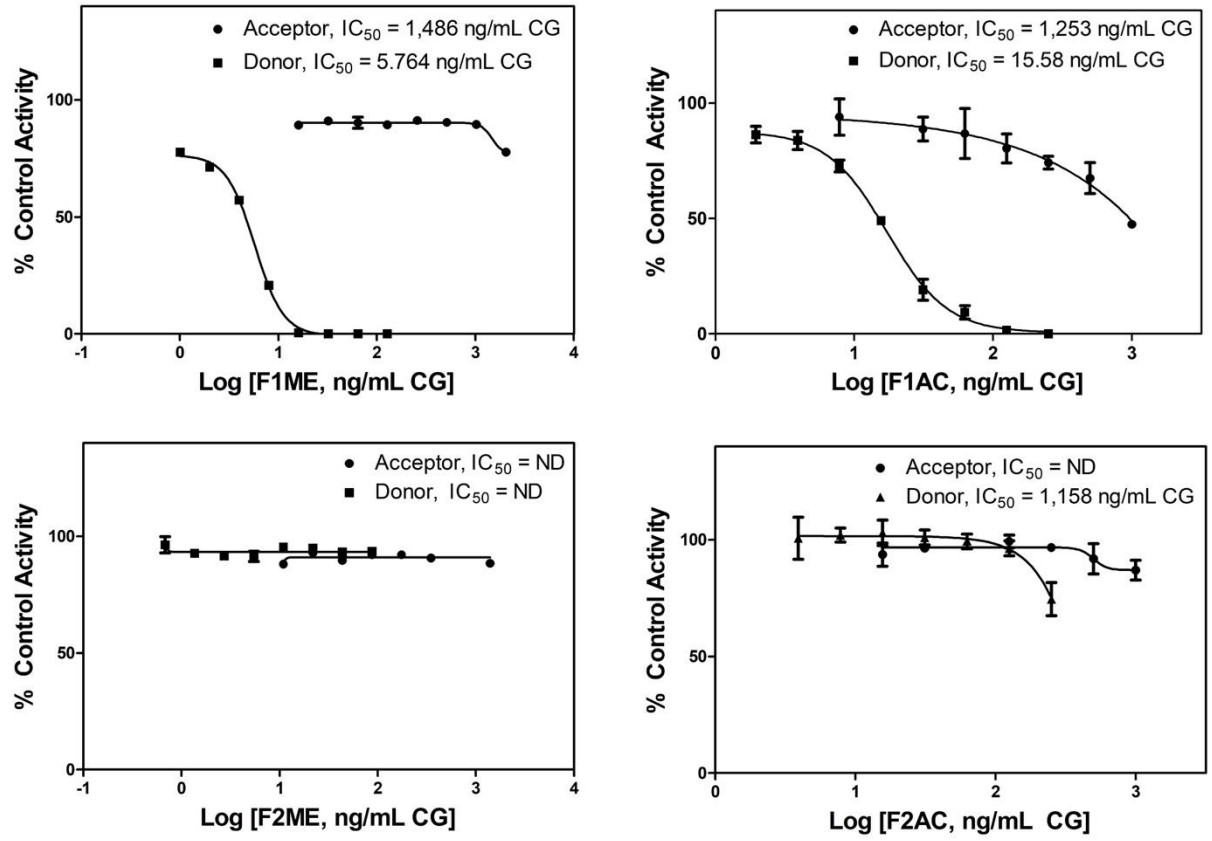

Figure 16. Inhibition curves for the inhibition of CYP3A4 by non-passively diffused (from PAMPA donor compartment) and passively diffused (from PAMPA acceptor compartment) compounds in açaí BDS formulations. Activity expressed as the percentage of the remaining activity compared with DMSO control (F1AC and F2AC extracts required no DMSO). Data expressed as mean ± SD of three independent experiments. IC_{50} values were calculated based on concentrations of PAMPA donor compartment at time 0.

3.3.2 LC-MS-based chemical characterization of BDS extracts

A method was made to perform chemical fingerprinting of the samples to identify potential CYP3A4 inhibitors from BDS extracts. In our previous work quantifying anthocyanins in açaí extracts including BDS samples, we found that the Poroshell 120 SB-C18 column provided good separation for anthocyanins from other compound classes found in açaí such as organic acids, flavonoids, terpenoids, and fatty acids [126]. This method was developed through the pooling of the four extracts and trying various gradients until optimal separation was achieved by employing the same mobile phase as our previously optimized approach and assessing a variety of chromatographic gradients and flow rates (including other mobile phases, such as aqueous phase (A): water with added FA and organic phase (B): MeOH:ACN (50:50) with added FA) [125]. The method was then assessed for intraday and interday reproducibility by running the samples twice on the same day and seven days apart. The chromatographic method which showed the best chromatographic separation and peak shape was the binary mobile phase consisting of 0.1% FA in water and 0.1% FA in MeOH at a flow rate of 0.2 mL/min. A method was developed to separate various compound classes with a broad polarity range in complex açaí BDS extracts.

Previously, Zhang et al. (2019) was the first to use MassHunter Profinder and Mass Profiler Professional (MPP) as part of a permeability study. Here it was used to examine similarities and differences between constituents of F1 and F2 extracts as well as the permeability of their constituents. When comparing the entities of F1 and F2 extracts, sample groups included the BDS extracts dissolved in acMeOH for chemical analysis. After batch recursive feature extraction and data alignment, each extract's total number of features was 40, 73, 45, and 97 for F1AC, F1ME, F2AC, and F2ME, respectively (**Figure 17**). Out of a total of 40 entities in F1AC, 9 were found to be unique. For F1ME, 23 chemical entities were unique to this extract. Only 3 unique extracts were

found in F2AC while the greatest number of unique compounds (38) were found in F2ME. There were 21 compounds shared only between the two ME extracts and 6 compounds found only in AC extracts. Our previous assessment of raw organic açaí fruit powder extracts found many more compounds present (715 in MeOH açaí extract), which leads us to believe that the BDS powders are less chemically complex than raw materials due to processing and dilution with excipients. The lack of chemical complexity could be why the inhibitory effects of açaí BDS extracts were not observed compared to those previously shown with MeOH açaí fruit powder extracts.

Our permeability studies found that 35, 65, 55, and 85 entities were extracted from PAMPA donor compartments of F1AC, F1ME, F2AC, and F2ME, respectively (**Figure 18**). Background ions found in DMSO/buffer control were excluded from analysis using Profinder software before visualization using MPP.

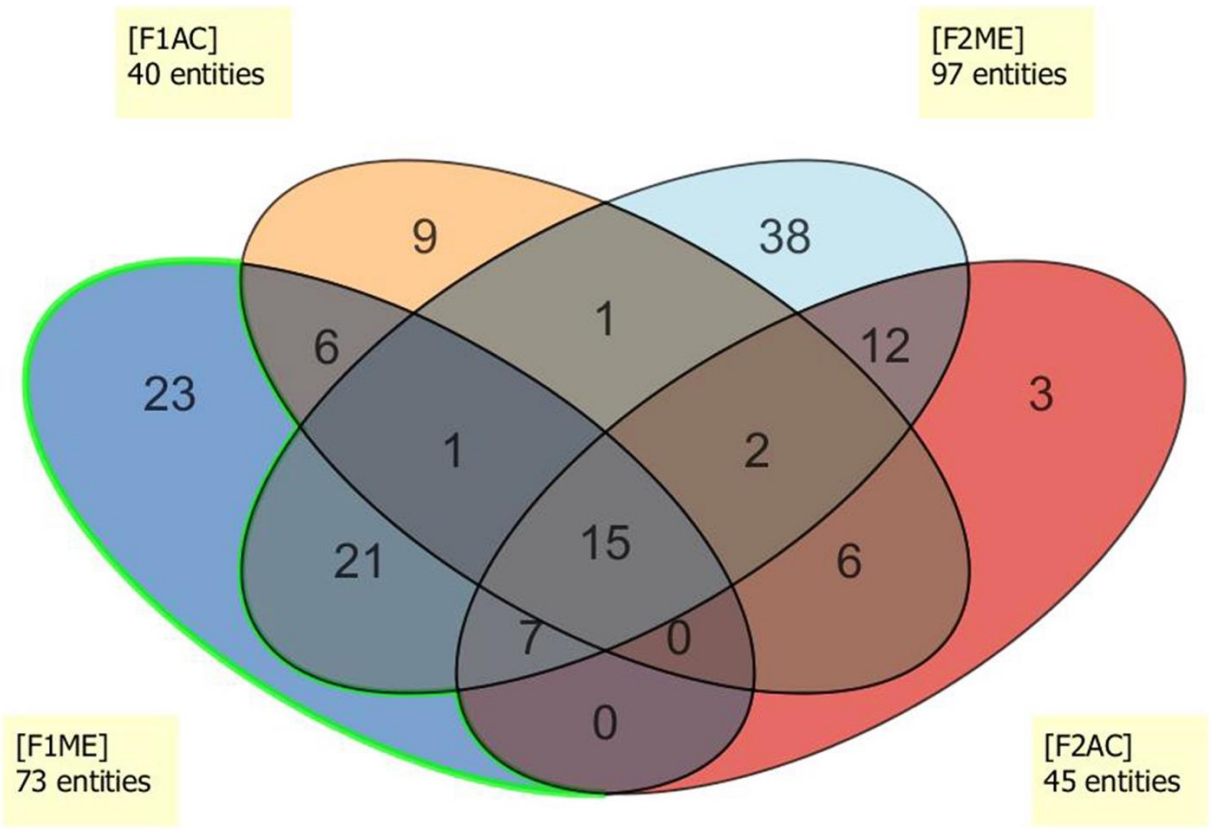

Figure 17. Venn diagram of BDS extract compounds present in each of the four BDS extracts. Compounds unique to F1ME (23) which were further examined are highlighted in green.

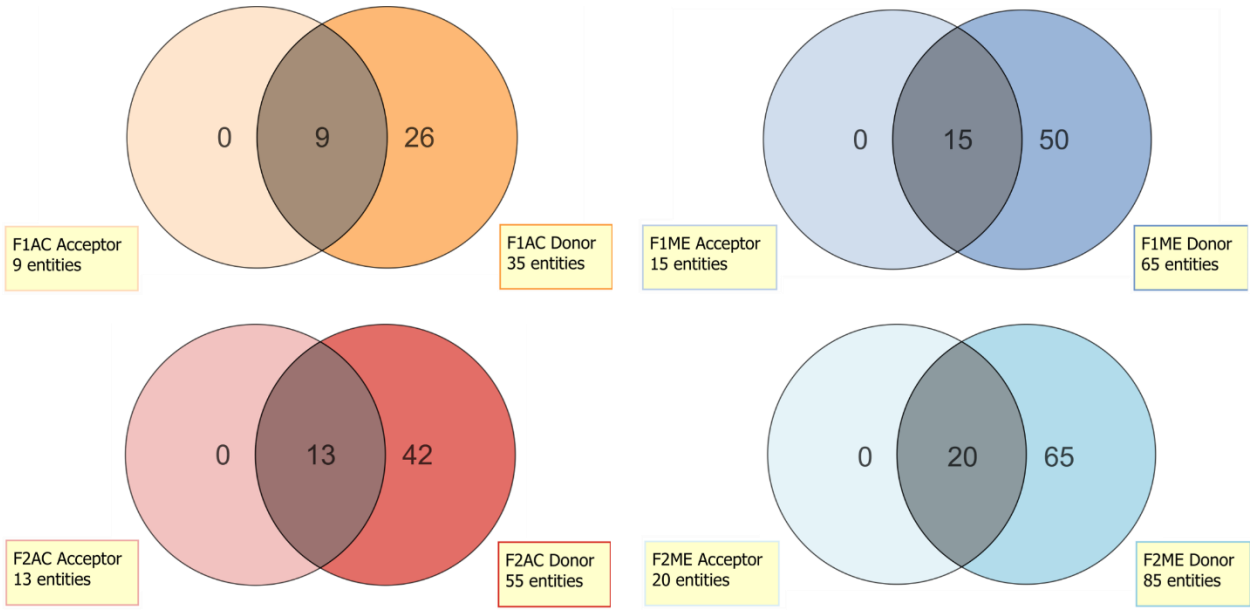

Figure 18. Venn diagrams of BDS extract compound passive permeability. Entities from DMSO buffer control were excluded as part of Profinder analysis.

3.3.3 Structural elucidation of constituents with CYP3A4 inhibition activity

In a previous work predicting and identifying antibacterial compounds from *Psidium guajava* L, we demonstrated the power of having an automatic dashboard that integrates mass spectrometry and bioactivity data into a molecular network for fast identification of bioactive natural products [120]. For complex mixtures, getting MS/MS data for all compounds present in the mixture can be challenging. However, all features can be examined using full-scan mass spectrometry data. Non-passively diffused constituents of F1ME showed the highest CYP3A4 inhibition potential. Therefore, we used this tool to find 6 features with significant bioactivity scores ($p < 0.05$) predicted to be CYP3A4 inhibitors listed in **Table 9** with their assigned formulas, RTs, and MS and MS/MS data. Out of these 6 compounds, only compound **3** could be tentatively identified as betaine (N-trimethyl glycine) with an MS/MS fragmentation match of 92.52% at 40 eV.

Compound **3** was assigned as betaine according to the reported MS/MS spectra in the METLIN database, where the compound contained matching characteristic fragment ions including *m/z* 118, 59, 58 [145]. Betaine is a common metabolite of plants and animals whose main function in plants is to shield cells against osmotic inactivation. It is primarily found in wheat bran and wheat germ, beets, and spinach. In humans, betaine has been found to reduce vascular risk factors, protect internal organs, and boost performance [146]. The GNPS-Bioactivity tool predicted betaine from the correlation between the uniqueness and abundance of mass spectral features and bioactivity of the sample. However, due to its small size and lack of affinity for CYP3A4, we do not believe that betaine is an inhibitor of CYP3A4 *in vivo.*

For the other five compounds, MS/MS experiments performed up to 60 eV collision energies provided fragmentation patterns that did not yield compound matches in any of the 18 databases searched. Even though most libraries only include fragmentation spectrum up to 45 eV, we hoped increasing collision energy would provide additional fragments and give more structural information. Five compounds, **1**, **2**, **4**, **5,** and **6**, could not be identified, but they are believed to be some form of unknown phospholipid based on the RT and MS/MS fragment losses. All five compounds have neutral losses of 119.96 (C_2HO_4P) and 79.96 (HPO_3) in ESI^+ as well as fragment ions 96.96 ($H_2PO_4^-$) and 78.95 (PO_3^-) in ESI^- (data not shown) [147]. For compounds **2** and **6** the loss of 79.96 is much more minor than in the other three unknown compounds. While compound **5** had a very high match to LysoPI (13:0/0:0) in our METLIN library based only on parent mass, the fragmentation pattern was not a match according to LIPID MAPS (which only provided a ESI^- *in silico* list of MS/MS fragments).

Table 9. Predicted bioactive compounds for CYP3A4 inhibition from F1ME extract.

	RT[a]	*m/z* [Adduct]	Molecular Formula	Error (ppm)	Score[b]	ESI-MS/MS fragment m/z (% base peak)	P-value	Compound Name
1	24.53	575.2833 $[M+H]^+$	$C_{24}H_{47}O_{13}P$	0.35	91.21	40 eV CE: 575.27 (100), 495.33 (4), 455.33 (21), 142.94 (6) 60 eV CE: 455.36 (46), 142.90 (100), 107.04 (51)	0.0021	*Unknown*
2	24.7	619.3094 $[M+H]^+$	$C_{26}H_{51}O_{14}P$	0.10	92.64	40 eV CE: 619.30 (100), 539.34 (4), 499.35 (19), 142.94 (3) 60 eV CE: 619.29 (30), 499.36 (54), 287.14 (54), 237.06 (45.8), 142.93 (100), 57.07 (49)	0.0024	*Unknown*
3	1.23	118.0862 $[M]^+$	$C_5H_{12}NO_2$	0.24	92.52	20 eV CE: 118.08 (22), 59.07 (50), 58.06 (100) 40 eV CE: 59.07 (1), 58.06 (100), 43.04 (6), 42.03 (8)	0.0039	Betaine

4	24.84	663.3356 $[M+H]^+$	$C_{28}H_{55}O_{15}P$	0.25	93.87	40 eV CE: 663.33 (100), 543.38 (12) 60 eV CE: 663.34 (100), 543.38 (99), 309.13 (36), 239.08 (20), 221.07 (21), 151.03 (21), 142.93 (30)	0.0097	*Unknown*
5	24.33	531.2573 $[M+H]^+$	$C_{22}H_{43}O_{12}P$	0.24	88.35	20 eV CE: 531.25 (100), 411.30 (5) 40 eV CE: 531.25 (100), 411.30 (32), 142.94 (19)	0.0363	*Unknown*
6	24.95	707.3618 $[M+H]^+$	$C_{30}H_{59}O_{16}P$	0.14	92.43	40 eV CE: 707.35 (100), 587.41 (8) 60 eV CE: 707.35 (98), 587.41 (100), 543.38 (11), 309.12 (10), 239.07 (14), 221.08 (17), 142.93 (20).	0.0411	*Unknown*

[a]Retention time in minutes.

[b]Score for molecular formula generated based on mass, isotopic abundance, and isotopic spacing except for compound **3** which the score is for formula generation and MS/MS fragmentation match.

3.4 UGT inhibition studies

3.4.1 Method development for quantitation of glucuronide metabolites

The goal was to develop a method quantifying glucuronide metabolites and an IS with a run time that allows for high throughput analysis. The six metabolites and their respective isoforms are listed in **Table 10**. The structures of the UGT metabolites used are included in **Figure 19.** A method has not been published previously for the separation of these six UGT metabolites with the internal standard chlorpropamide. Previous methods for UGT cocktail assays have alternatively used 4-hydroxyindole for UGT1A4 [148], zidovudine for UGT2B7 [149, 150], etoposide for UGT1A1 and isoferulic acid for UGT1A9 [150]. Chen et al. also used chlorpropamide as an internal standard, but only for ESI^- ions. Neither Seo et al. nor Gradinaru et al. used internal standards for their metabolite quantification. All three methods published previously used various C18 stationary phases for their separations.

Our method development began by using our previously published method for CYP3A4-mediated midazolam metabolism quantitation. When this method was unsuccessful in resolving the metabolites, we tried various chromatographic gradients until an optimal one could be reached. After this, two additional stationary phases were tried including an end-capped C18 column and a phenyl hexyl column. The ZORBAX Eclipse Plus Phenyl-Hexyl (Agilent Technologies) column provided the greatest amount of separation using a binary mobile phase consisting of 0.1% FA in water and 0.1% FA in ACN at a flow rate of 0.5 mL/min. A comparison of the separations using a C18 column and the phenyl hexyl column, each with optimized methods, is shown in **Figure 20**.

Using a C18 column, we were able to separate well compounds trifluoperazine N-glucuronide (**3**) and propofol glucuronide (**5**), which is a separation that was not achieved by Seo

et al. (**Figure 20A**). Similarly, Seo et al. found separating the metabolites of UGT1A6 (**4**) and UGT2B7 (**6**) to be difficult, even when using 4-hydroxyindole glucuronide rather than serotonin glucuronide. These glucuronide metabolites **4** and **6** were also poorly retained using C18 as a stationary phase with retention times around 1 minute. Using the phenyl-hexyl column, compounds **4** and **6** were retained more in addition to being completely resolved from one another.

In similar fashion to Chen et al., compound **2** could not be resolved from IS chlorpropamide (**7**) when using C18 as a stationary phase (**Figure 20A**). The phenyl-hexyl column was able to separate metabolite **2** from **7**, although not completely resolved from propofol glucuronide (**5**) (**Figure 20B**). However, the peak apexes of **2** and **5**, which are most important when performing quantitation with a QTOF, are not overlapping. In addition to being able to retain compounds based on hydrophobic interactions, like a C18 column, the phenyl-hexyl column provides increased specificity for compounds with pi bonds and exposed lone pairs which allowed for better separation of metabolites and the IS. Glucuronide metabolites for UGT isoforms 1A1, 1A3, 1A4, 1A6, 1A9, and 2B7 eluted at 4.292, 4.749, 4.498, 1.920, 4.703, and 2.105 min, respectively (**Table 10**). The IS chlorpropamide eluted at 5.163 min. Isotopically labeled standards are available for each of the glucuronide metabolites, but chlorpropamide was chosen to be the IS instead due to reliable commercial availability in addition to ionization in both ESI^+ and ESI^- (as seen in **Figure 21**). All metabolites and the IS could be detected accurately within a range of 5 ppm. Because of the resolution of each of the compounds, this method could be used in isolated assays which measure inhibition of metabolite formation in only one UGT isoform and potentially has use in UGT cocktail assays (which assay multiple UGT enzymes for inhibited substrate metabolism at once).

Table 10. LC-MS detection of glucuronide metabolites from in-vitro assay conditions.

	UGT	Metabolite name	RT (min)	Ion Formula	Adducts	*m/z*	Dif (ppm)
1	1A1	17-beta-estradiol glucuronide	4.292	$C_{24}H_{31}O_8$	$[M-H]^-$	447.2025	2.58
2	1A3	Chenodeoxycholic acid 24-acyl-glucuronide	4.749	$C_{30}H_{47}O_{10}$	$[M-H]^-$	567.3201	4.63
3	1A4	Trifluoperazine N-glucuronide	4.498	$C_{27}H_{32}F_3N_3O_6S$	$[M+H]^+$	584.2034	-0.46
4	1A6	Serotonin glucuronide	1.920	$C_{16}H_{21}N_2O_7$	$[M+H]^+$	353.1341	-0.64
5	1A9	Propofol glucuronide	4.703	$C_{18}H_{25}O_7$	$[M-H]^-$	353.1626	5.73
6	2B7	Naloxone 3-beta-glucuronide	2.105	$C_{25}H_{30}NO_{10}$	$[M+H]^+$	504.1860	-0.84
7	IS[a]	Chlorpropamide	5.163	$C_{10}H_{12}ClN_2O_3S$	$[M-H]^-$	275.0276	4.86
				$C_{10}H_{14}ClN_2O_3S$	$[M+H]^+$	277.0406	-0.78

[a]Internal Standard

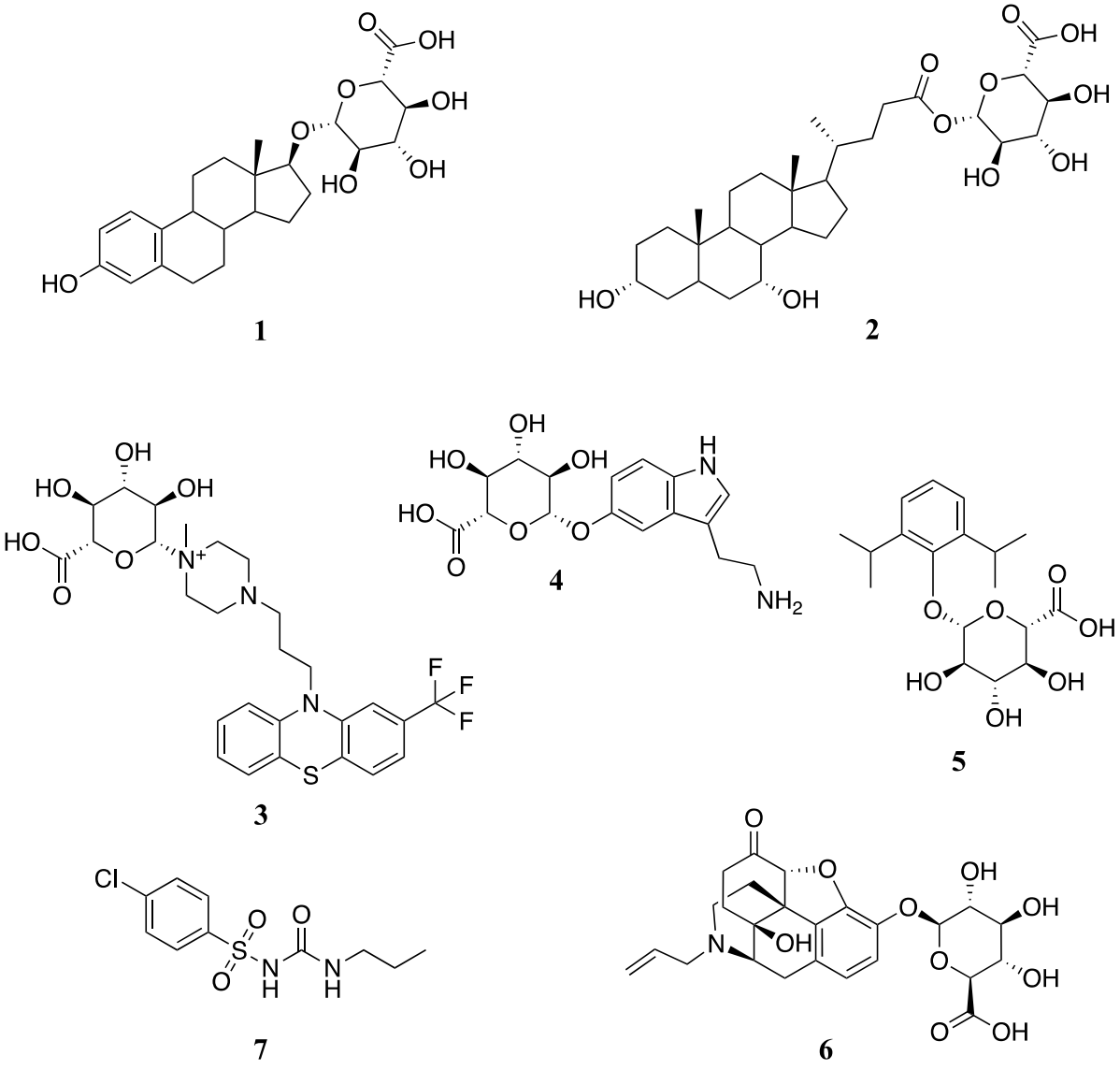

Figure 19. Structures of UGT metabolites used in development of LC-MS assay. Compounds are labeled according to Table 10.

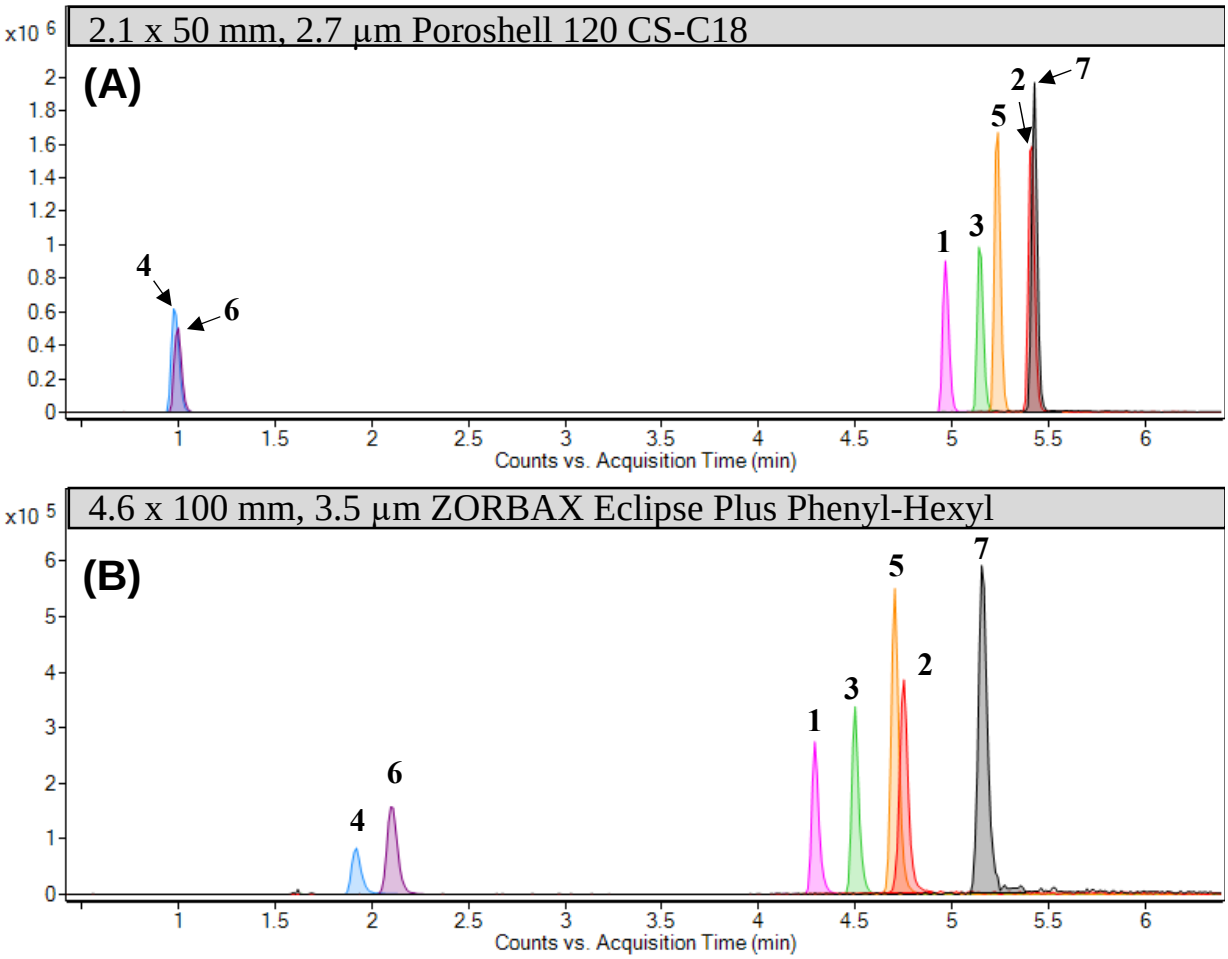

Figure 20. Comparison of (**A**) traditional C18 and (**B**) phenyl-hexyl stationary phases for the separation of UGT metabolites (**1-6**) and IS (**7**). Metabolites are labeled according to Table 10.

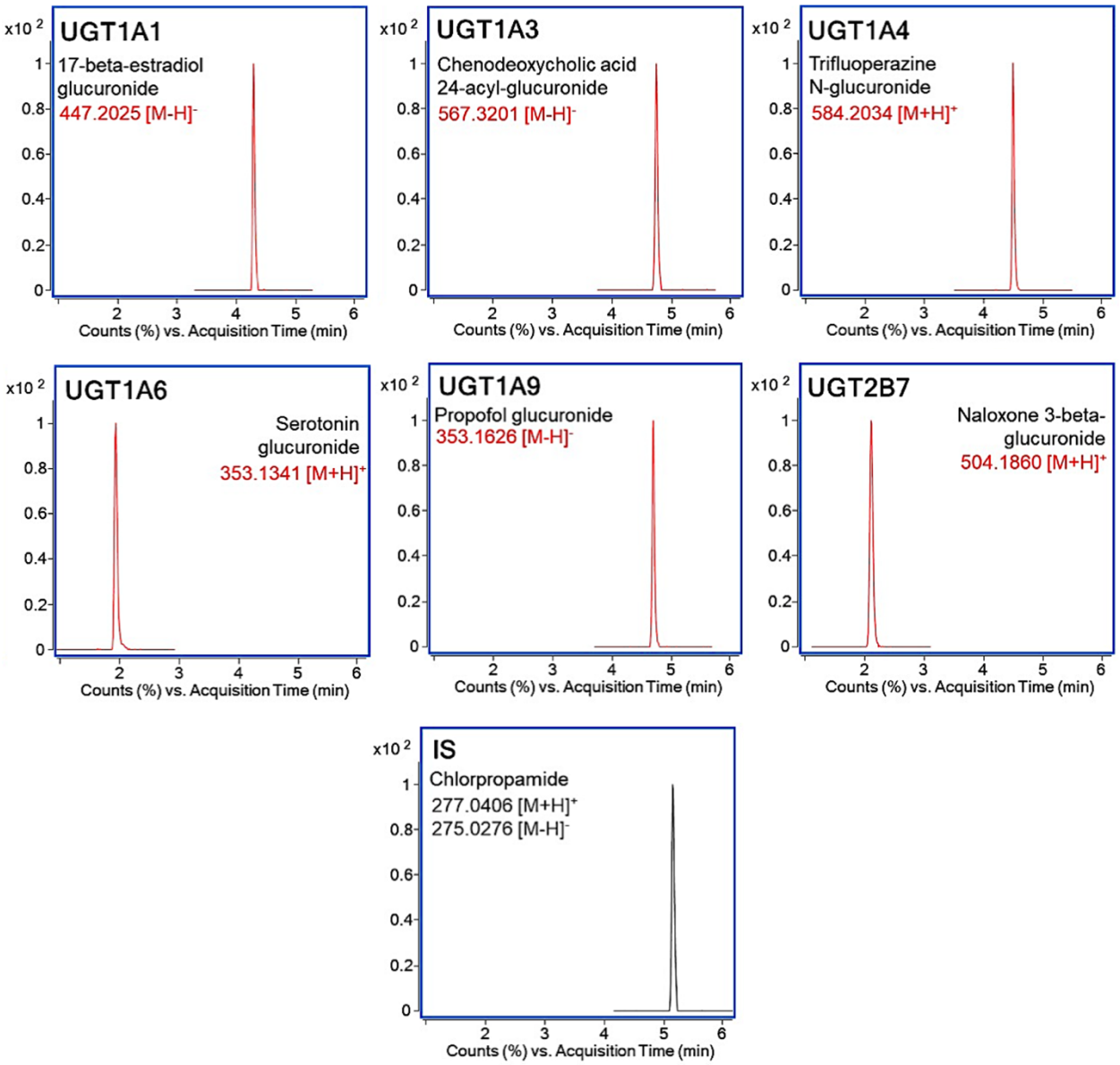

Figure 21. Extracted ion chromatograms (EICs) for UGT metabolites and IS chlorpropamide by LC-MS.

4. Conclusions and Future Directions

Cancer remains the leading cause of death worldwide, and BDS are often consumed more by cancer patients than otherwise healthier patients without cancer to alleviate side effects of chemotherapy drugs and/or increase quality of life. However, many patients do not know the risks of concomitant use of BDS with anticancer drugs and the possibility for increased AEs, which may be life-threatening. Açaí is a popular botanical which cancer patients use to complement their anticancer agents. The FAERS database indicated potential for life-threatening AEs when patients used anticancer drugs and BDS containing açaí synchronously, but the mechanism of this interaction remains unknown. Our group previously found that both passively and non-passively diffused compounds in MeOH açaí fruit extract displayed significant inhibition of hepatic CYP3A4 – suggesting potential for interactions between açaí BDS and CYP3A4-interactive drugs. Before testing this hypothesis, analytical methods to chemically characterize and standardize açaí products prior to *in vitro* testing were needed.

An LC-MS method was generated for chemical fingerprinting, untargeted metabolomics, and identification of chemical constituents of 16 açaí extracts from different origins and extraction types. This method allowed for the identification of several compound classes, including fatty acids, flavonoids, phenols, organic acids, and amino acid derivatives, among other constituents. Of these 173 compounds that were found, 138 have not previously been reported in açaí to our knowledge. The success of the compound identification and specificity of the statistical models created indicates that our strategy for LC-MS and LC-MS/MS analysis could be used for additional botanicals in the future that are of interest for BDIs. This LC-MS/MS method can be made into a targeted metabolomics approach specific to compounds of interest that may have been important to the PCA or HCA models that were not previously identified using an untargeted approach.

The future of this work will result in the characterization of compounds from açaí which are either passively or non-passively permeable after oral consumption. Because the açaí extracts have been examined and constituents described, many compounds that are intestinally permeable may have been tentatively or positively identified in this work. This LC-MS chemical fingerprinting method will be used to characterize samples from *in-vitro* PAMPAs in addition to *in-vivo* bioavailability studies using rats.

Extracts from botanical natural products should be chemically standardized to certain concentrations of bioactive or marker compounds prior to testing *in vitro* to allow for concentrations that can best represent physiological conditions. Only one compound, cyanidin 3-*O*-glucoside, has been quantified in human plasma previously, so it and three additional anthocyanins were quantified in our açaí extracts.

In past literature, methods using MS to quantify anthocyanins in açaí extracts ranged from 35-120 minutes per injection. These methods with long run times make the quantitation very difficult and time-consuming. In this study, we reported a 10-minute quantitative method for anthocyanins that is fast while remaining reproducible, sensitive, and accurate. In conclusion, the column used in this quantitative method was a 2.1 x 100 mm, 2.7 μm Poroshell 120 EC-C18 column which greatly enhanced our chromatographic method and allowed for shorter run times, sharper peaks, and greater sensitivity to our analytes. All four anthocyanins were present in each of our twelve extracts with a similar analyte profile with cyanidin 3-*O*-rutinoside being the highest in concentration followed by cyanidin 3-*O*-glucoside. This is the first comparison of açaí anthocyanin profiles between the fresh fruits and processed powders and BDS capsules, where we found that the highest concentration of anthocyanins was found in the açaí organic fruit powder. The lowest concentration of anthocyanins was found in the BDS capsules, in which the two

formulations had different anthocyanin profiles despite both being made from aqueous açaí extracts. In addition to the differences between profiles, the Natrol dietary supplement capsule (F2) had nearly twice the anthocyanin content of the Nature Way dietary supplement capsule (F1). The anthocyanins in these açaí extracts were also found to be very stable except for the F1ME and F1AC extracts in which one anthocyanin, peonidin 3-rutinoside (**4**) could not be quantified after 30 days. Lastly, we were able to generate a LC-MS method for this purpose that was assessed for linearity, sensitivity, accuracy, intermediate precision, and repeatability. A fast and robust method is necessary for the quantitation of bioactive compounds so that botanical extracts can be standardized accurately before testing in biological assays. This method can be used to measure anthocyanins reproducibly in a variety of açaí extract types for industrial or academic purposes.

In the project prior, our group elucidated that both passively and non-passively diffused compounds in MeOH açaí fruit extract displayed significant inhibition of hepatic CYP3A4. This led to the current project which investigated the potential for constituents in açaí BDS to inhibit CYP3A4 metabolism of midazolam. Our research demonstrated that non-passively diffused compounds in the F1ME extract had the greatest potential to inhibit CYP3A4 and result in CYP3A4-mediated BDIs. The identities of one compound, betaine, and descriptions of 5 unidentified compounds characterized by uniqueness and high abundance in F1ME were reported. This method, which makes use of PAMPA, could reduce the tendency for *in vitro* drug metabolism studies to produce inflated results. This method may be applied to further improve the accuracy of measuring *in vitro* BDIs. While açaí BDS may not inhibit CYP3A4 through passively diffused compounds, the non-passively diffused compounds may be absorbed through other mechanisms and should be further examined om a subsequent project.

UGTs are an understudied enzyme family for their potential to be a target of BDIs. A literature search performed found that many anticancer drugs metabolized by UGTs may have serious AEs related to cardiovascular symptoms if taken concomitantly with a UGT inhibitor. Based on this, we believed that UGTs could be a potential target for BDIs caused by açaí constituents when taken synchronously. In this study, we report an LC-MS method that can be used to quantify the metabolites of six UGT probe substrates so that these UGT isoforms can be assessed for *in vitro* inhibition by açaí extracts. A method had not been previously published using these six UGT metabolites with the internal standard chlorpropamide. The method created was able to separate the 6 metabolites and IS within a complex matrix with minimal sample preparation in under 6 minutes with a two-minute re-equilibration time (for a total run time of 8 minutes per sample) using a phenyl-hexyl stationary phase. This method was capable of separating UGT metabolites trifluoperazine glucuronide and propofol glucuronide, in addition to the separation of chenodeoxycholic acid glucuronide from the internal standard chlorpropamide. These two separations had not been successfully achieved in previously published methods. Later, this method will be used to elucidate enzyme kinetics and develop these *in vitro* assays before testing the inhibition potential of açaí extracts.

References

[1] Sung, H., J. Ferlay, R.L. Siegel, M. Laversanne, I. Soerjomataram, A. Jemal, and F. Bray, *Global Cancer Statistics 2020: GLOBOCAN Estimates of Incidence and Mortality Worldwide for 36 Cancers in 185 Countries.* CA: A Cancer Journal for Clinicians, 2021. **71**(3): p. 209-249.

[2] Alwhaibi, M., Y. AlRuthia, T.M. Alhawassi, H. Almalag, H. Alsalloum, and B. Balkhi, *Polypharmacy and comorbidities among ambulatory cancer patients: A cross-sectional retrospective study.* Journal of Oncology Pharmacy Practice, 2019. **26**(5): p. 1052-1059.

[3] van Leeuwen, R.W., E.L. Swart, F.A. Boom, M.S. Schuitenmaker, and J.G. Hugtenburg, *Potential drug interactions and duplicate prescriptions among ambulatory cancer patients: a prevalence study using an advanced screening method.* BMC cancer, 2010. **10**(1): p. 1-5.

[4] Popa, M.A., K.J. Wallace, A. Brunello, M. Extermann, and L. Balducci, *Potential drug interactions and chemotoxicity in older patients with cancer receiving chemotherapy.* Journal of geriatric oncology, 2014. **5**(3): p. 307-314.

[5] Tamura, B.K., C.L. Bell, M. Inaba, and K.H. Masaki, *Outcomes of polypharmacy in nursing home residents.* Clinics in geriatric medicine, 2012. **28**(2): p. 217-236.

[6] Goldberg, R.M., J. Mabee, L. Chan, and S. Wong, *Drug-drug and drug-disease interactions in the ED: analysis of a high-risk population.* The American journal of emergency medicine, 1996. **14**(5): p. 447-450.

[7] Li, C., R.A. Hansen, C. Chou, A.I. Calderón, and J. Qian, *Trends in botanical dietary supplement use among US adults by cancer status: The National Health and Nutrition Examination Survey, 1999 to 2014.* Cancer, 2018. **124**(6): p. 1207-1215.

[8] Werneke, U., J. Earl, C. Seydel, O. Horn, P. Crichton, and D. Fannon, *Potential health risks of complementary alternative medicines in cancer patients.* Br J Cancer, 2004. **90**(2): p. 408-13.

[9] Tascilar, M., F.A. de Jong, J. Verweij, and R.H. Mathijssen, *Complementary and alternative medicine during cancer treatment: beyond innocence.* Oncologist, 2006. **11**(7): p. 732-41.

[10] Frenkel, M., D.I. Abrams, E.J. Ladas, G. Deng, M. Hardy, J.L. Capodice, M.F. Winegardner, J.K. Gubili, K.S. Yeung, H. Kussmann, and K.I. Block, *Integrating dietary supplements into cancer care.* Integr Cancer Ther, 2013. **12**(5): p. 369-84.

[11] Marian, M.J., *Dietary Supplements Commonly Used by Cancer Survivors: Are There Any Benefits?* Nutrition in Clinical Practice, 2017. **32**(5): p. 607-627.

[12] Velicer, C.M. and C.M. Ulrich, *Vitamin and mineral supplement use among US adults after cancer diagnosis: a systematic review.* J Clin Oncol, 2008. **26**(4): p. 665-73.

[13] Ávila-Gálvez, M., J.A. Giménez-Bastida, J.C. Espín, and A. González-Sarrías, *Dietary Phenolics against Breast Cancer. A Critical Evidence-Based Review and Future Perspectives.* Int J Mol Sci, 2020. **21**(16).

[14] Drozdoff, L., E. Klein, M. Kalder, C. Brambs, M. Kiechle, and D. Paepke, *Potential Interactions of Biologically Based Complementary Medicine in Gynecological Oncology.* Integr Cancer Ther, 2019. **18**: p. 1534735419846392.

[15] Alschuler, L.N. and K.A. Gazella, *The Definitive Guide to Cancer: An Integrative Approach to Prevention, Treatment, and Healing.* 3rd ed. 2010, Berkeley, CA: Celestial Arts.

[16] Yamaguchi, K.K.d.L., L.F.R. Pereira, C.V. Lamarão, E.S. Lima, and V.F. da Veiga-Junior, *Amazon acai: Chemistry and biological activities: A review.* Food Chemistry, 2015. **179**: p. 137-151.

[17] Smith, T., F. Majid, V. Eckl, and C.M. Reynolds, *Herbal Supplements Sales in US Increase by Record-Breaking 17.3% in 2020: Sales of immune health, stress relief, and heart health supplements grow during COVID-19 pandemic.* HerbalGram, 2021(131): p. 52-65.

[18] Fahim, S.M., A.U. Mishuk, N. Cheng, R. Hansen, A.I. Calderón, and J. Qian, *Adverse event reporting patterns of concomitant botanical dietary supplements with CYP3A4 interactive & CYP3A4 non-interactive anticancer drugs in the U.S. Food and Drug Administration Adverse Event Reporting System (FAERS).* Expert Opinion on Drug Safety, 2019. **18**(2): p. 145-152.

[19] Lee, J., *Anthocyanins of açai products in the United States.* NFS Journal, 2019. **14-15**: p. 14-21.

[20] *Center for Food Safety and Applied Nutrition Center (CFSAN) Adverse Event Reporting System (CAERS)*. United States Food and Drug Administration.

[21] Guillemette, C., É. Lévesque, and M. Rouleau, *Pharmacogenomics of Human Uridine Diphospho-Glucuronosyltransferases and Clinical Implications.* Clinical Pharmacology & Therapeutics, 2014. **96**(3): p. 324-339.

[22] Allain, E.P., M. Rouleau, E. Lévesque, and C. Guillemette, *Emerging roles for UDP-glucuronosyltransferases in drug resistance and cancer progression.* British Journal of Cancer, 2020. **122**(9): p. 1277-1287.

[23] *Atazanavir sulfate (Reyataz®) product package insert.* Bristol-Meyers Squibb: Princeton, NJ.

[24] Zientek, M.A., T.C. Goosen, E. Tseng, J. Lin, J.N. Bauman, G.S. Walker, P. Kang, Y. Jiang, S. Freiwald, D. Neul, and B.J. Smith, *In Vitro Kinetic Characterization of Axitinib Metabolism.* Drug Metabolism and Disposition, 2016. **44**(1): p. 102.

[25] Abdel-Rahman, O. and M. Fouad, *Risk of cardiovascular toxicities in patients with solid tumors treated with sunitinib, axitinib, cediranib or regorafenib: an updated systematic review and comparative meta-analysis.* Crit Rev Oncol Hematol, 2014. **92**(3): p. 194-207.

[26] Ramalingam, S.S., C.P. Belani, C. Ruel, P. Frankel, B. Gitlitz, M. Koczywas, I. Espinoza-Delgado, and D. Gandara, *Phase II Study of Belinostat (PXD101), a Histone Deacetylase Inhibitor, for Second Line Therapy of Advanced Malignant Pleural Mesothelioma.* Journal of Thoracic Oncology, 2009. **4**(1): p. 97-101.

[27] Peer, C.J., A.K.L. Goey, T.M. Sissung, S. Erlich, M.-J. Lee, Y. Tomita, J.B. Trepel, R. Piekarz, S. Balasubramaniam, S.E. Bates, and W.D. Figg, *UGT1A1 genotype-dependent dose adjustment of belinostat in patients with advanced cancers using population pharmacokinetic modeling and simulation.* Journal of clinical pharmacology, 2016. **56**(4): p. 450-460.

[28] Mincu, R.I., A.A. Mahabadi, L. Michel, S.M. Mrotzek, D. Schadendorf, T. Rassaf, and M. Totzeck, *Cardiovascular Adverse Events Associated With BRAF and MEK Inhibitors: A Systematic Review and Meta-analysis.* JAMA Network Open, 2019. **2**(8): p. e198890-e198890.

[29] Badowski, M.E., B. Burton, K.M. Shaeer, and J. Dicristofano, *Oral oncolytic and antiretroviral therapy administration: dose adjustments, drug interactions, and other considerations for clinical use.* Drugs Context, 2019. **8**: p. 212550.

[30] Pai, V.B. and M.C. Nahata, *Cardiotoxicity of Chemotherapeutic Agents.* Drug Safety, 2000. **22**(4): p. 263-302.

[31] Wen, Z., M.N. Tallman, S.Y. Ali, and P.C. Smith, *UDP-glucuronosyltransferase 1A1 is the principal enzyme responsible for etoposide glucuronidation in human liver and intestinal microsomes: structural characterization of phenolic and alcoholic glucuronides of etoposide and estimation of enzyme kinetics.* Drug Metab Dispos, 2007. **35**(3): p. 371-80.

[32] Matrone, G., J.J. Mullins, C.S. Tucker, and M.A. Denvir, *Effects of Cyclin Dependent Kinase 9 inhibition on zebrafish larvae.* Cell cycle (Georgetown, Tex.), 2016. **15**(22): p. 3060-3069.

[33] Hagenauer, B., A. Salamon, T. Thalhammer, O. Kunert, E. Haslinger, P. Klingler, A.M. Senderowicz, E.A. Sausville, and W. Jäger, *In vitro glucuronidation of the cyclin-dependent kinase inhibitor flavopiridol by rat and human liver microsomes: involvement of UDP-glucuronosyltransferases 1A1 and 1A9.* Drug Metab Dispos, 2001. **29**(4 Pt 1): p. 407-14.

[34] Blandizzi, C., B. De Paolis, R. Colucci, A. Di Paolo, R. Danesi, and M. Del Tacca, *Acetylcholinesterase Blockade Does Not Account for the Adverse Cardiovascular Effects of the Antitumor Drug Irinotecan: A Preclinical Study.* Toxicology and Applied Pharmacology, 2001. **177**(2): p. 149-156.

[35] Paoluzzi, L., A.S. Singh, D.K. Price, R. Danesi, R.H. Mathijssen, J. Verweij, W.D. Figg, and A. Sparreboom, *Influence of genetic variants in UGT1A1 and UGT1A9 on the in vivo glucuronidation of SN-38.* J Clin Pharmacol, 2004. **44**(8): p. 854-60.

[36] Ameri, P., G. Tini, P. Spallarossa, V. Mercurio, C.G. Tocchetti, and I. Porto, *Cardiovascular safety of the tyrosine kinase inhibitor nintedanib.* Br J Clin Pharmacol, 2021. **87**(10): p. 3690-3698.

[37] Lamb, Y.N., *Nintedanib: A Review in Fibrotic Interstitial Lung Diseases.* Drugs, 2021. **81**(5): p. 575-586.

[38] Goldman, L. and A.I. Schafer, *Goldman-Cecil medicine*. 26th edition. ed. 2020, Philadelphia, PA: Elsevier.

[39] Moore, D., *Panobinostat (Farydak): A Novel Option for the Treatment of Relapsed Or Relapsed and Refractory Multiple Myeloma.* P & T : a peer-reviewed journal for formulary management, 2016. **41**(5): p. 296-300.

[40] Francucci, C.M., A. Camilletti, and M. Boscaro, *Raloxifene and cardiovascular health: its relationship to lipid and glucose metabolism, hemostatic and inflammation factors and cardiovascular function in postmenopausal women.* Curr Pharm Des, 2005. **11**(32): p. 4187-206.

[41] Kokawa, Y., N. Kishi, H. Jinno, T. Tanaka-Kagawa, S. Narimatsu, and N. Hanioka, *Effect of UDP-glucuronosyltransferase 1A8 polymorphism on raloxifene glucuronidation.* European Journal of Pharmaceutical Sciences, 2013. **49**(2): p. 199-205.

[42] Fisher, B., J.P. Costantino, D.L. Wickerham, C.K. Redmond, M. Kavanah, W.M. Cronin, V. Vogel, A. Robidoux, N. Dimitrov, and J. Atkins, *Tamoxifen for prevention of breast cancer: report of the National Surgical Adjuvant Breast and Bowel Project P-1 Study.* JNCI: Journal of the National Cancer Institute, 1998. **90**(18): p. 1371-1388.

[43] Romero-Lorca, A., A. Novillo, M. Gaibar, F. Bandrés, and A. Fernández-Santander, *Impacts of the Glucuronidase Genotypes UGT1A4, UGT2B7, UGT2B15 and UGT2B17 on Tamoxifen Metabolism in Breast Cancer Patients.* PLoS One, 2015. **10**(7): p. e0132269.

[44] Beumer, J.H., J.M. Rademaker-Lakhai, H. Rosing, M.J. Hillebrand, T.M. Bosch, L. Lopez-Lazaro, J.H. Schellens, and J.H. Beijnen, *Metabolism of trabectedin (ET-743, Yondelis) in patients with advanced cancer.* Cancer Chemother Pharmacol, 2007. **59**(6): p. 825-37.

[45] Iacovelli, R., C. Ciccarese, E. Bria, M. Romano, E. Fantinel, D. Bimbatti, A. Muraglia, A.B. Porcaro, S. Siracusano, M. Brunelli, R. Mazzarotto, W. Artibani, and G. Tortora, *The Cardiovascular Toxicity of Abiraterone and Enzalutamide in Prostate Cancer.* Clin Genitourin Cancer, 2018. **16**(3): p. e645-e653.

[46] Vaillancourt, J., V. Turcotte, P. Caron, L. Villeneuve, L. Lacombe, F. Pouliot, É. Lévesque, and C. Guillemette, *Glucuronidation of Abiraterone and Its Pharmacologically Active Metabolites by UGT1A4, Influence of Polymorphic Variants and Their Potential as Inhibitors of Steroid Glucuronidation.* Drug Metab Dispos, 2020. **48**(2): p. 75-84.

[47] Brown, J.R., J.C. Byrd, P. Ghia, J.P. Sharman, P. Hillmen, D.M. Stephens, C. Sun, W. Jurczak, J.M. Pagel, and A. Ferrajoli, *Cardiovascular adverse events in patients with chronic lymphocytic leukemia receiving acalabrutinib monotherapy: pooled analysis of 762 patients.* Haematologica, 2020.

[48] Allain, E.P., M. Rouleau, K. Vanura, S. Tremblay, J. Vaillancourt, V. Bat, P. Caron, L. Villeneuve, A. Labriet, V. Turcotte, T. Le, M. Shehata, S. Schnabl, D. Demirtas, R. Hubmann, C. Joly-Beauparlant, A. Droit, U. Jäger, P.B. Staber, E. Lévesque, and C. Guillemette, *UGT2B17 modifies drug response in chronic lymphocytic leukaemia.* British journal of cancer, 2020. **123**(2): p. 240-251.

[49] Khosrow-Khavar, F., K.B. Filion, S. Al-Qurashi, N. Torabi, N. Bouganim, S. Suissa, and L. Azoulay, *Cardiotoxicity of aromatase inhibitors and tamoxifen in postmenopausal women with breast cancer: a systematic review and meta-analysis of randomized controlled trials.* Ann Oncol, 2017. **28**(3): p. 487-496.

[50] Kamdem, L.K., Y. Liu, V. Stearns, S.A. Kadlubar, J. Ramirez, S. Jeter, K. Shahverdi, B.A. Ward, E. Ogburn, M.J. Ratain, D.A. Flockhart, and Z. Desta, *In vitro and in vivo oxidative metabolism and glucuronidation of anastrozole.* Br J Clin Pharmacol, 2010. **70**(6): p. 854-69.

[51] Mulay, S. and A. Boruchov, *Recurrent and partially reversible cardiomyopathy occurring during treatment with bendamustine and rituximab.* Leukemia & lymphoma, 2015. **56**(3): p. 805-807.

[52] Azali, L., L. Hazelden, T. Wiczer, M. Palettas, R. Thomas, C. Aossey, J.S. Blachly, M.R. Grever, A.S. Kittai, K.A. Rogers, J.C. Byrd, J.A. Woyach, D. Addison, and S.A. Bhat, *Evaluation of the Incidence and Risk Factors Associated with Major Cardiovascular Events in Patients Receiving Acalabrutinib Therapy.* Blood, 2020. **136**: p. 29-30.

[53] Force, T., D.S. Krause, and R.A. Van Etten, *Molecular mechanisms of cardiotoxicity of tyrosine kinase inhibition.* Nature Reviews Cancer, 2007. **7**(5): p. 332-344.

[54] Lu, D., Q. Xie, and B. Wu, *N-glucuronidation catalyzed by UGT1A4 and UGT2B10 in human liver microsomes: Assay optimization and substrate identification.* J Pharm Biomed Anal, 2017. **145**: p. 692-703.

[55] Perez-Verdia, A., F. Angulo, F.L. Hardwicke, and K.M. Nugent, *Acute cardiac toxicity associated with high-dose intravenous methotrexate therapy: case report and review of the literature.* Pharmacotherapy, 2005. **25**(9): p. 1271-6.

[56] de Almagro, M.C., E. Selga, R. Thibaut, C. Porte, V. Noé, and C.J. Ciudad, *UDP-glucuronosyltransferase 1A6 overexpression in breast cancer cells resistant to methotrexate.* Biochem Pharmacol, 2011. **81**(1): p. 60-70.

[57] Clemons Bankston, P. and R.A. Al-Horani, *New Small Molecule Drugs for Thrombocytopenia: Chemical, Pharmacological, and Therapeutic Use Considerations.* Int J Mol Sci, 2019. **20**(12).

[58] Bussel, J., D.M. Arnold, E. Grossbard, J. Mayer, J. Treliński, W. Homenda, A. Hellmann, J. Windyga, L. Sivcheva, A.A. Khalafallah, F. Zaja, N. Cooper, V. Markovtsov, H. Zayed, and A.-M. Duliege, *Fostamatinib for the treatment of adult persistent and chronic immune thrombocytopenia: Results of two phase 3, randomized, placebo-controlled trials.* American journal of hematology, 2018. **93**(7): p. 921-930.

[59] Precht, J.C., W. Schroth, K. Klein, H. Brauch, E. Krynetskiy, M. Schwab, and T.E. Mürdter, *The letrozole phase 1 metabolite carbinol as a novel probe drug for UGT2B7.* Drug Metab Dispos, 2013. **41**(11): p. 1906-13.

[60] Gerisch, M., F.-T. Hafner, D. Lang, M. Radtke, K. Diefenbach, A. Cleton, and J. Lettieri, *Mass balance, metabolic disposition, and pharmacokinetics of a single oral dose of regorafenib in healthy human subjects.* Cancer chemotherapy and pharmacology, 2018. **81**(1): p. 195-206.

[61] Ye, L., X. Yang, E. Guo, W. Chen, L. Lu, Y. Wang, X. Peng, T. Yan, F. Zhou, and Z. Liu, *Sorafenib metabolism is significantly altered in the liver tumor tissue of hepatocellular carcinoma patient.* PLoS One, 2014. **9**(5): p. e96664.

[62] Martin, P., S. Oliver, S.J. Kennedy, E. Partridge, M. Hutchison, D. Clarke, and P. Giles, *Pharmacokinetics of vandetanib: three phase I studies in healthy subjects.* Clin Ther, 2012. **34**(1): p. 221-37.

[63] Han, K., J.Y. Jin, M. Marchand, S. Eppler, N. Choong, S.P. Hack, N. Tikoo, R. Bruno, M. Dresser, L. Musib, and N.R. Budha, *Population pharmacokinetics and dosing implications for cobimetinib in patients with solid tumors.* Cancer Chemother Pharmacol, 2015. **76**(5): p. 917-24.

[64] Sawyer, D.B., X. Peng, B. Chen, L. Pentassuglia, and C.C. Lim, *Mechanisms of anthracycline cardiac injury: can we identify strategies for cardioprotection?* Progress in cardiovascular diseases, 2010. **53**(2): p. 105-113.

[65] Parmar, S., J.C. Stingl, A. Huber-Wechselberger, A. Kainz, W. Renner, U. Langsenlehner, P. Krippl, J. Brockmöller, and E. Haschke-Becher, *Impact of UGT2B7 His268Tyrpolymorphism on the outcome of adjuvant epirubicin treatment in breast cancer.* Breast Cancer Research, 2011. **13**(3): p. R57.

[66] Gestl, S.A., M.D. Green, D.A. Shearer, E. Frauenhoffer, T.R. Tephly, and J. Weisz, *Expression of UGT2B7, a UDP-glucuronosyltransferase implicated in the metabolism of 4-hydroxyestrone and all-trans retinoic acid, in normal human breast parenchyma and in invasive and in situ breast cancers.* Am J Pathol, 2002. **160**(4): p. 1467-79.

[67] Didagelos, M., A. Boutis, N. Diamantopoulos, M. Sotiriadou, and C. Fotiou, *Bleomycin cardiotoxicity during chemotherapy for an ovarian germ cell tumor.* Hippokratia, 2013. **17**(2): p. 187-188.

[68] Koçan, F., U. Avcıbaşı, P. Unak, F.Z. Müftüler, C.A. Içhedef, H. Demiroğlu, and F.G. Gümüşer, *Metabolic comparison of radiolabeled bleomycin and bleomycin-glucuronide labeled with 99mTc.* Cancer Biother Radiopharm, 2011. **26**(5): p. 573-84.

[69] Schmidinger, M., C.C. Zielinski, U.M. Vogl, A. Bojic, M. Bojic, C. Schukro, M. Ruhsam, M. Hejna, and H. Schmidinger, *Cardiac toxicity of sunitinib and sorafenib in patients with metastatic renal cell carcinoma.* J Clin Oncol, 2008. **26**(32): p. 5204-12.

[70] Suter, T.M. and M.S. Ewer, *Cancer drugs and the heart: importance and management.* European Heart Journal, 2013. **34**(15): p. 1102-1111.

[71] Kingwell, E., M. Koch, B. Leung, S. Isserow, J. Geddes, P. Rieckmann, and H. Tremlett, *Cardiotoxicity and other adverse events associated with mitoxantrone treatment for MS.* Neurology, 2010. **74**(22): p. 1822-1826.

[72] Shimizu, M., H. Suemizu, M. Mitsui, N. Shibata, F.P. Guengerich, and H. Yamazaki, *Metabolic profiles of pomalidomide in human plasma simulated with pharmacokinetic data in control and humanized-liver mice.* Xenobiotica; the fate of foreign compounds in biological systems, 2017. **47**(10): p. 844-848.

[73] Miyawaki, H., H. Kioka, K. Sato, M. Kurashige, T. Ozawa, H. Shibayama, S. Hikoso, E. Morii, K. Yamauchi-Takihara, and Y. Sakata, *Long-term Effects of the Janus Kinase 1/2 Inhibitor Ruxolitinib on Pulmonary Hypertension and the Cardiac Function in a Patient with Myelofibrosis.* Internal medicine (Tokyo, Japan), 2020. **59**(2): p. 229-233.

[74] Shilling, A.D., F.M. Nedza, T. Emm, S. Diamond, E. McKeever, N. Punwani, W. Williams, A. Arvanitis, L.G. Galya, M. Li, S. Shepard, J. Rodgers, T.-Y. Yue, and S. Yeleswaram, *Metabolism, Excretion, and Pharmacokinetics of [¹⁴C]INCB018424, a Selective Janus Tyrosine Kinase 1/2 Inhibitor, in Humans.* Drug Metabolism and Disposition, 2010. **38**(11): p. 2023.

[75] Wang, A.Y., H. Weiner, M. Green, H. Chang, N. Fulton, R.A. Larson, O. Odenike, A.S. Artz, M.R. Bishop, L.A. Godley, M.J. Thirman, S. Kosuri, J.E. Churpek, E. Curran, K. Pettit, W. Stock, and H. Liu, *A phase I study of selinexor in combination with high-dose cytarabine and mitoxantrone for remission induction in patients with acute myeloid leukemia.* Journal of hematology & oncology, 2018. **11**(1): p. 4-4.

[76] Kasamon, Y.L., L.S.L. Price, O.O. Okusanya, N.C. Richardson, R.-J. Li, L. Ma, Y.-T. Wu, M. Theoret, R. Pazdur, and N.J. Gormley, *FDA Approval Summary: Selinexor for Relapsed or Refractory Diffuse Large B-Cell Lymphoma.* The Oncologist, 2021. **26**(10): p. 879-886.

[77] van Breemen, R.B., H.H.S. Fong, and N.R. Farnsworth, *The Role of Quality Assurance and Standardization in the Safety of Botanical Dietary Supplements.* Chemical Research in Toxicology, 2007. **20**(4): p. 577-582.

[78] Garg, V., V.J. Dhar, A. Sharma, and R. Dutt, *Facts about standardization of herbal medicine: a review.* Zhong Xi Yi Jie He Xue Bao, 2012. **10**(10): p. 1077-83.

[79] Manwill, P.K., L. Flores-Bocanegra, M. Khin, H.A. Raja, N.B. Cech, N.H. Oberlies, and D.A. Todd, *Kratom (Mitragyna speciosa) Validation: Quantitative Analysis of Indole and Oxindole Alkaloids Reveals Chemotypes of Plants and Products.* Planta Med, 2022.

[80] *NCCIH Policy: Natural Product Integrity.* National Center for Complimentary and Integrative Health, 2022.

[81] Bijauliya, R.K.K., S. Alok, D.K. Chanchal, and M. Kumar. *A COMPREHENSIVE REVIEW ON STANDARDIZATION OF HERBAL DRUGS*. 2017.

[82] Tistaert, C., B. Dejaegher, and Y.V. Heyden, *Chromatographic separation techniques and data handling methods for herbal fingerprints: A review.* Analytica Chimica Acta, 2011. **690**(2): p. 148-161.

[83] Raut, J.S. and S.M. Karuppayil, *A status review on the medicinal properties of essential oils.* Industrial Crops and Products, 2014. **62**: p. 250-264.

[84] Kharbach, M., I. Marmouzi, M. El Jemli, A. Bouklouze, and Y. Vander Heyden, *Recent advances in untargeted and targeted approaches applied in herbal-extracts and essential-oils fingerprinting - A review.* Journal of Pharmaceutical and Biomedical Analysis, 2020. **177**: p. 112849.

[85] Mulabagal, V., W.J. Keller, and A.I. Calderón, *Quantitative analysis of anthocyanins in Euterpe oleracea (açaí) dietary supplement raw materials and capsules by Q-TOF liquid chromatography/mass spectrometry.* Pharmaceutical Biology, 2012. **50**(10): p. 1289-1296.

[86] Lavine, B.K., *Pattern Recognition.* Critical Reviews in Analytical Chemistry, 2006. **36**(3-4): p. 153-161.

[87] Berrueta, L.A., R.M. Alonso-Salces, and K. Héberger, *Supervised pattern recognition in food analysis.* Journal of Chromatography A, 2007. **1158**(1): p. 196-214.

[88] Goodarzi, M., P.J. Russell, and Y. Vander Heyden, *Similarity analyses of chromatographic herbal fingerprints: A review.* Analytica Chimica Acta, 2013. **804**: p. 16-28.

[89] Laurindo, L.F., S.M. Barbalho, A.C. Araújo, E.L. Guiguer, A. Mondal, G. Bachtel, and A. Bishayee, *Açaí (Euterpe oleracea Mart.) in Health and Disease: A Critical Review.* Nutrients, 2023. **15**(4).

[90] Del Pozo-Insfran, D., C.H. Brenes, and S.T. Talcott, *Phytochemical Composition and Pigment Stability of Açai (Euterpe oleracea Mart.).* Journal of Agricultural and Food Chemistry, 2004. **52**(6): p. 1539-1545.

[91] Bobbio, F.O., J.I. Druzian, P.A. AbrÃO, P.A. Bobbio, and S. Fadelli, *Identificação e quantificação das antocianinas do fruto do açaizeiro (Euterpe oleracea) Mart.* Food Science and Technology, 2000. **20**.

[92] Gallori, S., A.R. Bilia, M.C. Bergonzi, W.L.R. Barbosa, and F.F. Vincieri, *Polyphenolic constituents of fruit pulp of Euterpe oleracea Mart. (Açai palm).* Chromatographia, 2004. **59**(11-12): p. 739-743.

[93] Kang, J., Z. Li, T. Wu, G.S. Jensen, A.G. Schauss, and X. Wu, *Anti-oxidant capacities of flavonoid compounds isolated from acai pulp (Euterpe oleracea Mart.).* Food Chemistry, 2010. **122**(3): p. 610-617.

[94] Kang, J., C. Xie, Z. Li, S. Nagarajan, A.G. Schauss, T. Wu, and X. Wu, *Flavonoids from acai (Euterpe oleracea Mart.) pulp and their antioxidant and anti-inflammatory activities.* Food Chemistry, 2011. **128**(1): p. 152-157.

[95] Lichtenthäler, R., R.B. Rodrigues, J.G.S. Maia, M. Papagiannopoulos, H. Fabricius, and F. Marx, *Total oxidant scavenging capacities of Euterpe oleracea Mart. (Açaí) fruits.* International Journal of Food Sciences and Nutrition, 2005. **56**(1): p. 53-64.

[96] Pacheco-Palencia, L.A., C.E. Duncan, and S.T. Talcott, *Phytochemical composition and thermal stability of two commercial açai species, Euterpe oleracea and Euterpe precatoria.* Food Chemistry, 2009. **115**(4): p. 1199-1205.

[97] Ribeiro, J.C., L.M.G. Antunes, A.F. Aissa, J.D.a.C. Darin, V.V. De Rosso, A.Z. Mercadante, and M.d.L.P. Bianchi, *Evaluation of the genotoxic and antigenotoxic effects after acute and subacute treatments with açai pulp (Euterpe oleracea Mart.) on mice using the erythrocytes micronucleus test and the comet assay.* Mutation Research/Genetic Toxicology and Environmental Mutagenesis, 2010. **695**(1): p. 22-28.

[98] Schauss, A.G., X. Wu, R.L. Prior, B. Ou, D. Patel, D. Huang, and J.P. Kababick, *Phytochemical and Nutrient Composition of the Freeze-Dried Amazonian Palm Berry, Euterpe oleraceae Mart. (Acai).* Journal of Agricultural and Food Chemistry, 2006. **54**(22): p. 8598-8603.

[99] Mantovani, I.S.B., S.B.O. Fernandes, and F.S. Menezes, *Constituintes apolares do fruto do açaí (Euterpe oleracea M. - Arecaceae).* Revista Brasileira de Farmacognosia, 2003. **13**.

[100] Nascimento, R.J.S.d., S. Couri, R. Antoniassi, and S.P. Freitas, *Composição em ácidos graxos do óleo da polpa de açaí extraído com enzimas e com hexano.* Revista Brasileira de Fruticultura, 2008. **30**.

[101] Schauss, A.G., X. Wu, R.L. Prior, B. Ou, D. Huang, J. Owens, A. Agarwal, G.S. Jensen, A.N. Hart, and E. Shanbrom, *Antioxidant Capacity and Other Bioactivities of the Freeze-Dried Amazonian Palm Berry, Euterpe oleraceae Mart. (Acai).* Journal of Agricultural and Food Chemistry, 2006. **54**(22): p. 8604-8610.

[102] Yuyama, L.K.O., J.P.L. Aguiar, D.F. Silva Filho, K. Yuyama, M.d. Jesus Varejão, D.I.T. Fávaro, M.B.A. Vasconcellos, S.A. Pimentel, and M.S.F. Caruso, *Caracterização físico-química do suco de açaí de Euterpe precatoria Mart. oriundo de diferentes ecossistemas amazônicos.* Acta Amazonica, 2011. **41**.

[103] Chin, Y.-W., H.-B. Chai, W.J. Keller, and A.D. Kinghorn, *Lignans and Other Constituents of the Fruits of Euterpe oleracea (Açai) with Antioxidant and Cytoprotective Activities.* Journal of Agricultural and Food Chemistry, 2008. **56**(17): p. 7759-7764.

[104] Oliveira, A.R., A.E.C. Ribeiro, É.R. Oliveira, M.C. Garcia, M.S. Soares JÚNior, and M. Caliari, *Structural and physicochemical properties of freeze-dried açaí pulp (Euterpe oleracea Mart.).* Food Science and Technology, 2020. **40**.

[105] Mertens-Talcott, S.U., J. Rios, P. Jilma-Stohlawetz, L.A. Pacheco-Palencia, B. Meibohm, S.T. Talcott, and H. Derendorf, *Pharmacokinetics of Anthocyanins and Antioxidant Effects after the Consumption of Anthocyanin-Rich Açai Juice and Pulp (Euterpe oleracea Mart.) in Human Healthy Volunteers.* Journal of Agricultural and Food Chemistry, 2008. **56**(17): p. 7796-7802.

[106] Vera de Rosso, V., S. Hillebrand, E. Cuevas Montilla, F.O. Bobbio, P. Winterhalter, and A.Z. Mercadante, *Determination of anthocyanins from acerola (Malpighia emarginata DC.) and açai (Euterpe oleracea Mart.) by HPLC–PDA–MS/MS.* Journal of Food Composition and Analysis, 2008. **21**(4): p. 291-299.

[107] Gallori, S., A.R. Bilia, M.C. Bergonzi, W.L.R. Barbosa, and F.F. Vincieri, *Polyphenolic constituents of fruit pulp of Euterpe oleracea Mart.(açai palm).* Chromatographia, 2004. **59**(11): p. 739-743.

[108] Bucar, F., A. Wube, and M. Schmid, *Natural product isolation – how to get from biological material to pure compounds.* Nat Prod Rep, 2013. **30**(4): p. 525-545.

[109] Nothias, L.F., M. Nothias-Esposito, R. da Silva, M. Wang, I. Protsyuk, Z. Zhang, A. Sarvepalli, P. Leyssen, D. Touboul, J. Costa, J. Paolini, T. Alexandrov, M. Litaudon, and P.C. Dorrestein, *Bioactivity-Based Molecular Networking for the Discovery of Drug Leads in Natural Product Bioassay-Guided Fractionation.* J Nat Prod, 2018. **81**(4): p. 758-767.

[110] Wang, M., J.J. Carver, V.V. Phelan, L.M. Sanchez, N. Garg, Y. Peng, D.D. Nguyen, J. Watrous, C.A. Kapono, T. Luzzatto-Knaan, C. Porto, A. Bouslimani, A.V. Melnik, M.J. Meehan, W.T. Liu, M. Crüsemann, P.D. Boudreau, E. Esquenazi, M. Sandoval-Calderón, R.D. Kersten, L.A. Pace, R.A. Quinn, K.R. Duncan, C.C. Hsu, D.J. Floros, R.G. Gavilan, K. Kleigrewe, T. Northen, R.J. Dutton, D. Parrot, E.E. Carlson, B. Aigle, C.F. Michelsen, L. Jelsbak, C. Sohlenkamp, P. Pevzner, A. Edlund, J. McLean, J. Piel, B.T. Murphy, L. Gerwick, C.C. Liaw, Y.L. Yang, H.U. Humpf, M. Maansson, R.A. Keyzers, A.C. Sims, A.R. Johnson, A.M. Sidebottom, B.E. Sedio, A. Klitgaard, C.B. Larson, C.A.B. P, D. Torres-Mendoza, D.J. Gonzalez, D.B. Silva, L.M. Marques, D.P. Demarque, E. Pociute,

E.C. O'Neill, E. Briand, E.J.N. Helfrich, E.A. Granatosky, E. Glukhov, F. Ryffel, H. Houson, H. Mohimani, J.J. Kharbush, Y. Zeng, J.A. Vorholt, K.L. Kurita, P. Charusanti, K.L. McPhail, K.F. Nielsen, L. Vuong, M. Elfeki, M.F. Traxler, N. Engene, N. Koyama, O.B. Vining, R. Baric, R.R. Silva, S.J. Mascuch, S. Tomasi, S. Jenkins, V. Macherla, T. Hoffman, V. Agarwal, P.G. Williams, J. Dai, R. Neupane, J. Gurr, A.M.C. Rodríguez, A. Lamsa, C. Zhang, K. Dorrestein, B.M. Duggan, J. Almaliti, P.M. Allard, P. Phapale, L.F. Nothias, T. Alexandrov, M. Litaudon, J.L. Wolfender, J.E. Kyle, T.O. Metz, T. Peryea, D.T. Nguyen, D. VanLeer, P. Shinn, A. Jadhav, R. Müller, K.M. Waters, W. Shi, X. Liu, L. Zhang, R. Knight, P.R. Jensen, B.O. Palsson, K. Pogliano, R.G. Linington, M. Gutiérrez, N.P. Lopes, W.H. Gerwick, B.S. Moore, P.C. Dorrestein and N. Bandeira, *Sharing and community curation of mass spectrometry data with Global Natural Products Social Molecular Networking.* Nat Biotechnol, 2016. **34**(8): p. 828-837.

[111] Nothias, L.-F., D. Petras, R. Schmid, K. Dührkop, J. Rainer, A. Sarvepalli, I. Protsyuk, M. Ernst, H. Tsugawa, M. Fleischauer, F. Aicheler, A.A. Aksenov, O. Alka, P.-M. Allard, A. Barsch, X. Cachet, A.M. Caraballo-Rodriguez, R.R. Da Silva, T. Dang, N. Garg, J.M. Gauglitz, A. Gurevich, G. Isaac, A.K. Jarmusch, Z. Kameník, K.B. Kang, N. Kessler, I. Koester, A. Korf, A. Le Gouellec, M. Ludwig, C. Martin H, L.-I. McCall, J. McSayles, S.W. Meyer, H. Mohimani, M. Morsy, O. Moyne, S. Neumann, H. Neuweger, N.H. Nguyen, M. Nothias-Esposito, J. Paolini, V.V. Phelan, T. Pluskal, R.A. Quinn, S. Rogers, B. Shrestha, A. Tripathi, J.J.J. van der Hooft, F. Vargas, K.C. Weldon, M. Witting, H. Yang, Z. Zhang, F. Zubeil, O. Kohlbacher, S. Böcker, T. Alexandrov, N. Bandeira, M. Wang, and P.C. Dorrestein, *Feature-based molecular networking in the GNPS analysis environment.* Nature methods, 2020. **17**(9): p. 905-908.

[112] Phelan, V.V., *Feature-Based Molecular Networking for Metabolite Annotation.* Methods Mol Biol, 2020. **2104**: p. 227-243.

[113] Baskiyar, S., C. Ren, K.L. Heck, A.M. Hall, M. Gulfam, S. Packer, C.D. Seals, and A.I. Calderón, *Bioactive Natural Products Identification Using Automation of Molecular Networking Software.* Journal of Chemical Information and Modeling, 2022.

[114] Pluskal, T., S. Castillo, A. Villar-Briones, and M. Orešič, *MZmine 2: Modular framework for processing, visualizing, and analyzing mass spectrometry-based molecular profile data.* BMC Bioinf, 2010. **11**(1): p. 395.

[115] Shannon, P., A. Markiel, O. Ozier, N.S. Baliga, J.T. Wang, D. Ramage, N. Amin, B. Schwikowski, and T. Ideker, *Cytoscape: a software environment for integrated models of biomolecular interaction networks.* Genome Res, 2003. **13**(11): p. 2498-504.

[116] Zdouc, M.M., M. Iorio, S.I. Maffioli, M. Crüsemann, S. Donadio, and M. Sosio, *Planomonospora: A Metabolomics Perspective on an Underexplored Actinobacteria Genus.* Journal of Natural Products, 2021. **84**(2): p. 204-219.

[117] Fox Ramos, A.E., C. Pavesi, M. Litaudon, V. Dumontet, E. Poupon, P. Champy, G. Genta-Jouve, and M.A. Beniddir, *CANPA: Computer-Assisted Natural Products Anticipation.* Analytical Chemistry, 2019. **91**(17): p. 11247-11252.

[118] Nothias-Esposito, M., L.F. Nothias, R.R. Da Silva, P. Retailleau, Z. Zhang, P. Leyssen, F. Roussi, D. Touboul, J. Paolini, P.C. Dorrestein, and M. Litaudon, *Investigation of Premyrsinane and Myrsinane Esters in Euphorbia cupanii and Euphobia pithyusa with MS2LDA and Combinatorial Molecular Network Annotation Propagation.* Journal of Natural Products, 2019. **82**(6): p. 1459-1470.

[119] Kang, K.B., E.J. Park, R.R. da Silva, H.W. Kim, P.C. Dorrestein, and S.H. Sung, *Targeted Isolation of Neuroprotective Dicoumaroyl Neolignans and Lignans from Sageretia theezans Using in Silico Molecular Network Annotation Propagation-Based Dereplication.* Journal of Natural Products, 2018. **81**(8): p. 1819-1828.

[120] Hall, A.M., S. Baskiyar, K.L. Heck, M.D. Hayden, C. Ren, C. Nguyen, C.D. Seals, E. Monu, and A.I. Calderón, *Investigation of the chemical composition of antibacterial Psidium guajava extract and partitions against foodborne pathogens.* Food Chemistry, 2022.

[121] Alcazar Magana, A., K. Wright, A. Vaswani, M. Caruso, R.L. Reed, C.F. Bailey, T. Nguyen, N.E. Gray, A. Soumyanath, J. Quinn, J.F. Stevens, and C.S. Maier, *Integration of mass spectral fingerprinting analysis with precursor ion (MS1) quantification for the characterisation of botanical extracts: application to extracts of Centella asiatica (L.) Urban.* Phytochemical Analysis, 2020. **31**(6): p. 722-738.

[122] Dührkop, K., M. Fleischauer, M. Ludwig, A.A. Aksenov, A.V. Melnik, M. Meusel, P.C. Dorrestein, J. Rousu, and S. Böcker, *SIRIUS 4: a rapid tool for turning tandem mass spectra into metabolite structure information.* Nature Methods, 2019. **16**(4): p. 299-302.

[123] Dührkop, K., H. Shen, M. Meusel, J. Rousu, and S. Böcker, *Searching molecular structure databases with tandem mass spectra using CSI:FingerID.* Proc Natl Acad Sci U S A, 2015. **112**(41): p. 12580-5.

[124] Yuan, R., S. Madani, X.-X. Wei, K. Reynolds, and S.-M. Huang, *Evaluation of Cytochrome P450 Probe Substrates Commonly Used by the Pharmaceutical Industry to*

Study in Vitro Drug Interactions. Drug Metabolism and Disposition, 2002. **30**(12): p. 1311-1319.

[125] Zhang, Y., T.A. Rants'o, D. Jung, E. Lopez, K. Abbott, S.R. Pondugula, L. McLendon, J. Qian, R.A. Hansen, and A.I. Calderón, *Screening for CYP3A4 inhibition and induction coupled to parallel artificial membrane permeability assay (PAMPA) for prediction of botanical-drug interactions: The case of açaí and maca.* Phytomedicine : international journal of phytotherapy and phytopharmacology, 2019. **59**: p. 152915.

[126] Heck, K.L., L.M. Walters, M.L. Kunze, and A.I. Calderón, *Standardization of açaí extracts for in-vitro assays based on anthocyanin quantitation.* Journal of Food Composition and Analysis, 2023. **118**: p. 105155.

[127] Rabizadeh, F., M.S. Mirian, R. Doosti, R. Kiani-Anbouhi, and E. Eftekhari, *Phytochemical Classification of Medicinal Plants Used in the Treatment of Kidney Disease Based on Traditional Persian Medicine.* Evid Based Complement Alternat Med, 2022. **2022**: p. 8022599.

[128] Earling, M., T. Beadle, and E.D. Niemeyer, *Açai Berry (Euterpe oleracea) Dietary Supplements: Variations in Anthocyanin and Flavonoid Concentrations, Phenolic Contents, and Antioxidant Properties.* Plant Foods for Human Nutrition, 2019. **74**(3): p. 421-429.

[129] Pacheco-Palencia, L.A., S. Mertens-Talcott, and S.T. Talcott, *Chemical Composition, Antioxidant Properties, and Thermal Stability of a Phytochemical Enriched Oil from Açai (Euterpe oleracea Mart.).* Journal of Agricultural and Food Chemistry, 2008. **56**(12): p. 4631-4636.

[130] Lv, L., Y. Liu, L. Li, F.-L. Qin, C.-J. Li, Y.-Q. Zhou, Y.-N. Zhou, H. Wang, Y. Jiao, and L. Zhao, *Pharmacokinetics and tissue distribution of Ebracteolatain A, a potential anti-cancer compound, as determined by an optimized ultra-performance liquid chromatography tandem mass spectrometry method.* Journal of Pharmaceutical and Biomedical Analysis, 2019. **169**: p. 279-287.

[131] Li, Y.-Q., C.-J. Li, L. Lv, Q.-q. Cao, X. Qian, S.w. Li, H. Wang, and L. Zhao, *A UPLC-MS/MS method for simultaneous determination of five flavonoids from Stellera chamaejasme L. in rat plasma and its application to a pharmacokinetic study.* Biomedical Chromatography, 2018. **32**(6): p. e4189.

[132] Fu, Z., Y. Ling, Z. Li, M. Chen, Z. Sun, and C. Huang, *HPLC-Q-TOF-MS/MS for analysis of major chemical constituents of Yinchen–Zhizi herb pair extract.* Biomedical Chromatography, 2014. **28**(4): p. 475-485.

[133] Ling, Y., Z. Fu, Q. Zhang, L. Xu, and L. Liao, *Identification and structural elucidation of steroidal saponins from the root of Paris polyphylla by HPLC-ESI-QTOF-MS/MS.* Natural Product Research, 2015. **29**(19): p. 1798-1803.

[134] Ling, Y., K. Liu, Q. Zhang, L. Liao, and Y. Lu, *High performance liquid chromatography coupled to electrospray ionization and quadrupole time-of-flight–mass spectrometry as a powerful analytical strategy for systematic analysis and improved characterization of the major bioactive constituents from Radix Dipsaci.* Journal of Pharmaceutical and Biomedical Analysis, 2014. **98**: p. 120-129.

[135] Ling, Y. and Q. Zhang, *Structural characterisation and screening of triterpene saponins in the bark of Ilex rotunda using high-performance liquid chromatography coupled to electrospray ionisation and quadrupole time-of-flight mass spectrometry.* Phytochemical Analysis, 2021. **32**(3): p. 395-403.

[136] Xiao, W., X. Zhuang, G. Shen, Y. Zhong, M. Yuan, and H. Li, *Simultaneous quantification of l-tetrahydropalmatine and its urine metabolites by ultra high performance liquid chromatography with tandem mass spectrometry.* Journal of Separation Science, 2014. **37**(6): p. 696-703.

[137] Zheng, L., H. Cong, M. Xue, T. Xiang, Z. Yao, B. Wu, and W. Lin, *Characterization of chemical constituents and rats metabolites of Shuanghua Baihe tablets by HPLC-Q-TOF-MS/MS.* Biomedical Chromatography, 2015. **29**(1): p. 75-86.

[138] Steimer, S. and P.J.R. Sjöberg, *Anthocyanin Characterization Utilizing Liquid Chromatography Combined with Advanced Mass Spectrometric Detection.* Journal of Agricultural and Food Chemistry, 2011. **59**(7): p. 2988-2996.

[139] Silva, M.d. and D.R.d. Oliveira, *The new Brazilian legislation on access to the biodiversity (Law 13,123/15 and Decree 8772/16).* brazilian journal of microbiology, 2018. **49**(1): p. 1-4.

[140] Silva, M.d. *Brazilian Biodiversity law: Despite enhancements, new rules are criticized by the scientific community*. 2018.

[141] Lee, J., *Chapter 4. Blackberry fruit quality components, composition, and potential health benefits*. 2017. p. 49-62.

[142] Carvalho, A.V., T. Ferreira Ferreira da Silveira, R.d.A. Mattietto, M.d.S. Padilha de Oliveira, and H.T. Godoy, *Chemical composition and antioxidant capacity of açaí (Euterpe oleracea) genotypes and commercial pulps.* Journal of the Science of Food and Agriculture, 2017. **97**(5): p. 1467-1474.

[143] Kidd, P.M., *Bioavailability and activity of phytosome complexes from botanical polyphenols: the silymarin, curcumin, green tea, and grape seed extracts.* Altern Med Rev, 2009. **14**(3): p. 226-46.

[144] Awortwe, C., P.J. Bouic, C.M. Masimirembwa, and B. Rosenkranz, *Inhibition of major drug metabolizing CYPs by common herbal medicines used by HIV/AIDS patients in Africa-- implications for herb-drug interactions.* Drug Metab Lett, 2014. **7**(2): p. 83-95.

[145] Smith, C.A., G. O'Maille, E.J. Want, C. Qin, S.A. Trauger, T.R. Brandon, D.E. Custodio, R. Abagyan, and G. Siuzdak, *METLIN: a metabolite mass spectral database.* Ther Drug Monit, 2005. **27**(6): p. 747-51.

[146] Craig, S.A.S., *Betaine in human nutrition.* The American Journal of Clinical Nutrition, 2004. **80**(3): p. 539-549.

[147] Sud, M., E. Fahy, D. Cotter, A. Brown, E.A. Dennis, C.K. Glass, A.H. Merrill, Jr, R.C. Murphy, C.R.H. Raetz, D.W. Russell, and S. Subramaniam, *LMSD: LIPID MAPS structure database.* Nucleic Acids Research, 2006. **35**(suppl_1): p. D527-D532.

[148] Seo, K.-A., H.-J. Kim, E.S. Jeong, N. Abdalla, C.-S. Choi, D.-H. Kim, and J.-G. Shin, *In Vitro Assay of Six UDP-Glucuronosyltransferase Isoforms in Human Liver Microsomes, Using Cocktails of Probe Substrates and Liquid Chromatography–Tandem Mass Spectrometry.* Drug Metabolism and Disposition, 2014. **42**(11): p. 1803.

[149] Chen, A., X. Zhou, Y. Cheng, S. Tang, M. Liu, and X. Wang, *Design and optimization of the cocktail assay for rapid assessment of the activity of UGT enzymes in human and rat liver microsomes.* Toxicology Letters, 2018. **295**: p. 379-389.

[150] Gradinaru, J., S. Romand, L. Geiser, P.A. Carrupt, D. Spaggiari, and S. Rudaz, *Inhibition screening method of microsomal UGTs using the cocktail approach.* Eur J Pharm Sci, 2015. **71**: p. 35-45.